eman ta zabal zazu

Universidad del País Vasco

Euskal Herriko Unibertsitatea

Design and evaluation of novel electro-conductive alginate hydrogels based on graphene oxide and reduced graphene oxide with applications in tissue engineering

NanoBioCel Group, Laboratory of Pharmacy and Pharmaceutical Technology

Faculty of Pharmacy, University of the Basque Country UPV/EHU

Ahmed Khalaf Reyad Raslan

Vitoria-Gasteiz, 2022

eman ta zabal zazu

Universidad del País Vasco

Euskal Herriko Unibertsitatea

Design and evaluation of novel electro-conductive alginate hydrogels based on graphene oxide and reduced graphene oxide with applications in tissue engineering

NanoBioCel Group, Laboratory of Pharmacy and Pharmaceutical Technology

Faculty of Pharmacy, University of the Basque Country UPV/EHU

Ahmed Khalaf Reyad Raslan

Vitoria-Gasteiz, 2022

ACKNOWLEDGMENTS.

ACKNOWLEDGMENTS TO RESEARCH GROUPS

Dr. Laura Saenz del Burgo and Prof. Jose Luis Pedraz deserve my heartfelt thanks for their tireless support and patience in my Ph.D. study and related research. The guidance they provided me throughout the whole process of researching and writing this thesis was constructive. My Ph.D. program wouldn't have been complete without the assistance of my advisor and mentor.

Dr. Jesus Ciriza also deserves my sincere thanks.

My last word is to thank my fellow lab mates for stimulating talks.

Acknowledgments for the financial support.

This research was funded by the University of the Basque Country UPV/EHU and the Basque Country Government (Grupos Consolidados, No ref. IT907-16).

The authors also wish to thank the academic and technical assistance provided by the ICTS “NANBIOSIS,” more specifically by the Drug Formulation Unit (U10) of the CIBER in Bioengineering, Biomaterials, and Nanomedicine (CIBER-BBN) at the University of Basque Country (UPV/EHU).

ACKNOWLEDGMENT TO THE EDITORIALS.

The authors would like to thank the editorials for granting permission to reuse their previously published articles in this thesis.

PUBLICATIONS RELATED TO THIS Ph.D. THESIS

1- Raslan A, Saenz Del Burgo L, Ciriza J, Pedraz JL. Graphene oxide and reduced graphene oxide-based scaffolds in regenerative medicine. Int J Pharm. 2020 Apr 30;580.119226. DOI. 10.1016/j.ijpharm.2020.119226. (Appendix 1)

2- Raslan A, Saenz del Burgo L, Espona-Noguera A, Retana AMO, Sanjuán ML, Cañibano-Hernández A, Gálvez-Martín P, Ciriza J, Pedraz JL. BSA- and Elastin-Coated GO, but Not Collagen-Coated GO, Enhance the Biological Performance of Alginate Hydrogels. Pharmaceutics. 2020 Jun 11;12(6).543. doi.10.3390/pharmaceutics12060543. (Appendix 2)

3- Raslan, A.; Ciriza, J.; Ochoa de Retana, A.M.; Sanjuán, M.L.; Toprak, M.S.; Galvez-Martin, P.; Saenz-del-Burgo, L.; Pedraz, J.L. Modulation of Conductivity of Alginate Hydrogels Containing Reduced Graphene Oxide through the Addition of Proteins. Pharmaceutics 2021, 13, 1473. https.//doi.org/10.3390/pharmaceutics13091473. (Appendix 3)

GLOSSARY.

IFNγ. Interferon-gamma

DEX Dextran

EDC. 1-ethyl-3-(3-dimethyl aminopropyl) carbodiimide hydrochloride

HA. Hydroxyapatite.

PADM. Porcine acellular dermal matrix

PHA. Phytohaemagglutinin

2D. Two-dimensional

3D. Three-dimensional

APA. Alginate-poly-L-lysine-alginate

BSA. Bovine Serum Albumin

C2C12. Immortalized mouse myoblast cell line

CCK-8. Cell counting kit-8

CNS. Central nervous system

CPC. Calcium phosphate cement

DMEM. Dulbecco´s modified Eagle´s medium

DMSO. Dimethyl sulfoxide

DPBS. Dulbecco-s phosphate-buffered saline

EG. Ethylene glycol

FBS. Fetal bovine serum

G. α-L-guluronic acid

GLP-1. Glucagon-like peptide 1

GMP. Good manufacturing procedures

GO. Graphene Oxide

rGO.Reduced graphene oxide

IL-6. Interleukin 6

iPS. Induced pluripotent stem cells

LDH. Lactate dehydrogenase

mcDNA. Minicircle DNA

MSC-Epo. D1 mesenchymal stem cells engineered to release EPO

PBS. Phosphate-buffered saline

PEG. Poly-ethylene-glycol

PEX. Hemopexin-like protein

PLGA Poly(d,l lactide-co-glycolide

PLGA. Poly(lactic-co-glycolic acid

SC. Stem cells

Sh-Sy5Y. Thrice-subcloned cell line derived from the SK-N-SH neuroblastoma cell

TLR4. Toll-like receptor 4

HeLa.Henrietta Lacks cells

SKBR3. Sloan Kettering breast cancer cells

MCF7. Michigan cancer foundation-7 breast cancer cells

TENG. Triboelectric nanogenerators

$CaSO_4$. Calcium sulfate

$CaCO_3$. Calcium carbonate

$CaCl_2$. Calcuim chrolide

OD. Oxidation degree

BMP-2. The bone morphogenetic protein-2

RES. Reticuloendothelial system

HAp Hydroxyapatite

β-TCP. β-tricalcium phosphate

Index

Chapter 1

Introduction

1. State of the art.

In the past, the field of biomaterials has experienced tremendous growth, which has resulted in a huge amount of research and development.

The term 'biomaterials' refers to substances created for interacting with biological systems, either therapeutically (treating, augmenting, repairing, or replacing body functions) or diagnostically. They include metal components, polymers, ceramics, and composites [1, 2].

Those biomaterials have many applications in the medical field and are frequently incorporated into or attached to a biological system or medical device that performs, strengthens, or replaces normal function [1, 2]. Although these materials differ in composition and properties, they all have common design standards: (a) provide mechanical support; (b) have high porosity to allow mass transport; (c) promote cell proliferation and differentiation; (d) induce a minimal host immune response [3]. It is essential to consider these requirements when developing a biomaterial-based system. Due to their excellent properties, these biomaterials are widely used in hydrogels preparation for regenerative medicine [4].

A hydrogel is a three-dimensional scaffold (3D) made from a highly hydrophilic polymer [4-7]. Importantly, hydrogels can absorb large amounts of water, thus becoming elastic similarly to normal tissues [8]. Hydrogels possess a broad spectrum of excellent characteristics, including high biocompatibility, biodegradability, and a highly porous surface [2, 4-7]. All these characteristics make hydrogels suitable for a variety of biomedical applications, including the development of soft contact lenses [9], tissue engineering [10, 11], diagnostics [12], and cell encapsulation (figure 1) [7].

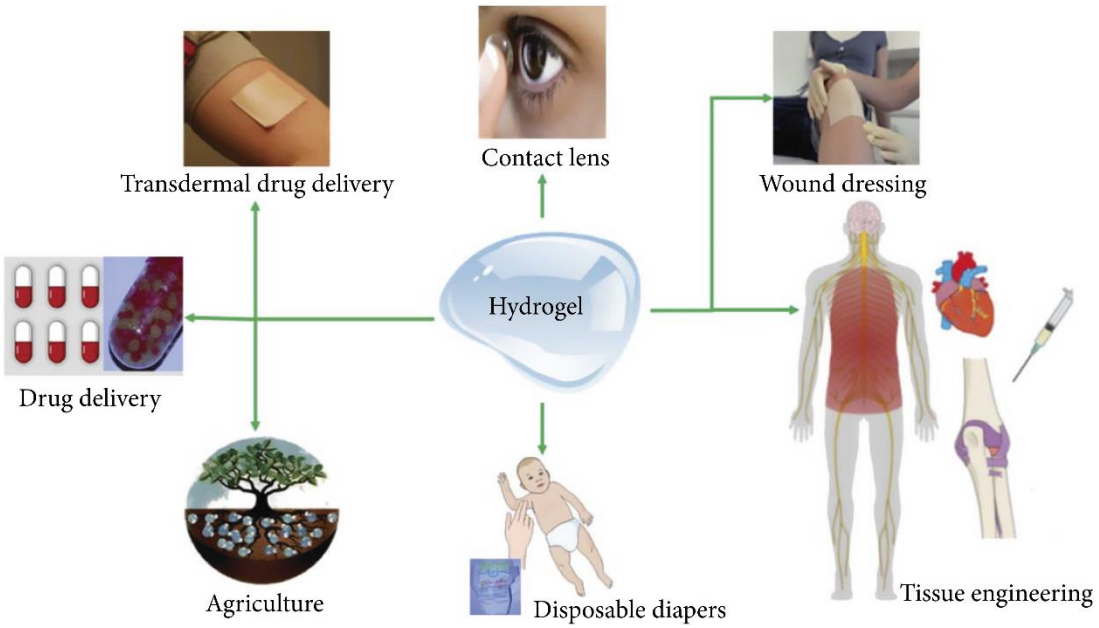

Figure 1. Applications of hydrogels in potential technological fields[13].

Two centuries ago, hydrogels were synthesized for the first time. However, the use of hydrogels in tissue engineering appeared in the 20th century [14]. In the beginning, hydrogels were designed with a limited range of properties, such as having a high content of water, good mechanical strength, and simple functionality [14]. Moreover, these hydrogels show a high-water content [10, 15], so they mimic the extracellular matrix, making them suitable for tissue engineering. Generally, hydrogels are known for their outstanding properties, including the ability to exchange nutrients and oxygen while releasing waste products and therapeutic proteins outside. A hydrogel also protects embedded cells from the immune system, preventing rejection [15]. To improve the surface properties of hydrogels and their function, fundamental structural and functional modifications have been made since the first studies were published [16-18].

Depending on the type of bonds that bind the copolymers together or by the source of the original polymer, it is possible to classify hydrogels in several ways [4, 5, 7]. In terms of the bonds, hydrogels can be classified as either physical or chemical hydrogels. A biological hydrogel is formed by physical bonds, such as hydrogen bonds or hydrophobic interactions [4, 5, 7]. This hydrogel is characterized by its instability and sensitivity to environmental conditions, such as temperature and pH. On the other hand, chemical hydrogels are composed of co-polymers attached by covalent bonds. Their stability and inert nature make them non-degradable [4].

Hydrogels can also be classified based on their origin, whether naturally derived hydrogels or synthetic hydrogels. Natural hydrogels are obtained from plant materials, microorganisms, and human tissues. All of these are examples of naturally derived hydrogels, including alginate, chitosan, collagen, elastin, fibrin, glycosaminoglycans, and hyaluronic acid (HA) [4, 17, 19]. While synthetic hydrogels can be designed to display desirable physical and chemical properties, they do not possess inherent biological activity; for example, polyethylene glycol (PEG) and polyethylene oxide (PEO) [2, 16, 20, 21].

In vivo, natural hydrogels such as collagen, fibrin, chitosan, and alginate are the most biocompatible hydrogels since they are components of the extracellular matrix (ECM)[22].There are still many limitations to using natural hydrogels in clinical applications due to poor mechanical strength and rapid drug release [7, 23].

Various biological applications have been investigated using alginate and its hydrogels in biomedical fields, including drug delivery, tissue regeneration, wound healing, 3D printing, and in vitro modeling. Many soft and hard tissues have been repaired using alginate-based biomaterials, including skin, heart, bone [22, 24]. Alginate-based hydrogels' chemical modification is frequently employed in these fields [7, 24-27]. Despite its biocompatibility, alginate is highly hydrophilic with low protein adsorption, making it a non-fouling material. Cell-interactive domains also make alginate hydrogels non-adhesive as cells cannot attach directly to the alginate [7, 24-27]. While this feature may seem disadvantageous, it can contribute to the design of biomaterials since non-modified alginate can be used as a blank slate and can be chemically modified to result in specific biological responses [24].

1.1 Alginate hydrogels.

Biomaterials such as alginate can be found in nature and have been widely used in tissue engineering applications. In addition to brown algae such as Laminaria, Macrocystis, and Ascophyllum, alginate can also be extracted from sphagnum moss [15]. As a biopolymer, this material has excellent properties, including biocompatibility, biodegradability, hydrophilicity [7, 28-31].

For decades, alginates have been considered one of the most efficient biomaterials for the assembly and fabrication of functional hydrogels due to their excellent biocompatibility and high porosity [32]. As a bridge, bivalent elements, such as Ca++, are added to alginate solutions to produce the crosslinking of the gluconate blocks of one polymer chain with those of adjacent chains (Fig. 2).

The high solubility of $CaCl_2$ crystals in water usually leads to rapid gelation, which cannot be controlled. There are several other alternatives. For example, Calcium phosphate solution (Calcium hexametaphosphate) allows the controlled and relatively slow gel formation by competing with the alginate carboxyl groups in the reaction with calcium ions. The lower solubility of calcium sulfate ($CaSO_4$) and calcium carbonate ($CaCO_3$) can also slow gel formation rates and prolong the gelation times of alginate [33].

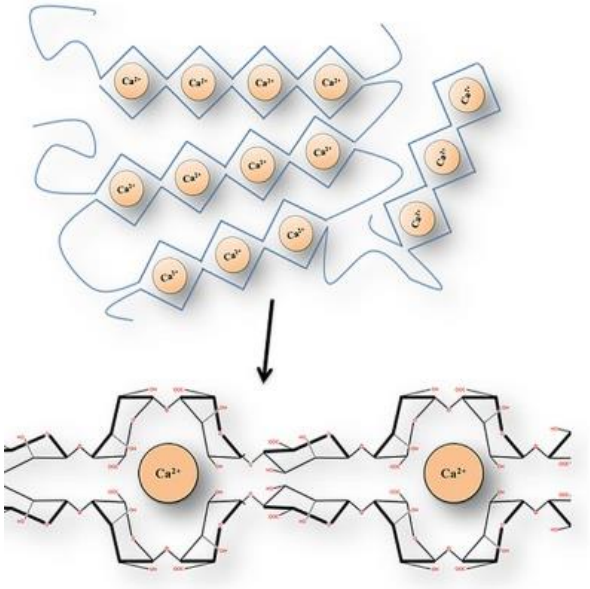

Figure 2. The crosslinking process of alginate with Ca^{++} [22]

Degradation of alginate hydrogels.

It is well known that mammals lack enzymes capable of degrading alginate, like the enzyme alginase which can cleave the polymer chains of the alginate [33]. Although alginate is not degradable, ionically cross-linked alginate hydrogels can dissolve when the divalent ions that bind the hydrogel are released via reactions with monovalent cations, sodium citrate [33]. However, it has been found that the partial oxidation of

alginate chains can make alginate biodegradable under physiological conditions and after log periods [34].

Applications of alginate hydrogels.

There have been extensive studies on the use of alginate hydrogels in cancer therapies, wound healing, cell-based therapies, and as scaffolds for tissue engineering (Figure 1) [10, 19, 20].

Conventional cancer therapies are associated with many side effects [7], so it is imperative to develop unorthodox treatments that can safely and precisely deliver drugs to the tumor site to target cancer cells [35-38]. Also, on the other side, it is necessary to understand tumor biology. In this sense, alginate scaffolds can be used to make models that can help improve the therapy of some tumors [7]. The ability of alginate hydrogels to achieve multi-practical therapeutic objectives, such as creating three-dimensional scaffolds that mimic the tumor environment, makes alginate hydrogels a strong candidate to be used in cancer therapy improvement [7]. In parallel, alginate hydrogels are the best drug delivery vehicles in cancer treatment, both for low molecular weight drugs and large molecules, including proteins and genes. Since they have a low aggregation force and good stability in biological fluids [39]. Depending on the pH, the release of the drug can be controlled. In addition, the period during which the drug will be released can also be regulated. The high surface porosity of the alginate hydrogel allows for the control of drug release [7].

Apart from cancer treatments, alginate is biocompatible and biodegradable, and it can also facilitate wound healing by preserving a moist environment and limiting microbial growth [15]. In addition, alginate hydrogels can support living cells and provide them with a suitable micro-environment to maintain their viability.

Cells classified as stem cells show self-renewal capacity and differentiation into different cell types depending on the environment in which they are found [37, 40]. Therefore, they can produce embryogenic tissues and regeneration throughout adulthood [37, 40]. Various types of stem cells, including mesenchymal stem cells (mesoderm), hematopoietic stem cells (mesoderm), and neural stem cells (ectoderm), are present and

active in virtually every tissue of the body. Additionally, their germ-layer progenitors occupy a hierarchical position between their differentiated and organ tissues [37, 40].

Cell encapsulation technology refers to the immobilization of cells within biocompatible, semipermeable membranes [41-45]. Rather than using therapeutic products, cells are encapsulated to deliver molecules of interest for a long period, as these molecules are continuously released. Moreover, genetically engineered cells can be immobilized to express any desired protein in vivo without changing the host's genome [46, 47]. Compared to protein encapsulation, stem cell encapsulation offers a considerable advantage since it allows the prolonged and controlled administration of therapeutic compounds, resulting in better physiological concentrations [46, 47]. The use of biodegradable hydrogels and extracellular matrix (ECM) components to encapsulate stem cells has been shown to promote cell survival, prevent immunity, and facilitate in vivo transplantation. [46, 47]. Several different biomaterials such as alginate, hyaluronic acid, agarose, and other polymers have been used for this purpose [47]. Chronic diseases, for example, are often the result of malfunctioning cells. The encapsulation of stem cells is a promising technology that provides an alternative for organ transplantation.

Alginate hydrogels drawbacks.

Although alginate represents excellent characteristics, the clinical applications of alginate hydrogels are limited due to lack of mechanical strength, leakage of alginate cell attachments, and fast drug release [15, 27]. Minimizing immune responses is also a challenge [17]. To solve these drawbacks, incorporating different nanomaterials into the alginate-based hydrogels seems an excellent strategy to improve its mechanical and functional characteristics depending on its application [17, 44].

1.2 Graphene oxide (GO) and reduced Graphene oxide (rGO).

Over the last ten years, advances in nanotechnology in the previous ten years have demonstrated their potential as a material for combining with alginate hydrogels to give support to living cells and create a suitable microenvironment. In this respect, graphene has proven to be an excellent candidate for improving the mechanical strength of alginate [6, 26, 27]. Graphene is formed by hybridizing thin, single-thick layers of carbon atoms [28, 48]. The concept of single-layer graphene was first proposed by P.R. Wallace in 1947.. Besides having good electrochemical properties, it also has high thermal conductivity [49, 50], gas impermeability, a large surface area, and high mechanical strength. These excellent characteristics have significantly increased applications in various fields, including electronics. It is being utilized increasingly in the biomedical field to develop new drug delivery systems, in gene therapy, or improve diagnostic imaging contrast media [51-54].

In recent years, the most extensively investigated derivative forms of graphene are graphene oxide (GO) and its reduced form, the reduced graphene oxide (rGO). These materials research and development have been conducted in different fields such as electronics and optics sensors [51, 55, 56]. Due to their modulation abilities, graphene derivatives may also highly impact biomedicine, including developing new drug delivery systems, gene therapy applications, and improved contrast agents for medical images [51, 55, 56].

In an acidic environment, graphite is oxidized to create GO, as per Hummers and Offermann. GO can be made by dispersing flake graphites in concentrated sulfuric acid solutions. Then those flakes are oxidized with $KMnO_4$ and K_2FeO_4 and stabilized with boric acid after further oxidation [57]. This is followed by hydrolysis of the product at 95ºC in deionized water. This produces a brown solution, indicating an absolute exfoliation of the intercalated graphite oxide. Afterward, H_2O_2, HCl, and water are used several times to remove residual oxidants from this product [51, 58]

There are several outstanding properties of GO, including a high surface area (890 m^2g^{-1}) [58], strong mechanical properties (Young's modulus of ~1.0 and breaking strength of ~130 GPa) [59], and low production cost, which make it an excellent material (Figure 3).

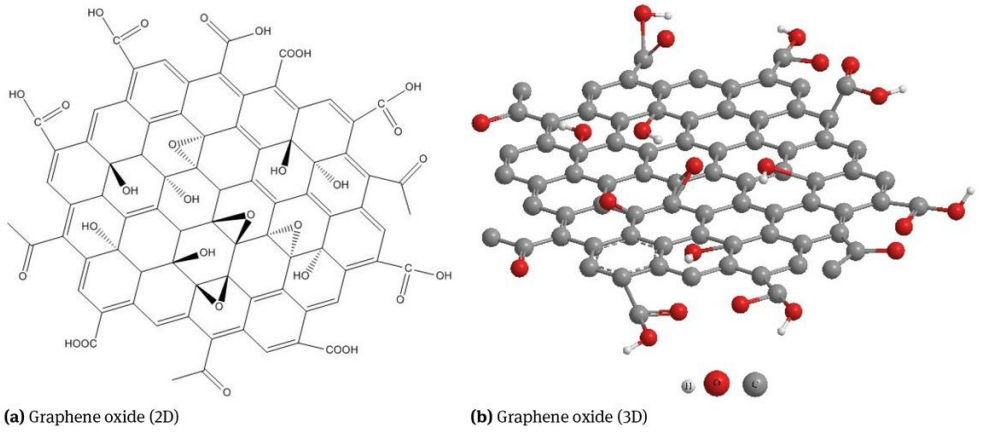

Figure 3. Structure of GO in 2D (a) and 3D (b) [60]

As a result, the graphene oxidation to GO increases the hydrophilic properties of its base plane, including the presence of hydroxyl, carboxyl, carbonyl, phenol, lactone, and quinone groups (figure 3) [55, 61, 62]. These oxygenated groups change the properties of graphene, permitting GO to disperse in an aqueous medium and other polar solvents [55, 63]. In addition, these oxygenated groups allow chemical reactions at the basal plane and on its sides [63]. Moreover, GO surfaces can be functionalized with proteins, antibodies, and DNA fragments with these reactions [39, 43], allowing various biological applications [64-68].

GO also has a high capacity to adsorb antibodies and proteins. It has been demonstrated that proteins adsorbed to GO are exceptionally resistant to proteolysis [69, 70], enabling their use as protein delivery systems [71] or as biosensors incorporating antibodies [69, 70].

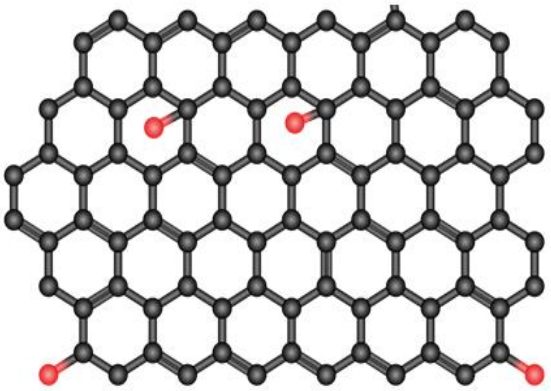

Figure 4. Reduced Graphene oxide structure [60]

This oxidized form of graphene, GO, can be also be reduced to produce the reduced graphene oxide (rGO) (figure 4) [60, 64]. Various methods can be used to produce rGO,

so its properties might vary as well [72]. In the most popular technique for rGO synthesis [73], GO is reduced chemically by chemical agents such as $NaBH_4$ [74], phenylhydrazine [75], hydrazine hydrate [76], or hydroxylamine [75]. The reducing agents are toxic, and the reduction process leads to a low carbon/oxygen ratio in the final product [77] and a poor-quality powder [72]. The production of high-quality rGO occurs under vacuum and in an inert or reducing atmosphere [66], at temperatures between 300°C and 2000°C [72]. Also, dry GO can be reduced in a solid-state by using a microwave oven [78]. In addition, GO can be photothermally reduced in a vacuum using a laser beam with wavelengths under 390 nm (energy >3.2 eV) [78].

As a result of the GO reduction, GO surface properties undergo dramatic changes, including significant changes in its mechanical strength, stability, dispersibility, and reactivity [79, 80]. This material has an excellent electrical conductivity of 6300 S cm−1 and high mobility of 320 cm^2 $V^{-}1$ $s^{-}1$, respectively [81]. rGO's physicochemical properties have led to its use in a variety of fields, such as electronics [82], energy storage and conversion devices, such as supercapacitors [64], or chemical sensors and biosensors [77]. Although rGO has lower conductivity than graphene, it still contains residual oxygen and structural defects. Due to the chemical reduction process involved in obtaining rGO, these defects and vacancies can be difficult, if not impossible, to restore [83]. Importantly, rGO demonstrates high mechanical strength. It has a Young modulus of 32GPa and a fracture strength of 120MPa (theoretically 2630 m2/g for single-layer graphene) [59].

Several studies have investigated the effects of GO and rGO on stem cell differentiation in regenerative medicine. A general observation has been that GO and rGO enhance stem cell differentiation. Cardiomyocytes (figure 5), neurons, and mesenchymal stem cells (MSCs) are highly affected by the GO surface on their adhesion capacity, cell proliferation [84-86], and differentiation [87, 88] into osteogenic lineages [89].

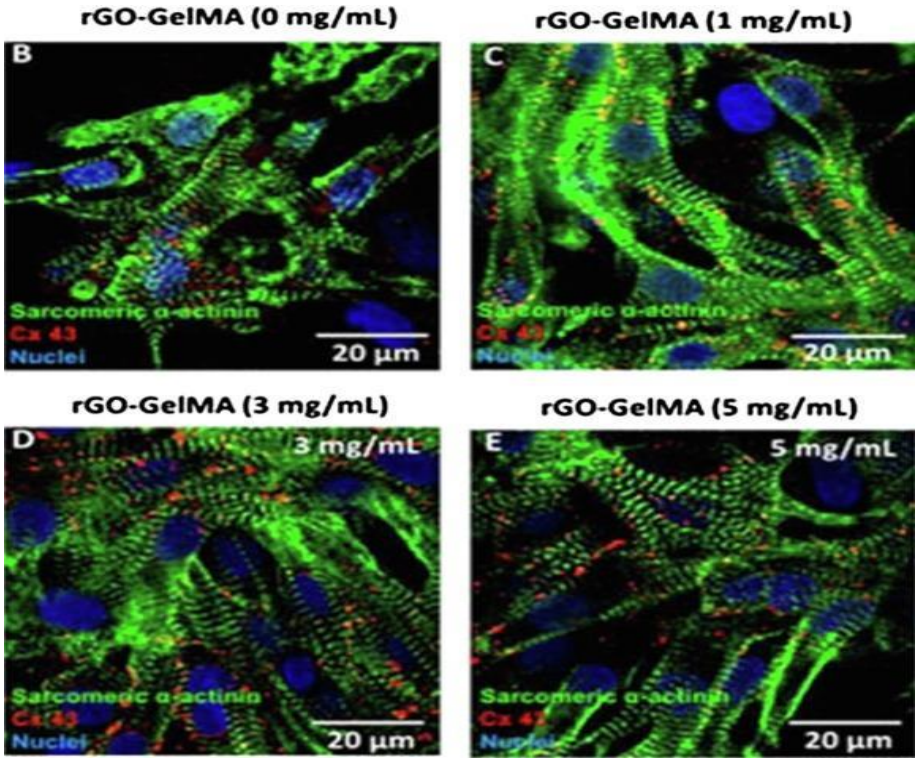

Figure 5. Images of cardiomyocytes immunostained for sarcomeric α-actinin (green) and connexin 43 (red) after eight days of culture on pristine GelMA and rGO-GelMA hydrogels at different concentrations of rGO. (B) 0 mg mL^{-1}, (C) 1 mg mL^{-1}, (D) 3 mg mL^{-1}, (E) 5 mg mL^{-1}. Note: nucleus (blue).[18]

Citotoxicity of graphene and derivatives

Studies conducted to date have shown conflicting results regarding the cytotoxicity of these carbon-derived materials [54, 90]. Some studies reported no effects from graphene or its derivatives on cell behavior at specific doses [90, 91], while others have shown that they can induce cellular damage [90, 91]. Due to these conflicting published results, a graphene derivative was suggested to be more biocompatible than graphene. For example, GO prepared by a modified Hummers method at doses lower than 20 µg/mL did not show toxicity in human fibroblast cells, while doses higher than 50 µg/mL did, decreasing cell adhesion, activating cell apoptosis pathways, and showing the presence of carbon material within lysosomes, mitochondrion, endoplasm, and the cell nucleus [92]. When studied *in vivo*, a low dose of this GO at the range of 0.1 µg-0.25 µgdid not demonstrate significant toxicity in mice, while higher doses did [93]. Similarly, GO can cause cytotoxicity and oxidative stress in BF-2 cells, in a dosage and time-dependent manner, even at low concentrations of GO (40µg/ ml) and short incubation [94]. The high chemical stability of GO allows it to be retained within the body. A substantial amount of injectable GO can be reached in different body organs, such as the lungs, liver, spleen,

and bone marrow [95]. In contrast, functionalized GO, like GO-PEG, is primarily found in the liver and spleen [96].

GO injection of mice exhibited high cytotoxicity, such as the development of lung granulomas, mainly in the lung, liver, spleen, and kidney, which caused the mice to die [92, 97]. However, GO has a long blood circulation time (half-time 5.3 ± 1.2 h) and is less able to penetrate the reticuloendothelial system than other graphene derivatives [98].

Radioisotope studies and morphological measurements of GO clearance in mice showed that the level of GO in the urine gradually increased within one hour after treatments, reaching a maximum level after six hours. The GO in the lung was cleared three months after treatments since it diffused through the alveolar-capillary barrier easily and was quickly excreted in the urine [99].

Furthermore, it has also been shown that GO cytotoxicity can differ based on the cell line, for example, in Henrietta Lacks cells (HeLa), Sloan Kettering breast cancer cells (SKBR3), and Michigan cancer foundation-7 breast cancer cells (MCF7). Based on different endpoints (lactate dehydrogenase (LDH) release, cellular metabolism, lysosomal integrity, and cell proliferation) for cytotoxicity, it was found that these cell lines responded significantly differently to 1, 2-Distearoyl-sn-glycero-3-phosphoethanolamine-Poly(ethylene glycol) coated oxidized graphene nanoribbons (O-GNR-PEG-DSPE) formulations. Cell viability was generally dose- and time-dependent for all the cells. However, MCF7 and SKBR3 cells exhibited significantly lower levels of cytotoxicity than HeLa cells [100].

Advantages of 3D scaffolds based on GO and rGO.

The GO and rGO-based 3D scaffolds are more effective than other porous scaffolds for stimulating the proliferation and differentiation of stem cells for developing new tissues, such as bones, heart muscles, and neurons. Moreover, GO and rGO-based 3D scaffolds stimulate cell proliferation and differentiation by enhancing cell-cell or cell-scaffold interactions (chemical or electric) [101] due to their surface properties, mechanical electrical properties, high biocompatibility, and their ability to improve cell adhesion [65, 102]. Thus, incorporating GO or rGO into different types of scaffolds offers several benefits, including improving hydrophilicity, mechanical strength, protein adsorption and stability, cell adhesion, proliferation, or electrical properties [34, 61]. Moreover, the high

adsorption capacities offered by GO and rGO enable the bioconjugation of proteins, antibodies, and DNA fragments within scaffolds [103] and protect proteins from proteolysis [71]. For example, it has been found that GO-PLGA/HA microcarriers immobilized with BMP-2 increased the adhesion and differentiation of MC3T3-E1 cells [93]. Furthermore, incorporating GO into scaffold matrixes can also improve the adhesion of growth factors [104].

Regarding GO-based scaffolds, when chitosan (CS)/GO scaffolds are used as support for cardiomyocyte cultures, they exhibit increased electrical conductivity, similar to that observed on a porcine acellular dermal matrix (PADM) after the integration of rGO [105]. Also, it has been found that when GO was incorporated in PLGA/HA scaffolds, the scaffold became significantly more hydrophilic [106, 107]. Also, adding GO to alginate scaffolds strengthens these mechanically weak scaffolds [108]. Similarly, the incorporation of GO makes collagen scaffolds improve their mechanical strength. Also, the incorporation of GO promoted the osteogenic differentiation of human MSCs [109].

On the other hand, rGO scaffolds have also been extensively studied for their electrical conductivity, an essential characteristic in cardiac and neural cell culture. It has been proposed that rGO increases the conductivity of scaffolds, facilitating the cell interaction with them [110]. Also, incorporating rGO into gelatin methacryloyl (GelMA) hybrid hydrogels enhance their mechanical properties [18].

In conclusion, the high chemical stability, biocompatibility, and low production cost present GO and rGO as excellent platforms for delivering proteins and antibodies and promoting cell proliferation, adhesion, and differentiation [93]. In this sense, our group has incorporated GO into alginate matrixes used in cell-based therapies to increase cell attachments, proliferation, and viability [6, 27, 43, 60, 111]. Accordingly, we found that GO at a 50 µg/ml concentration positively impacts viability, metabolic activity, and membrane integrity of C_2C_{12}-EPO myoblasts in 3D cultures [39]. However, we encountered several problems. For example, because of its high surface activity, GO could bind the secreted therapeutic factors at its surface and, thus, reduce their release to the media [6, 26, 27]. To solve the GO adsorption problem, it is necessary to precoat the GO surface with a protecting corona that reduces its surface activity [6, 26, 27]. One option is to pre-coat these GO nanoparticles with fetal bovine serum (FBS). The incorporation of these coated GO nanoparticles into alginate-based microcapsules, was

able to enhance the viability of the encapsulated C_2C_{12}-EPO myoblasts [26].

The mechanism of interaction of GO and rGO with Proteins.

Understanding how adsorption works is necessary for creating an homogeneous coating of proteins on graphene or graphene derivative surfaces. A variety of essential factors for protein interaction with GO and rGO surfaces have been suggested, including the shape of the protein or hydrophobicity. As the oxidation degree (OD) increases, GO's adsorption behavior switches from Freundlich- to Langmuir-type [112]. Accordingly, depending on the type of adsorbed materials, the adsorption mechanism can differ; it may bind to the GO and rGO via hydrophobicity, via Van der Waals force, electrostatically, or via hydrogen bonding [113]. GO and rGO surfaces adsorb proteins due to their hydrophobic side interacting with the hydrophobic side of the GO and rGO. For instance, the adsorption of BSA on GO surfaces is mediated by hydrophobic interactions mediated by electron density and molecule shape [69, 70]. Also, the van der Waals forces have an essential role in the adsorption of hydrophobic drugs or nanocomposites on the GO surface [48]. At the same time, electrostatic interactions are most evident on GO and mostly occur in strong pH conditions (at pH < 6.0, the GO surface is more negatively charged) [70]. For example, positively charged compounds are attracted to negatively charged GO due to electrostatic attraction. Moreover, GO becomes more negatively charged when its oxygen-containing functional groups are deprotonated at low pH, which causes stable aqueous suspension by electrostatic repulsion among negatively charged GO particles. GO and rGO are also characterized by hydrogen bonding interactions, allowing nitrogen oxide to adsorb more strongly on GO than on graphene because –OH and nitrogen oxide form hydrogen bonds. Additionally, the π–π stacking interactions were attributed to the abundant π electrons on the basal plane of the GO and rGO surface. The π–π stacking interactions are one of the most important mechanisms for GO and rGO protein adsorption [70].

2. Methodology

A disadvantage of GO is that it can adsorb different proteins because of its high surface activity. As commented before, the addition of GO nanoparticles into alginate-based microcapsules containing C2C12-EPO myoblastss reduced the amount of EPO secreted.

The purpose of this thesis is to describe and characterize new methods for fabricating modified GO-protein-alginate and rGO-protein-alginate hydrogels that can simulate the cellular matrix of embedded cells and reduce high protein trapping. The GO and rGO particles will be mixed with proteins of the extracellular matrix (BSA, collagen, and elastin). Thus, our first step was to characterize the interactions between GO or rGO with those proteins . In this sense, it is relevant to investigate the impact of protein concertation, incubation time, and temperature. Moreover, through the blocking study, we determined if the coating layer is able to reduce the surface activity of GO and rGO.

Next, we prepared hybrid hidrogels containing alginate and graphene derivatives and analysed their electrochemical behavior. Also, we performed in vitro studies to determine the viability of C2C12-EPO myoblasts and the EPO release.

In order to get new knowledge on these point the subsequent studies and experiments were performed.

2.1- Characterization of GO-protein and rGO-protein interactions

To confirm the formation of the protein coating layer on the GO and rGO, we used Raman and FT-IR techniques in order to investigate the physical bonding between GO or rGO, and proteins.

Raman spectrum was acquired using a Confocal Raman Imaging Alpha 300 M (Company WITEC) with a 532 nm laser (5% laser power, an exposure time of the 50s, and 4 accumulations).

FT-IR spectroscopy measurements were performed with a BRUKER IFS 66/S Spectrometer, using 32 scans with 4 (cm−1) resolution in 4000–400 cm−1 region.

2.2. The effect of concentration.

We studied the impact of protein concentration on the adsorption capacity of GO and rGO. At a fixed time (2h) and temperature (37ºC), serial concentrations of each protein (0-2000g/mL) were incubated with GO and rGO. After centrifugation for 15 minutes at 14000 rpm, the GO-protein and rGO-protein suspensions were collected. A non-adsorbed protein was then be analyzed in the supernatant. The data were analyzed using Langmuir and Freundlich models.

Langmuir and Freundlich are two adsorption models commonly used in adsorption studies. The Langmuir isotherm describes monolayer adsorption.

Langmuir's Equation is described by Equations (1) and (2):

$$Ce/qe = Ce/qmax + 1/(qmax.KL) \quad (1)$$

$$RL = 1/(1 + KL \times C0) \quad (2)$$

Specifically, Ce (ug/mL) represents the concentration of the adsorbed protein at equilibrium, qe (ug/ug) represents the ability of GO and rGO to adsorb protein, q_{max} (ug/ug) represents the maximum protein absorption per unit weight of GO or rGO, KL (mL/g) indicates the Langmuir constant (C0) shows the initial protein concentration, and RL represents the separation factor.

The Freundlich isotherm is applied to multilayer adsorption on heterogeneous surfaces.Freundlich's Equation was simplified in Equation (3):

$$Log\ qe = log\ KF + 1/n \times log\ Ce \quad (3)$$

The Freundlich constant and adsorption intensity are represented by KF and n, respectively.

Langmuir and Freundlich's adsorption isotherms will be used to determine the adsorption isotherm and to investigate if protein adsorption occurs on a homogeneous surface, forming a homogeneous coating layer or not.

2.3 Kinetic study of protein adsorption.

To evaluate the effect of incubation time, a range of concentrations (0-2000g/ml) of BSA, collagen, and elastin was incubated at 37ºC with GO or rGO and, at different time points (1-24h), the non-adsorbed protein was quantified.

2.4 Thermodynamic of protein adsorption.

To evaluate the impact of incubation temperature, a range of concentrations (0-2000g/ml) of BSA, Collagen, and Elastin was incubated with GO or rGO for 2 hours at different temperatures (0-42ºC) and the non-adsorbed protein was quantified. Through thermodynamics experiments, the three basic thermodynamic parameters such as Gibbs free energy change (ΔG^{o}), entropy change (ΔS^{o}), and enthalpy change (ΔH^{o}) were determined.

ΔG° values indicate the nature of the adsorption: physico- or chemo-sorption, and spontaneous or non-spontaneous. On the other hand, $\Delta H°$ suggests the type of adsorption reaction: exothermic (adsorption decreases with temperature) or endothermic (adsorption increses with temperature).

ΔS° is an indicator of the degree of entropy during the adsorption of the proteins .

2.5 Preparation of GO and rGO containing hydrogels

We prepared hybrid alginate hydrogels containing GO, rGO, GO-proteins, rGO-proteins, as shown in (figure 6).

GO, rGO suspensions or mixtures of GO-protein and rGO-protein suspensions were prepared. After that, a solution of sodium alginate was prepared and then mixed with the different suspensions. Alginate final concentration was be 1.5% and GO, rGO, and GO-proteins and rGO-protein final concentration was 50ug/ml. Using these mixtures, alginate hydrogels were prepared after mixing with calcium sulfate through two luer lock syringes connected with a fluid dispensing connector. The resulting mixtures were kept for gelification between two glass plates with a separation of 2 mm.

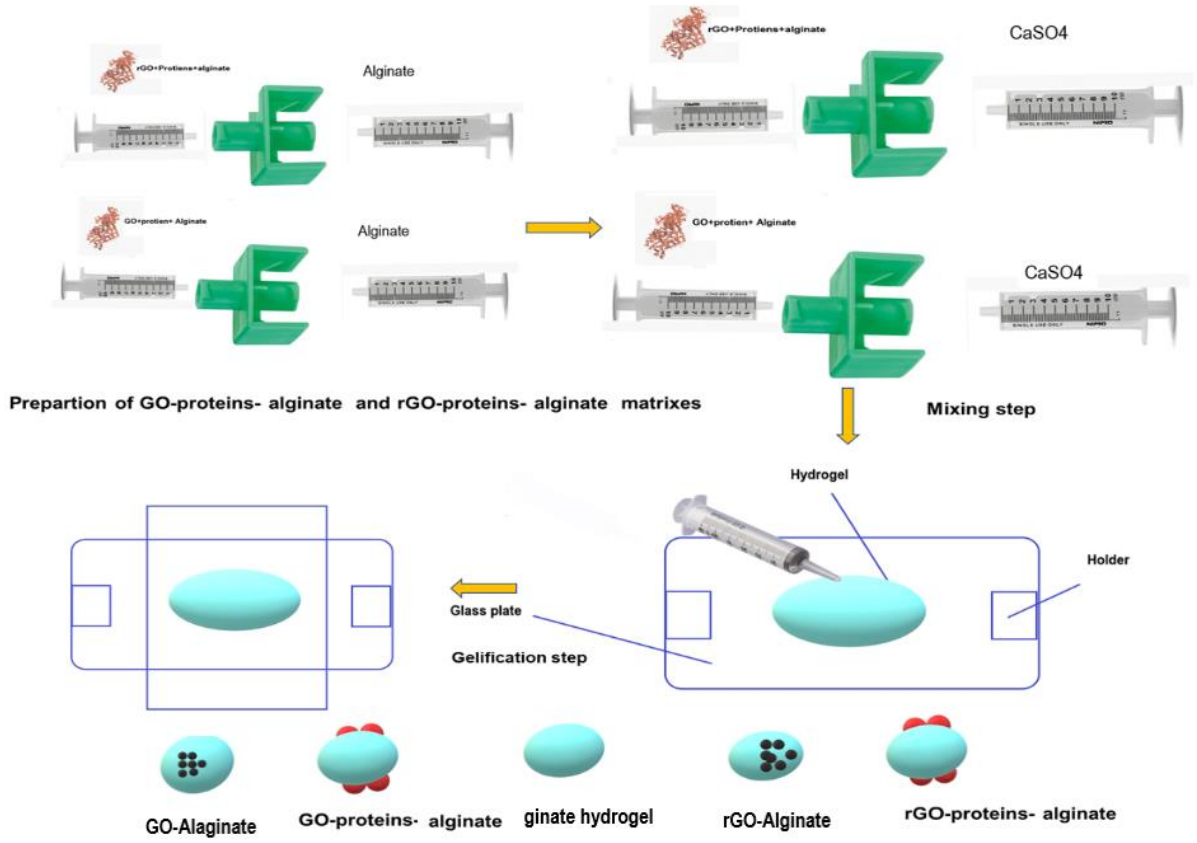

Figure 6. Diagram for preparing GO-Proteins-alginate and rGO-Proteins-alginate hydrogels .

2.6 Electrochemical study of hybrid hydrogels.

The obtained rGO containing hybrid hydrogels (see previous section) were cut into 14 mm diameter disks for electrochemical studies.

Electrochemical impedance spectroscopy (EIS) and cyclic voltammetry (CV) were performed using the Versa State-3 Electrochemical Impedance Spectrometer (Princeton Applied Research-US) and a screen-printed electrode (Dropsens-Spain). These measurements were utilized to determine the electrochemical activity of protein-coated-rGO nanoparticles embedded within alginate hydrogels. Within a range of frequencies from 10^{-1} to 10^{6} Hz, we calculated phase angle (deg) and impedance modulus (ohms) in EIS, followed by Bode model analysis to determine whether the studied hydrogels were conducting or insulating.

2.7 In vitro cell studies.

We performed several *in vitro* studies. Using murine C2C12 myoblasts genetically engineered to secrete erythropoietin (C2C12-EPO) we examined the biological effects of alginate hydrogels containing GO or GO with different adsorbed proteins (BSA, collagen, and elastin). Cells were embedded into different alginate-GO or –rGO (previously coated) containing hydrogels at a density of $5x10^6$ cells/ml.

2.7.1 Fluorescence microscopy viability imaging

The LIVE/DEAD® Viability/Cytotoxicity Kit (InvitrogenTM) was used to perform fluorescence microscopy viability imaging at various time points. This assay gave us a qualitative idea of the positive effect of the nanoparticles inside alginate hydrogels on cell viability.

2.7.2 Metabolic activity.

Sigma-Aldrich's Counting Kit-8 solution (CCK-8) was also used to study the metabolic activity of the embedded cells at various time points. This assay gave us a quantitative idea of the positive effect of the nanoparticles inside alginate hydrogels on cell viability.

2.7.3 EPO secretion.

EPO secretion was also quantified. C2C12-EPO containing hybrid alginate hydrogels of different conditions were incubated in culture media and the supernatants were collected. We measured the amount of released EPO using the Quantikine IVD EPO ELISA kit (R&D Systems).

2.8 EPO and insulin blocking studies.

We performed a blocking study for EPO and insulin as model of therapeutic substances relevant for the clinic.

First, GO-proteins and rGO-proteins mixtures were obtained in order to obtain a biocorona on the surface of both graphene derivatives. These mixtures were incubated

overnight with either recombinant EPO or insulin. Next, samples were spun for 5 minutes and the supernatants were colleted. The non-adsorbed EPO and insulin were quantified with the ELISA kits Quantikine IVD EPO ELISA kit (R&D Systems) and Insulin ELISA Kit (Mercodia), respectively. Thus, we were able to determine if the preformed biocorona on GO and rGO nanoparticles was enough for avoiding the adsorption of therapeutic proteins produced and released by cells than can be used in different cell therapies.

2.9 Statistical analysis.

SPSS software, version 24.00, or GraphPad Prism 8.0 (GraphPad Inc., San Diego, CA) were used to analyze the data.. We considered $p<0.05$ as significant for comparing groups.

3. Hypothesis and objectives

Technological advances and new challenges have profoundly transformed regenerative medicine. Cell embedding in hydrogels also contributes to a broader and more diverse research area. Three-dimensional (3D) scaffolds are designed to support living cells and facilitate their survival and proliferation.

For decades, alginate has proven to be an ideal material for fabricating functional hydrogels because of its high porosity and biocompatibility [26, 27]. However, limitations such as mechanical strength weakening, low cell attachment, and rapid drug release should also be considered [114]. To compensate for these flaws, various materials can be used to create more biomimetic support for the cells and enhance cell viability. In this sense, our group has proposed combining carbon-based materials with alginate to modify its properties, improve itsmechanical properties and enhance the viability of embedded therapeutic cells.

GO has shown to be able to improve cell viability and metabolic activity when introduced in alginate-based microcapsules [6, 26, 27]. However, due to the GO's high surface activity, secreted therapeutic agents from cells, such as EPO, are retained or absorbed on its surface; therefore, incorporating GO into alginate matrixes might have some disadvantages.

As a solution for this high GO surface activity, we proposed the creation of a biocorona or pre-coating of proteins on the GO surface before introducing these GO nanoparticles into the alginate hydrogels. In previous studies, we pre-coated GO with FBS. This approach was effective as the therapeutic protein EPO was released into the media; thus, the FBS containing proteins were adsorbed into GO and formed a protein biocorona that even increased more cell viability. However, on those expereriments, it was difficult to know which of the proteins of the FBS mixture was getting attached into the GO surface.

On the other hand, the development of an electrically conductive scaffold with a porous structure that has similar conductive characteristics to the native heart or neural tissue, would be really useful in tissue engineering; particularly for the regeneration of neuronal and cardiac tissues. Integrating rGO into alginate hydrogels could enhance their conductive properties. Additionally, rGO has a lower surface activity than GO. Thus, it has a lower affinity for therapeutic proteins, which makes it suitable for incorporating into alginate matrixes.

Taking into account all the previously mentioned advantages of graphene derivatives as well as the difficulty of working with these materials we decided that the first objective of the thesis was to perform a review of the state of the art, (Appendix 1). Then the next main goals of this thesis is, to investigate the possibility of creating a protein biocorona on the GO surface that prevents therapeutic protein adsorptionand to enhance the biological performande of alginate hydrogels (Appendix 1). Thus, we aimed:

- To understand how BSA, type I collagen and elastin interact with GO surface in order to form a biocorona.
- To analyse their electrochemical characteristics after being embedded within alginate hydrogels.
- To evaluate the biological impact of protein-coated GO particles within alginate hydrogels on EPO producing cells.

On the other hand, the use of hybrid alginate-grahene derivates, specifically rGO, in order to obtain hydrogels with high conductivity is an interesting area of research related to several medical applications, such as cardio and neuro-regenerative medicine (Apendix 2). Thus, we aimed:

- To create conductive protein-rGO-alginate hybrid hydrogels using different protein-coatings; proteins that are usually present in FBS (BSA, collagen and elastin).
- To understand the adsorption phenomena involved on the interaction between rGO surface and these proteins and the effect of temperature.
- To determine of blocking the rGO surface precluded further adsorption of other proteins of interest.
- To analyse their electrochemical characteristics of protein-coated rGO-alginate hybrid hydrogels.

4.Results and discussion.

4.1 Advantages and disadvantages of GO and rGO containing scaffolds in tissue engineering.

Compared with other porous scaffolds, GO, and rGO-based scaffolds significantly influence stem cells' proliferation and differentiation processes which facilitates the development of new tissues [101], including bone [105, 115], cardiac tissue [23, 87], and neural tissue [116-119]. In fact, these components optimize the mechanical [66, 120], electrical [53, 101, 121], and adhesion properties of the scaffolds. As mentioned, the mechanical properties of GO and rGO containing scaffolds are excellent [66, 101, 122]. By adding GO to alginate, for example, the strength of the scaffold is enhanced [7, 15, 30]. Also, incorporating GO into collagen scaffolds increases their mechanical strength and encourages human MSC differentiation towards osteogenesis [123, 124]. Likewise, rGO enhances the mechanical properties of GelMA hybrid hydrogels [125].

On the other hand, GO and rGO containing scaffolds show an increase of their hydrophilicity, strength and stability [84, 104, 121, 126]. Also, these graphene derivatives have the capacity to bind and stabilize proteins. Thus, growth factors are more stable by remaining adsorbent to these carbon derivatives [70] .

These high protein adsorption properties of GO and rGO and their specific surface area facilitate bio-conjugation not only with proteins but also with DNA fragments within scaffolds, preventing their proteolysis [70].

Also, the fast adsorption of proteins through π-π interaction between the GO or rGO aromatic sides providing a biocompatible environment for cells to adhere and proliferate [104].

In conclusion, the high chemical stability, biocompatibility, and low production cost, present GO and rGO nanoparticles as excellent platforms for delivering proteins and antibodies and promoting cell proliferation, adhesion and differentiation [70].

While GO and rGO have certain advantages, they also have some drawbacks.

The GO cytotoxicity can be attributed to several factors, including the dose [26] that is used in *in vitro* assays, its lateral size [127], and its surface charge [128-130]. The modified Hummers method has shown to produce no toxicity in human fibroblast cells

when GO is used at doses between 20 µg/mL and 50 µg/mL [92, 97] . The cells undergo apoptosis, lose adhesion, and become carbon-rich when the dose is greater than 50 ug/mL [92]. Similarly, GO cytotoxicity appears to be dose-dependent since GO concentration lower than 50 ug/mL exhibits higher biocompatibility with no evident cytotoxicity [131].

Furthermore, the extent of cytotoxicity depends on the lateral size of the platelets.Due to their small size and sharp edges, small GO particles have shown high toxicity since they are able to penetrate cell membranes and enter the cytoplasm, damaging the cell membrane and causing cytoplasmic leakage. In contrast, particles larger than 200 nm are not toxic since they do not penetrate the cell membranes [132].

Additionally, the GO surface charge impacts [130, 133] both cellular uptakeand internalization. Usually, the strong electrostatic repulsion between GO molecules and membranes prevents these particles from absorbing to non-phagocytic cells. However, these negatively charged nanoparticles may penetrate non-phagocytic cell membranes through cationic sites [134]. In addition, the negative GO surface charge has shown to induce platelet activation and aggregation [102].

GO's chemical stability allows it to remain in the body for a long time. Moreover, when injected, GO is retained in many body organs, including the lungs, liver, spleen, and bone marrow [132]. In contrast, GO-PEG is mainly retained in the liver and spleen [132]. This GO can cause inflammation, cell infiltration, granulomas, and pulmonary edema in the lungs, among others [132]. Finally, these particles are excreted by the excretory system [135]. According to the GO particle size and surface modification different mechanisms can explain its clearance. Large sheets of GO are physically filtered in the spleen, whereas smaller particles can pass through the renal tubules to reach the urine, where they are excreted without apparent toxicity [132].By modifying the surface of GO, such as GO-PEG or GO-dex (GO-DEX), GO can be accumulated into the reticuloendothelial system (RES) of the liver and spleen without producing long-term toxicity. However, these compounds were detectable after three months of injection [96].

Taking into account these advantages and drawbacks of the graphene derivatives, the purpose of this thesis was, first, to develop a protein biocorona on GO and rGO particles in order to prevent or reduce the adsorption of the therapeutic proteins into their surface when these nanoparticles are incorporated into alginate-based scaffolds; thus, taking

advantage of the benefitial effect of graphene derivatives on cell viability at low concentrations, while avoiding the adsorption of the EPO protein. Factors such as concentration, time, and temperature were examined.

Secondly, this thesis also examined how the incorporation of rGO affected the electrochemical properties of alginate hydrogels.

4.2. Characterization of the GO-protein interactions.

To study the protein-GO interactions, Raman spectroscopy was used. Purified GO, BSA, collagen, and elastin, as well as combinations of GO with each protein, were analyzed. The proteins spectrum was hardly discernible after mixing with GO. In fact, GO has a high Raman activity with two bands characteristics of sp^2 graphite systems. Interestingly, it was evident a band (1100-1250 cm^1) that can be caused by the appearance of sp^3 bonds coming from the functionalization of the surface of the platelets. Thus, proving that a protein biocorona has formed. Moreover, when we analyzed the different bands on the spectra and the ratio between some of the bands, we could observed that the I/D ratio (I:band at 1100-1250cm^{-1}; D: band at 1340 cm^{-1}) was increased when proteins were mixed with the GO nanoparticles which suggests an enhancement of the functionalization degree of the platelets. In the same line, the FTIR spectroscopy confirmed the formation of a protein biocorona. In fact, after mixing each protein with GO nanoplatelets, the spectra of both (protein and GO) overlapped and new vibrations appeared as a signal of newly formed amide bonds. Also, the characteristic peak of GO at 1645 cm^{-1} (aromatic C=C group) was no longer detectable (Figure 7). This suggests that the bio-corona formation on GO surfaces occurs through the π-π interaction between the benzene ring from the proteins and the C=C from GO. However, this does not discard that other interactions, such as hydrogen bonds, could also be participating in the bio-corona formation [136].

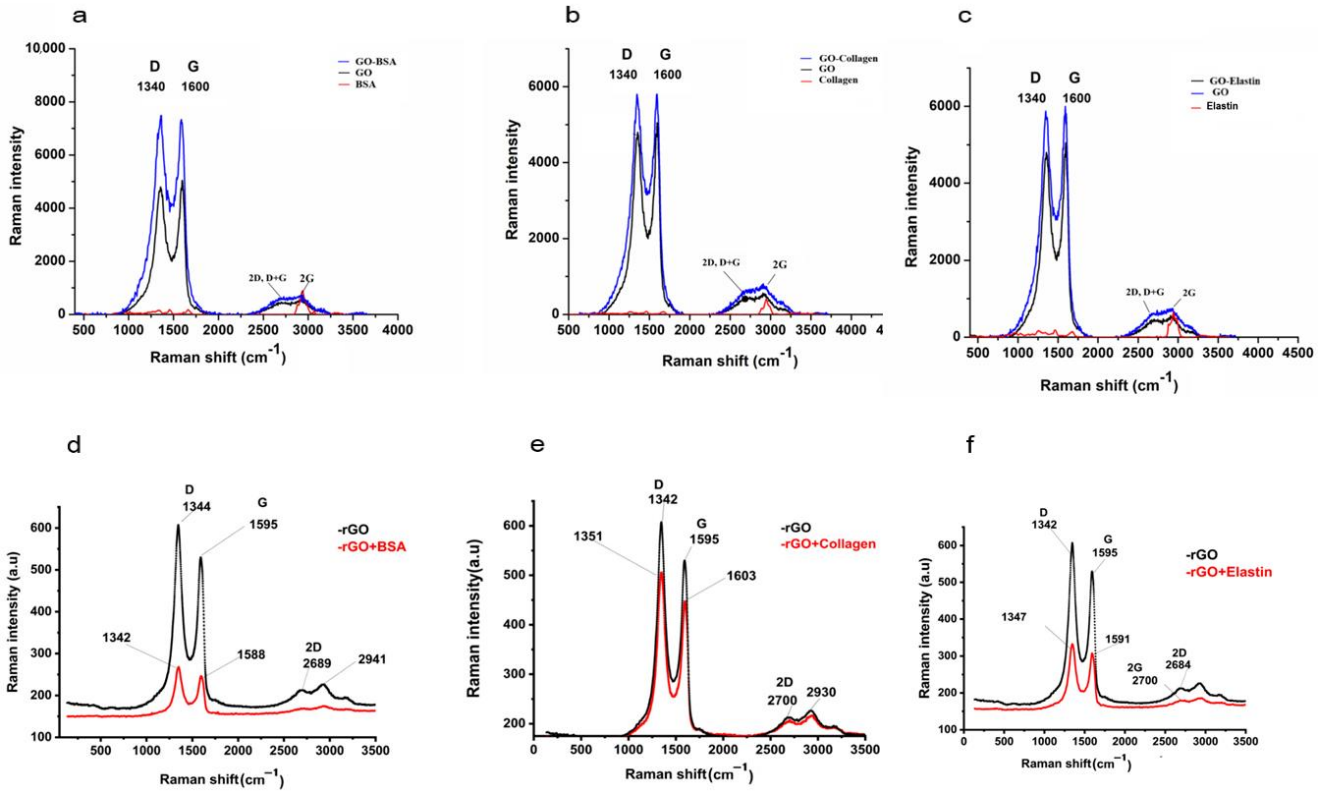

Figure 7. Raman spectrum of GO before and after the adsorption of BSA (**a**), collagen (**b**) and elastin (**c**). Same experiments performed on rGO: BSA (**d)**, collagen (**e**) and elastin (**f**).

In a similar way, the interaction between rGO and the studied proteins was analyzed (Figure 7). First, we could detect differences between GO and rGO, as an indication of the presence of defects due to the reduction process of the oxidized form of graphene. Then, the interactions between rGO and each protein was analyzed. . Raman spectra of rGO-proteins shown that the two main bands of the spectra shifted to the right and that the intensity ratios between some bands were higher than those previously seen when GO-protein interactions were studied. These intensity ratio changes would be attributable to the presence of more structural defects, probably due to the adsorption of the proteins to the surface of rGO [137]. In order to corroborate these results, the FTIR attenuated total reflectance technique was applied.

In the FT-IR spectrum of the rGO-proteins mixtures, a noticeable shift of the C=C and the C- stretching bands were detected, which are indicative of the binding of the benzene ring of the proteins and the rGO nanoparticles surface. From our view, these results suggest that the proteins adsorption on rGO surfaces is a result of π–π interactions [138].

4.3 Adsorption capacity of proteins on GO and rGO nanoplates depending on proteins concentration, molecular weight and hydrophilicity/hydrophobicity.

Based on our findings, as we increase the protein concentration, the GO's ability to adsorb protein also increases. In fact, higher protein concentrations, when adsorbed to the GO surface, helped decreasing the resistance of the particles to move from the aqueous solution to the GO platelets solid phase. However, this effect varied among the proteins studied (Figure 8). This effect of the inicial concentration was more intense for the BSA-GO interaction. When the initial BSA concentration was increased from 125 to 1000 µg/mL, the adsorption of BSA increased by 5.9-folds. In contrast, when modifiying the collagen concentration, the GO particles adsorption capacity (q_e) did not increase as much as with increasing concentrations of BSA or elastin.

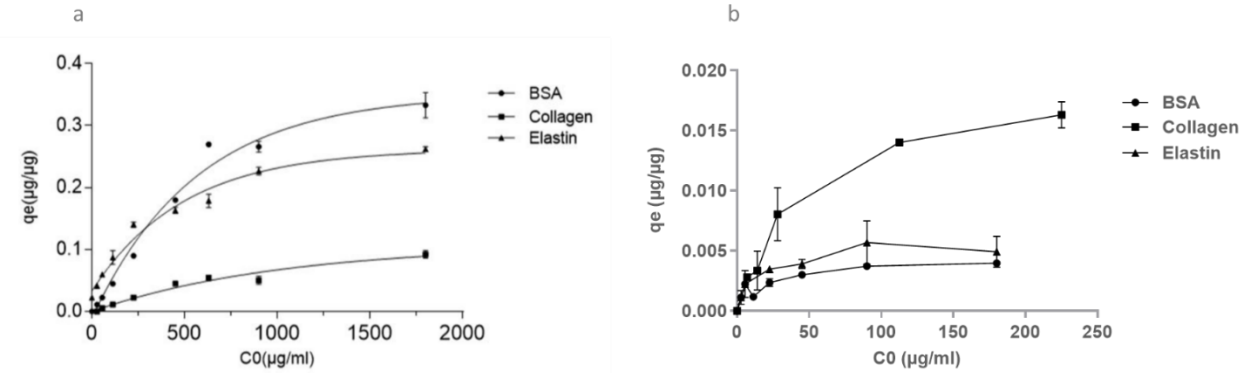

Figure 8. Effect on the GO (a) and rGO (b) adsorption capacity (qe) of the initial concentration (C0) of BSA, collagen and elastin.

In contrast, when the effect of protein concentration and rGO adsorption capacity was analysed, we saw that this capacity was increased at low protein dose values (Figure 8). In this case, collagen shown the highest q_e. However, other hydrophilic proteins, including BSA and elastin, displayed a low affinity for the surface of rGO..

In order to analyze how this adsorption fenomena takes place on GO and rGO nanoparticles at a constant temperature, both Langmuir and Freundlich models can be applied. As results have demonstrated, the three studied proteins are adsorbed on the graphene derivatives surface fitting better the Langmuir model (Table 1). This suggests that proteins are adsorbed on the surface of these GO and rGO platelets covering a finite

number of adsorption sites as a single layer, without interacting among adsorbed proteins on the surface.

Table 1. Parameters were calculated from experimental data for Langmuir model. Notes. qe: The amount of protein adsorbed per GO or rGO weight at equilibrium; q max: The Maximum amount of protein adsorbed per GO or rGO weight; KL: Langmuir constant; RL. Separation factor.

	qe (µg/µg)	qmax (µg/µg)	KL (ml/µg)	RL	R2
		For GO			
BSA	0.332	0.330	0.057	0.009	0.99
Elastin.	0.262	0.380	0.002	0.249	0.97
Collagen	0.122	0.071	0.023	0.044	0.97
		For rGO			
BSA	0.0070	0.0091	0.0297	0.1570	0.968
Elastin.	0.0049	0.0049	0.1980	0.0271	0.996
Collagen	0.0220	0.0230	0.0313	0.0660	0.987

On the other hand, it seems that the proteins molecular weight also plays a key role on the adsorption process. BSA and elastin are lower molecular weight proteins (66.5 KDa and 70 KDa, respectively). Collagen, in contrast, has a higher molecular weight (300 kDa). As the kinetic studies of protein adsorption on GO and rGO have demonstrated, this adsorption process follows a pseudo-second-order kinetic model, which suggests that each of the studied proteins can interact with two sorption sites on the surface of the nanoparticles. Moreover, results showed that the higher the molecular weight of the protein, the lowest affinity for the graphene derivate. In any case, due to the high number of available active sites on these nanoparticles, the adsorption process occurred very fast, and always before the first 20 minutes after mixing the proteins with GO or rGO particles the equilibrium was reached.

To better understand these interactions, the intra-particle diffusion model was studied, which considers the adsorption process to take place in three consecutive steps. This model showed that the low molecular weight proteins (BSA and elastin) have a higher intra-particle diffusion rate constant than collagen and that these smaller proteins interact with GO through hydrophilic interactions. In contrast, as mentioned, the higher molecular weight of collagen together with its more hydrophobic nature make the intra-particle diffusion rate constant to be lower as well as the thickness of the boundary layer. When the intra-particle diffusion model was applied to the interaction of proteins with rGO, we saw that collagen showed the highest diffusion rate constant and boundary layer thickness, which means that there is a strong hydrophobic interaction with the rGO

surface. In this case, the hydrophilicity of the two other smaller proteins BSA and elastin would provoke a reduction in the affinity for this reduced form of graphene.

Acording to the results obtained after the application of this model, we can also conclude that the the intraparticle-diffusion process is not the only one that takes place when these proteins and the carbone derivatives are mixed. In fact, the film diffusion process could also be taking place.

4.4 Thermodynamic analysis of protein-graphene derivatives interaction.

Next, we wanted to study the effect of increasing the temperature on the adsorption process of these proteins on GO and rGO surface (Table 2).

Table 2. Thermodynamic parameters for GO and rGO. Enthalpy change. ΔH°; Entropy change. ΔS°; Gibbs free energy change. ΔG° at 300 K.

	ΔH° (kJ/mol)	ΔS° (kJ/mol.K)	ΔG° (kJ/mol)	R2
	for GO			
BSA	2.598	−0.057887	20.543	0.981
Elastin	16.27	−0.008881	19.031	0.779
Collagen	17.363	−0.006935	19.513	0.935
	For rGO			
BSA	−40.34	−0.207	23.95	0.99
Collagen	2.44	−0.069	23.68	0.95
Elastin	−89.96	−0.358	28.4	0.94

We observed an increase in the GO adsorption capacity for BSA, collagen, and elastin with an increase in temperature. The positive ∆H° values indicate that the proteins adsorption process on the GO surface is endothermic. Moreover, the adsorption process consists of two steps; hydration of proteins in the solution (endothermic) and adsorption of proteins on the GO surface (exothermic)being the first step the most important one. We could also observed that the molecular weight of the proteins might have an effect on the adsorption process depending on the temperature. In fact, collagen showed the highest ∆S° values.

In contrast, when we performed the same experiments on rGO, we detected that this time the adsorption of the proteins was an exothermic process. However, the adsorption became endothermic for collagen when the temperature was enhanced. Thus, we believe that in this case, because of the hydrophobic nature of this protein, the hydratation step would require more energy in comparison with the rest of the analyzed proteins.

The positive ΔG° values reflect the non-spontaneous nature of the adsorption processes both on GO and rGO nanoparticles.

4.5 Effect of GO and rGO particles coating on hybrid alginate hydrogels containing graphene derivatives.

In contact with cells, GO may act as an electrochemical mediator as it can act as a semiconductor material. Thus, we wanted to study the effect of incorporating not only GO or rGO particles inside alginate hydrogels, but also, the effect of including a protein biocorona on these materials (Figure 9).

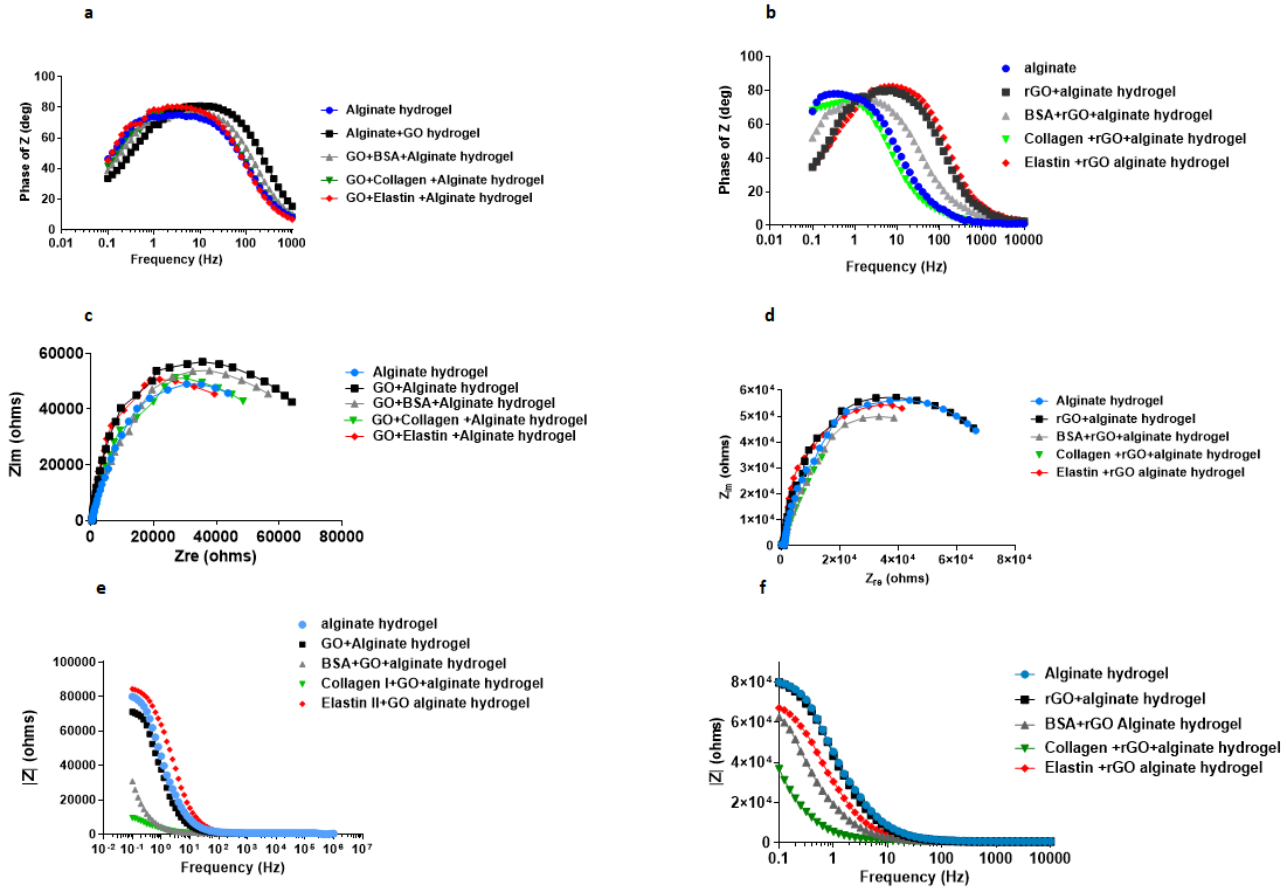

Figure 9. Electrochemical study from protein coated-GO alginate hydrogels and protein-coated rGO alginate hydrogels. a) and b) Bode plots (phar angle Z vs frequency). C and d) Nyquist diagram for GO containing hydrogels. e and f) Impredace modulus for rGO containing hydrogels.

The analysis of the electrochemical data revealed that protein-coated GO particles act as electrochemical mediators in alginate hydrogels . In fact, there was a higher impedance values in the GO containing alginate matrices than in the alginate hydrogels. Additionally, when there was a protein biocorona pre-formed in the GO particles, the impedance decreased in protein-GO-alginate hybrid hydrogels, which indicates an improvement in the conductive properties (Figure 9). Thus, it seems that GO provides insulating properties to alginate hydrogels and that the protein-biocorona enhances its conductivity behavior.

Regarding the effect of rGO, when protein-coated rGO particles were incorporated into alginate hydrogels, the capacitance was altered, being the collagen-coated rGO the condition in which we detected the highest capacitance values. Thus, it can be concluded that the collagen biocorona on rGO platelets is able to enhance the conductivity of rGO containing hybrid alginate hydrogels as well as simple alginate hydrogels (Figure 9).

4.6 Effect of protein-coated GO on the viability of C2C12 cells embedded on hybrid alginate hydrogels.

As previously published, the incorpotarion of GO particles into alginate-based microcapsules is benefitial for the viability of embedded C2C12 myoblasts. However, because of the protein adsorption capacity of GO, the therapeutic protein erythropoietin released by the encapsulated cells was not able to get to the media. Thus, it seemed necessary to pre-cover the GO particles surface with another protein biocorona that would avoid the adsorption of the therapeutic protein.

Thus, we covered the GO nanoparticles with the proteins of study (BSA, elastin and collagen) and analyzed by fluorescent microscopy the effect on EPO producing C2C12 myoblasts. The protein covered-GO particles enhanced the viability of C2C12 cells embedded in alginate hydrogels, being the effect more (Figure 10) significant in hydrogels containing collagen-GO and elastin-GO particles. This effect was already visible after one week and it was even more relevant during the second week after encapsulation.

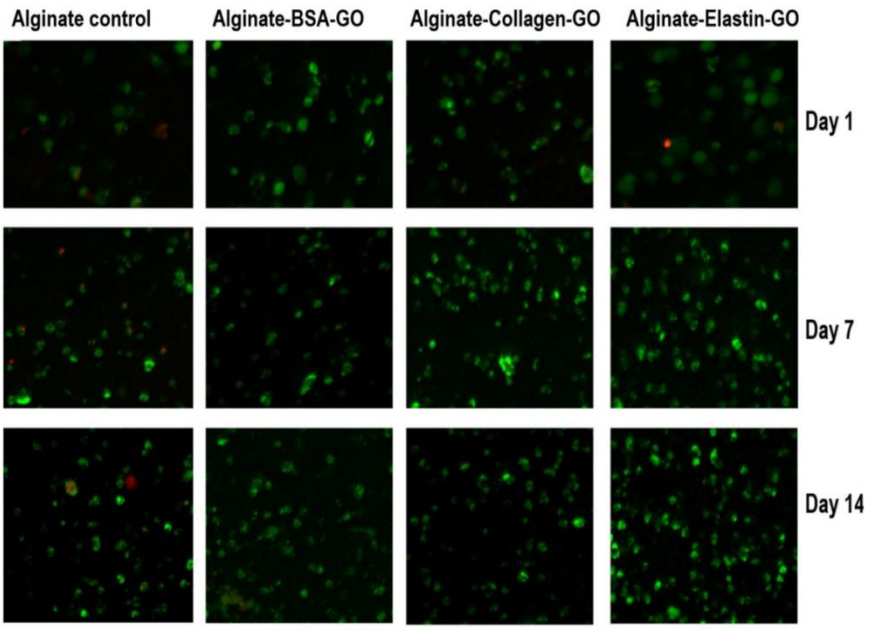

Figure 10. After calcein/ethidium staining for C2C12–EPO myoblasts, fluorescence microscopy images were incorporated within the modified alginate hydrogels based on GO-BSA, GO-collagen GO-elastin. Green. Live cells. Red. Dead cells. Scale bar. 100 µm.

In parallel, the measurement of the metabolic activity of the cells revealed that even after one day post-encapsulation, elastin-coated GO containing alginate hydrogels showed significantly higher activity (Figure 11). From then on, the effect of all the proteins biocorona seemed to have the same effect and statistically significat differences were only detected on the second week of analysis.

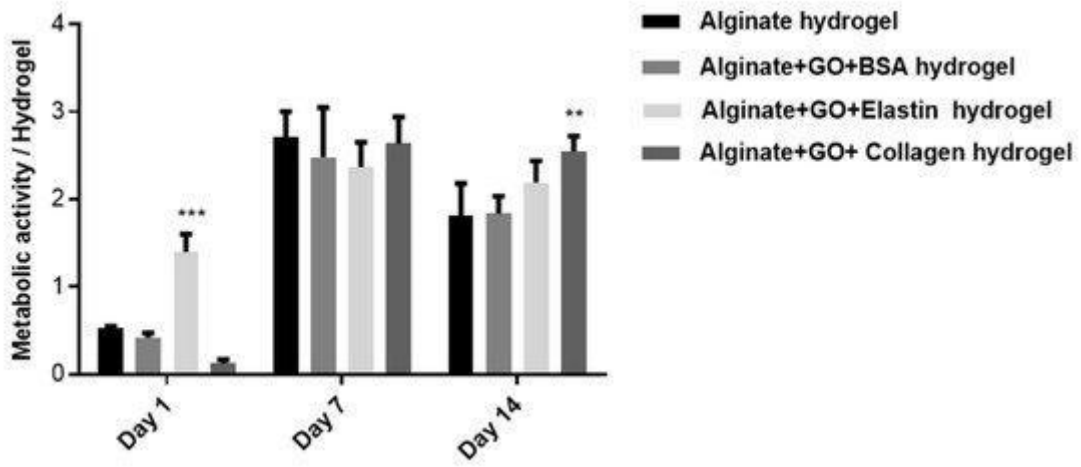

Figure 11. Metabolic activity of hybrid alginate-GO embedded C2C12-EPO myoblasts over two weeks. Note. **. $p < 0.01$; ***. $p < 0.001$ compared with cells encapsulated in alginate without GO.

Apart from knowing the metabolic activity of the embedded cells, it was also important to evaluate the production and release of the therapeutic factor that is being produced by these cells, EPO. According to the results, BSA-coated GO alginate hydrogels were the most effective in releasing EPO (figure 12). In contrast, collagen-coated GO-alginate hydrogels shown a lower release amount than than the control. We could have expected that as cell viability increases, the amount of EPO released into the media should also increase. However, the biocorona that is formed around GO nanoparticles is different depending on the protein used (BSA, elastin or collagen) and thus, the blocking that is achieved is also different which has an impact on the amount of therapeutic protein that is attached into the GO surface, and thus, released to the media. It seems that elastin and collagen are not able to form a stable or uniforme biocorona around GO and as a consequence, they are not avoiding completely the EPO adsorption into GO surface. Therefore, although cells shoed a high metabolic activity and, probably, they are producing high amount of EPO, this protein is not getting to the media, as it is getting attached to the GO particles.

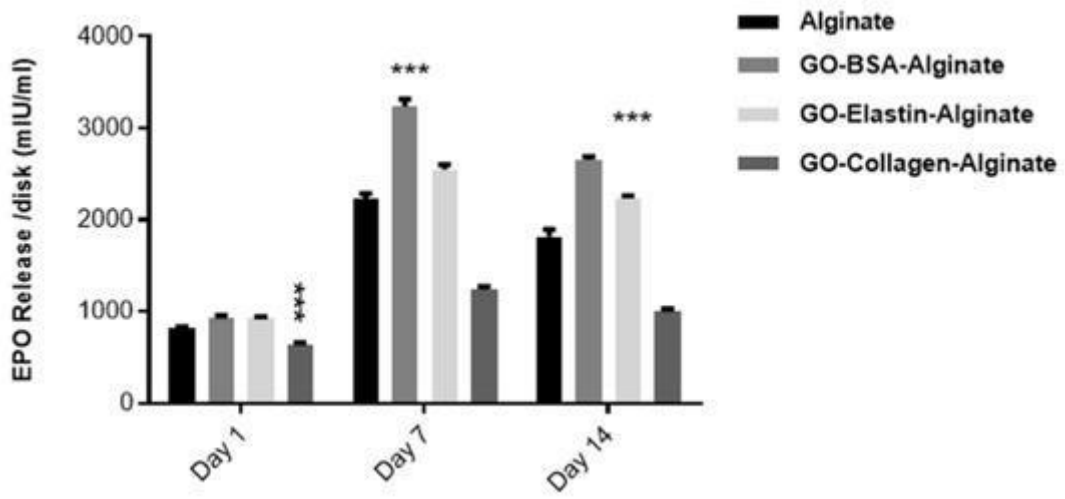

Figure 12. EPO production and release from C2C12-EPO myoblasts embedded in different hybrid protein-GO-alginate hydrogels. Note; ***. $p < 0.001$ compared with cells embedded in alginate without GO.

4.7 Capacity of BSA, elastin and collagen to block the active sites of GO for interacting with therapeutic proteins.

Taking into account the results explained in the previous section, we decided to study the capacity of these proteins to really block the adsorption of EPO on GO surface before making the hybrid GO-alginate hydrogels. We observed that when GO and EPO are mixed together, the graphene derivative adsorbs around 70% of the protein (Figure 13).

Interestingly, when BSA is used for making previously a biocorona and then, the BSA-GO nanoplatelets are mixed with EPO, we saw that this protein is able to almost completely block the adsorption of EPO on the GO surface. As a consequence, all the EPO produced by the cells encapsulated in these BSA-GO-alginate hydrogels is able to reach the media. In contrast, the other two proteins do not block completely the adsorption of EPO and thus, the therapeutic protein produced by the cells in retained inside the hydrogels. This would explain why in these to proteins, although cells showed high levels of viability, the amount of EPO detected in the media was lower.

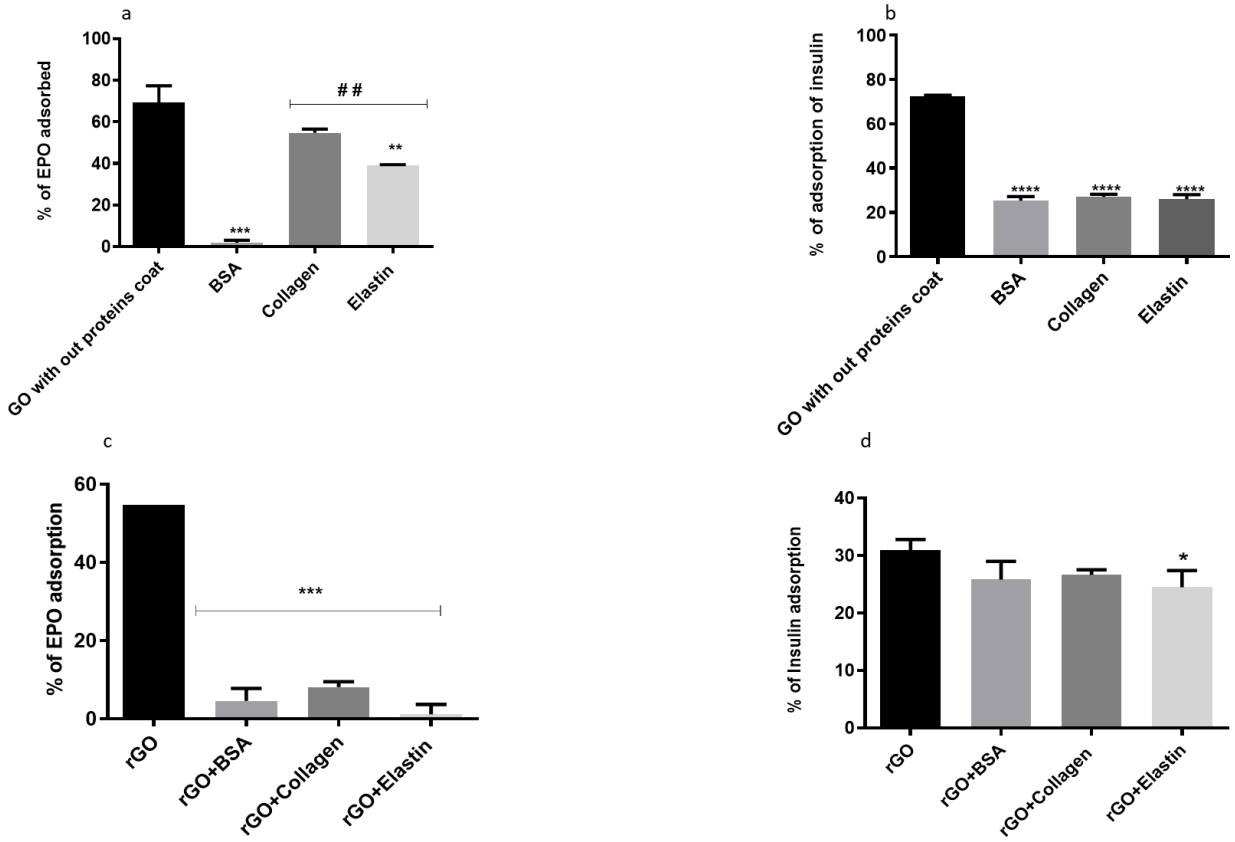

Figure 13. Percentage of (a) EPO and (b) insulin adsorbed by GO without coating, and BSA-, collagen- and elastin-coating. Percentage of (c) EPO and (d) insulin adsorbed by rGO without coating, and BSA-, collagen- and elastin-coating. p< 0.05; *. p < 0.01; **. p < 0.001; *** compared with non-coated platelets.

In order to investigate if this phenomeno takes places with other therapeutic proteins apart from EPO, we performed the same blockin experiment with insulin, since insulin-producing cells in alginate microcapsules or hydrogels could be an area of investigation for treating type 1 diabetes mellitus. The insulin adsorption on GO surface was similar to that for EPO and was approximately 70%. However, in contrast to EPO, the three studied proteins reduced insulin adsorption into the GO surface by around 60% (Figure 13).

In light of these findings, we speculated that because BSA and elastin are hydrophilic, they interfere with EPO's hydrophobic nature, reducing its affinity to adsorb on GO surfaces. In contrast, collagen, which is hydrophobic, would interact with the therapeutic protein, thus decreasing its ability to prevent the EPO's adsorption on the GO surface. On the other hand, due to its low molecular weightand high hydrophilic nature, insulin could compete with BSA, elastin and collagen for the GO binding sites, thus replacing a portion of the coating proteins.

4.8 Capacity of BSA, elastin and collagen to block the active sites of rGO for interacting with therapeutic proteins

In order to compare the adsorption of therapeutic proteins on rGO surface and the effect of blocking these active sites of rGO with different pre-coatings (BSA, elastin and collagen), we performed the same studies with rGO (Figure 13). Thi figure shows that rGO has a higher affinity for EPO (54.67%) than insulin (30.94%). Importantly, a significant reduction in EPO-adsoption was observed with the three preformed biocoronas. Among the three precoatings,elastin exhibited the highest capacity to prevent EPO adsorption on the rGO surface.

When insulin adsorption blocking was analyzed, the coating proteins BSa and collagen were not able to block the interaction between rGO particles and insulin. Elastin, however, showed a slightly higher capacity to prevent insulin from being trapped on the surface of rGO.

5. Bibliography

[1] "Biomaterials," *Biomaterials,* 1980.

[2] Q. Chai, Y. Jiao, and X. Yu, "Hydrogels for Biomedical Applications: Their Characteristics and the Mechanisms behind Them," *Gels,* vol. 3, no. 1, 2017, doi: 10.3390/gels3010006.

[3] A. Lückgen, "Alginate-based hydrogels with patterned biophysical and biochemical cues," Doctoral Thesis, Technische Universität Berlin, Technische Universität Berlin, Berlin, 2020. [Online]. Available: http://dx.doi.org/10.14279/depositonce-10013

[4] B. Kaczmarek, K. Nadolna, and A. Owczarek, "Chapter 6 - The physical and chemical properties of hydrogels based on natural polymers," in *Hydrogels Based on Natural Polymers*, Y. Chen Ed.: Elsevier, 2020, pp. 151-172.

[5] A. Serafin, C. Murphy, M. C. Rubio, and M. N. Collins, "Printable alginate/gelatin hydrogel reinforced with carbon nanofibers as electrically conductive scaffolds for tissue engineering," *Materials Science and Engineering: C,* vol. 122, p. 111927, 2021/03/01/ 2021, doi: https://doi.org/10.1016/j.msec.2021.111927.

[6] L. Saenz del Burgo *et al.*, "Hybrid Alginate–Protein-Coated Graphene Oxide Microcapsules Enhance the Functionality of Erythropoietin Secreting C2C12 Myoblasts," *Molecular Pharmaceutics,* vol. 14, no. 3, pp. 885-898, 2017, doi: 10.1021/acs.molpharmaceut.6b01078.

[7] F. Abasalizadeh *et al.*, "Alginate-based hydrogels as drug delivery vehicles in cancer treatment and their applications in wound dressing and 3D bioprinting," *Journal of Biological Engineering,* vol. 14, 2020, doi: 10.1186/s13036-020-0227-7.

[8] E. Caló and V. V. Khutoryanskiy, "Biomedical applications of hydrogels: A review of patents and commercial products," *European Polymer Journal,* vol. 65, pp. 252-267, 2015/04/01/ 2015, doi: https://doi.org/10.1016/j.eurpolymj.2014.11.024.

[9]] T. R. Hoare and D. S. Kohane, "Hydrogels in drug delivery: Progress and challenges," *Polymer,* vol. 49, no. 8, pp. 1993-2007, 2008/04/15/ 2008, doi: https://doi.org/10.1016/j.polymer.2008.01.027.

[10] L. Mei *et al.*, "Injectable hydrogels for cartilage and bone tissue engineering," *骨研究：英文,* vol. 5, no. 2, pp. 75-94, 2017.

[11] Y.-H. Tsou, J. Khoneisser, P.-C. Huang, and X. Xu, "Hydrogel as a bioactive material to regulate stem cell fate," *Bioactive Materials,* vol. 1, no. 1, pp. 39-55, 2016, doi: 10.1016/j.bioactmat.2016.05.001.

[12] H. J. van der Linden, S. Herber, W. Olthuis, and P. Bergveld, "Stimulus-sensitive hydrogels and their applications in chemical (micro)analysis," (in eng), *Analyst,* vol. 128, no. 4, pp. 325-31, Apr 2003, doi: 10.1039/b210140h.

[13] S. Petros, T. Tesfaye, and M. Ayele, "A Review on Gelatin Based Hydrogels for Medical Textile Applications," *Journal of Engineering,* vol. 2020, p. 8866582, 2020/12/23 2020, doi: 10.1155/2020/8866582.

[14] R. A. M. Osmani, E. Singh, U. Hani, S. Chavan, H. Kazi, and M. Menon, "5 - Bionanocomposite hydrogels for regenerative medicine and biomedical applications," in *Bionanocomposites in Tissue Engineering and Regenerative Medicine*, S. Ahmed and Annu Eds.: Woodhead Publishing, 2021, pp. 91-118.

[15] S. Radoor, J. Karayil, A. Jayakumar, E. Krishnankutty Radhakrishnan, J. Parameswaranpillai, and S. Siengchin, "18 - Alginate-based bionanocomposites in wound dressings," in *Bionanocomposites in Tissue Engineering and Regenerative Medicine*, S. Ahmed and Annu Eds.: Woodhead Publishing, 2021, pp. 351-375.

[16] W. Zhao, K. Odelius, U. Edlund, C. Zhao, and A.-C. Albertsson, "In Situ Synthesis of Magnetic Field-Responsive Hemicellulose Hydrogels for Drug Delivery," *Biomacromolecules,* vol. 16, no. 8, pp. 2522-2528, 2015, doi: 10.1021/acs.biomac.5b00801.

[17] Y. Zhang, J. Liu, L. Huang, Z. Wang, and L. Wang, "Design and performance of a sericin-alginate interpenetrating network hydrogel for cell and drug delivery," *Scientific reports,* vol. 5, no. 1, p. 12374, 2015, doi: 10.1038/srep12374.

[18] S. R. Shin *et al.*, "Reduced Graphene Oxide-GelMA Hybrid Hydrogels as Scaffolds for Cardiac Tissue Engineering," *Small,* vol. 12, no. 27, pp. 3677-3689, 2016, doi: 10.1002/smll.201600178.

[19] F. Raza *et al.*, "A Review on Recent Advances in Stabilizing Peptides/Proteins upon Fabrication in Hydrogels from Biodegradable Polymers," *Pharmaceutics,* vol. 10, no. 1, 2018, doi: 10.3390/pharmaceutics10010016.

[20] U. S. K. Madduma-Bandarage and S. V. Madihally, "Synthetic hydrogels: Synthesis, novel trends, and applications," *Journal of Applied Polymer Science,* vol. 138, no. 19, p. 50376, 2021, doi: https://doi.org/10.1002/app.50376.

[21] E. C. González-Díaz and S. Varghese, "Hydrogels as Extracellular Matrix Analogs," (in eng), *Gels (Basel, Switzerland),* vol. 2, no. 3, p. 20, 2016, doi: 10.3390/gels2030020.

[22] N. Chirani, L. H. Yahia, L. Gritsch, F. Motta, S. Chirani, and S. Farè, "History and Applications of Hydrogels," *Journal of Biomedical Sciences,* vol. Vol. 4, pp. 13-23, 12/01 2015, doi: 10.4172/2254-609X.100013.

[23] J. Cutts, M. Nikkhah, and D. A. Brafman, "Biomaterial Approaches for Stem Cell-Based Myocardial Tissue Engineering," *Biomarker insights,* vol. 10, no. Suppl 1, p. 77, 2015.

[24] M. I. Neves, L. Moroni, and C. C. Barrias, "Modulating Alginate Hydrogels for Improved Biological Performance as Cellular 3D Microenvironments," (in English), *Frontiers in Bioengineering and Biotechnology,* Review vol. 8, 2020-June-30 2020, doi: 10.3389/fbioe.2020.00665.

[25] K. T. Campbell, D. J. Hadley, D. L. Kukis, and E. A. Silva, "Alginate hydrogels allow for bioactive and sustained release of VEGF-C and VEGF-D for lymphangiogenic therapeutic applications," *PLOS ONE,* vol. 12, no. 7, p. e0181484, 2017, doi: 10.1371/journal.pone.0181484.

[26] J. Ciriza *et al.*, "Graphene oxide increases the viability of C2C12 myoblasts microencapsulated in alginate," *International Journal of Pharmaceutics,* vol. 493, no. 1-2, pp. 260-270, 2015, doi: 10.1016/j.ijpharm.2015.07.062.

[27] J. Ciriza *et al.*, "Graphene oxide enhances alginate encapsulated cells viability and functionality while not affecting the foreign body response," *Drug delivery,* vol. 25, no. 1, pp. 1147-1160, 2018, doi: 10.1080/10717544.2018.1474966.

[28] A. Syarifuddin, Hasmiyani, and A. Dirpan, "Impedance analysis of Sodium alginate : - Graphene oxide composite," ed.

[29] E. Axpe and M. L. Oyen, "Applications of Alginate-Based Bioinks in 3D Bioprinting," *International Journal of Molecular Sciences,* vol. 17, no. 12, 2016, doi: 10.3390/ijms17121976.

[30] C. Barron and J.-Q. He, "Alginate-based microcapsules generated with the coaxial electrospray method for clinical application," *Journal of Biomaterials Science, Polymer Edition,* vol. 28, no. 13, pp. 1245-1255, 2017, doi: 10.1080/09205063.2017.1318030.

[31] F. Bigoni, F. D. Giorgio, F. Soavi, and C. Arbizzani, "Sodium Alginate: A Water-Processable Binder in High-Voltage Cathode Formulations," doi: 10.1149/2.0281701jes.

[32] A. Espona-Noguera *et al.*, "Tunable injectable alginate-based hydrogel for cell therapy in Type 1 Diabetes Mellitus," vol. 107, ed, 2018, pp. 1261-1269.

[33] K. Y. Lee and D. J. Mooney, "Alginate: Properties and biomedical applications," *Progress in Polymer Science,* vol. 37, no. 1, pp. 106-126, 2012, doi: 10.1016/j.progpolymsci.2011.06.003.

[34] H. Park and K. Lee, "Cartilage regeneration using biodegradable oxidized alginate/hyaluronate hydrogels," *Journal of biomedical materials research. Part A,* vol. 102, 02/01 2014, doi: 10.1002/jbm.a.35126.

[35] Z. Yu, R. G. Pestell, T. G. Pestell, and M. P. Lisanti, "Cancer stem cells," *International Journal of Biochemistry and Cell Biology,* vol. 44, no. 12, pp. 2144-2151, 2012, doi: 10.1016/j.biocel.2012.08.022.

[36] D. L. Dragu, L. G. Necula, C. Bleotu, C. C. Diaconu, and M. Chivu-Economescu, "Therapies targeting cancer stem cells: Current trends and future challenges," *World Journal of Stem Cells,* vol. 7, no. 9, pp. 1185-1201, 2015, doi: 10.4252/wjsc.v7.i9.1185.

[37] K. Chen, Y.-h. Huang, and J.-l. Chen, "Understanding and targeting cancer stem cells: therapeutic implications and challenges," *Acta Pharmacologica Sinica,* vol. 34, no. 6, pp. 732-740, 2013, doi: 10.1038/aps.2013.27.

[38] J. A. Ajani, S. Song, H. S. Hochster, and I. B. Steinberg, "Cancer stem cells: the promise and the potential," *Seminars in Oncology,* vol. 42 Suppl 1, p. 3, 2015, doi: 10.1053/j.seminoncol.2015.01.001.

[39] M. M. Yallapu, M. Jaggi, and S. C. Chauhan, "Design and engineering of nanogels for cancer treatment," (in eng), *Drug Discov Today,* vol. 16, no. 9-10, pp. 457-63, May 2011, doi: 10.1016/j.drudis.2011.03.004.

[40] M. P. Prabhakaran, J. R. Venugopal, and S. Ramakrishna, "Mesenchymal stem cell differentiation to neuronal cells on electrospun nanofibrous substrates for nerve tissue engineering," vol. 30, ed, 2009, pp. 4996-5003.

[41] G. Orive, E. Santos, J. L. Pedraz, and R. M. Hernandez, "Application of cell encapsulation for controlled delivery of biological therapeutics," *Advanced Drug Delivery Reviews,* vol. 67-68, pp. 3-14, 2014, doi: 10.1016/j.addr.2013.07.009 [doi].

[42] R. M. A. Hernández, G. Orive, A. Murua, and J. L. Pedraz, "Microcapsules and microcarriers for in situ cell delivery," *Advanced Drug Delivery Reviews,* vol. 62, no. 7-8, pp. 711-730, 2010, doi: 10.1016/j.addr.2010.02.004.

[43] A. Garate *et al.*, "Assessment of the Behavior of Mesenchymal Stem Cells Immobilized in Biomimetic Alginate Microcapsules," *Molecular Pharmaceutics,* vol. 12, no. 11, pp. 3953-3962, 2015, doi: 10.1021/acs.molpharmaceut.5b00419.

[44] T. Billiet, M. Vandenhaute, J. Schelfhout, S. Van Vlierberghe, and P. Dubruel, "A review of trends and limitations in hydrogel-rapid prototyping for tissue engineering," (in eng), *Biomaterials,* vol. 33, no. 26, pp. 6020-41, Sep 2012, doi: 10.1016/j.biomaterials.2012.04.050.

[45] A. Ashimova, S. Yegorov, B. Negmetzhanov, and G. Hortelano, "Cell Encapsulation Within Alginate Microcapsules: Immunological Challenges and Outlook," (in English), *Frontiers in Bioengineering and Biotechnology,* Mini Review vol. 7, no. 380, 2019-December-03 2019, doi: 10.3389/fbioe.2019.00380.

[46] G. D. Prestwich, "Engineering a clinically-useful matrix for cell therapy," *Organogenesis,* vol. 4, no. 1, pp. 42-47, 2008/01/01 2008, doi: 10.4161/org.6152.

[47] K. Shah, "Encapsulated stem cells for cancer therapy," *Biomatter,* vol. 3, no. 1, p. e24278, 2013/01/01 2013, doi: 10.4161/biom.24278.

[48] E. J.-C. Amieva, J. López-Barroso, A. L. Martínez-Hernández, and C. Velasco-Santos, "Graphene-Based Materials Functionalization with Natural Polymeric Biomolecules," *Recent Advances in Graphene Research,* 2016, doi: 10.5772/64001.

[49] X. Huang *et al.*, "Graphene-based materials: synthesis, characterization, properties, and applications," *Small (Weinheim an Der Bergstrasse, Germany),* vol. 7, no. 14, pp. 1876-1902, 2011, doi: 10.1002/smll.201002009.

[50] Y. Yang, A. M. Asiri, Z. Tang, D. Du, and Y. Lin, "Graphene based materials for biomedical applications," vol. 16, ed, 2013, pp. 365-373.

[51] V. B. Mohan, K.-t. Lau, D. Hui, and D. Bhattacharyya, "Graphene-based materials and their composites: A review on production, applications and product limitations," vol. 142, ed, 2018, pp. 200-220.

[52] J. Liu, L. Cui, and D. Losic, "Graphene and graphene oxide as new nanocarriers for

drug delivery applications," *Acta Biomaterialia,* vol. 9, no. 12, pp. 9243-9257, 2013, doi: 10.1016/j.actbio.2013.08.016.

[53] L. Feng and Z. Liu, "Graphene in biomedicine: opportunities and challenges," *Nanomedicine (London, England),* vol. 6, no. 2, pp. 317-324, 2011, doi: 10.2217/nnm.10.158.

[54] L. Yan, F. Zhao, S. Li, Z. Hu, and Y. Zhao, "Low-toxic and safe nanomaterials by surface-chemical design, carbon nanotubes, fullerenes, metallofullerenes, and graphenes," *Nanoscale,* vol. 3, no. 2, pp. 362-382, 2011, doi: 10.1039/c0nr00647e.

[55] D. Sharma, S. Kanchi, M. I. Sabela, and K. Bisetty, "Insight into the biosensing of graphene oxide: Present and future prospects," *Arabian Journal of Chemistry,* vol. 9, no. 2, pp. 238-261, 2016, doi: 10.1016/j.arabjc.2015.07.015.

[56] D. Chen, H. Feng, and J. Li, "Graphene oxide: preparation, functionalization, and electrochemical applications," *Chemical Reviews,* vol. 112, no. 11, pp. 6027-6053, 2012, doi: 10.1021/cr300115g.

[57] H. Yu, B. Zhang, C. Bulin, R. Li, and R. Xing, "High-efficient Synthesis of Graphene Oxide Based on Improved Hummers Method," *Scientific reports,* vol. 6, no. 1, p. 36143, 2016, doi: 10.1038/srep36143.

[58] P. Bradder, S. K. Ling, S. Wang, and S. Liu, "Dye Adsorption on Layered Graphite Oxide," *Journal of Chemical & Engineering Data,* vol. 56, no. 1, pp. 138-141, 2011, doi: 10.1021/je101049g.

[59] J. W. Suk, R. D. Piner, J. An, and R. S. Ruoff, "Mechanical properties of monolayer graphene oxide," *ACS nano,* vol. 4, no. 11, pp. 6557-6564, 2010, doi: 10.1021/nn101781v.

[60] A. Raslan, L. Saenz del Burgo, J. Ciriza, and J. Luis Pedraz, "Graphene oxide and reduced graphene oxide-based scaffolds in regenerative medicine," ed, 2020, p. 119226.

[61] S. Park and R. S. Ruoff, "Chemical methods for the production of graphenes," *Nature Nanotechnology,* vol. 4, no. 4, pp. 217-224, 2009, doi: 10.1038/nnano.2009.58.

[62] L. Zhang, Z. Lu, Q. Zhao, J. Huang, H. Shen, and Z. Zhang, "Enhanced chemotherapy efficacy by sequential delivery of siRNA and anticancer drugs using PEI-grafted graphene oxide," *Small (Weinheim an Der Bergstrasse, Germany),* vol. 7, no. 4, pp. 460-464, 2011, doi: 10.1002/smll.201001522.

[63] B. Konkena and S. Vasudevan, "Understanding Aqueous Dispersibility of Graphene Oxide and Reduced Graphene Oxide through pKa Measurements," *The journal of physical chemistry letters,* vol. 3, no. 7, p. 867, 2012.

[64] C. Chung, Y.-K. Kim, D. Shin, S.-R. Ryoo, B. H. Hong, and D.-H. Min, "Biomedical Applications of Graphene and Graphene Oxide," *Accounts of chemical research,* vol. 46, no. 10, pp. 2211-2224, 2013, doi: 10.1021/ar300159f.

[65] S. Agarwal *et al.*, "Interfacing live cells with nanocarbon substrates," *Langmuir: the ACS journal of surfaces and colloids,* vol. 26, no. 4, pp. 2244-2247, 2010, doi: 10.1021/la9048743.

[66] S. Baradaran *et al.*, "Mechanical properties and biomedical applications of a nanotube hydroxyapatite-reduced graphene oxide composite," vol. 69, ed, 2014, pp. 32-45.

[67] E. Campbell, M. T. Hasan, C. Pho, K. Callaghan, G. R. Akkaraju, and A. V. Naumov, "Graphene Oxide as a Multifunctional Platform for Intracellular Delivery, Imaging, and Cancer Sensing," *Scientific Reports,* vol. 9, no. 1, pp. 1-9, 2019, doi: 10.1038/s41598-018-36617-4.

[68] M. de Sousa *et al.*, "Covalent functionalization of graphene oxide with d-mannose: evaluating the hemolytic effect and protein corona formation," *Journal of Materials Chemistry B,* vol. 6, no. 18, pp. 2803-2812, 2018, doi: 10.1039/C7TB02997G.

[69] D. Y. Lee, Z. Khatun, J.-H. Lee, Y.-K. Lee, and I. In, "Blood compatible graphene/heparin conjugate through noncovalent chemistry," *Biomacromolecules,* vol. 12, no. 2, pp.

336-341, 2011, doi: 10.1021/bm101031a.

[70] M. Simsikova and T. Sikola, "Interaction of Graphene Oxide with Proteins and Applications of their Conjugates," *Journal of Nanomedicine Research,* vol. 5, no. 2, pp. 1-0, 2017, doi: 10.15406/jnmr.2017.05.00109.

[71] H. Yan *et al.*, "Effects of the oxidation degree of graphene oxide on the adsorption of methylene blue," *Journal of Hazardous Materials,* vol. 268, pp. 191-198, 2014, doi: 10.1016/j.jhazmat.2014.01.015.

[72] P. Zhang, Z. Li, S. Zhang, and G. Shao, "Recent Advances in Effective Reduction of Graphene Oxide for Highly Improved Performance Toward Electrochemical Energy Storage," *ENERGY & ENVIRONMENTAL MATERIALS,* vol. 1, no. 1, pp. 5-12, 2018, doi: 10.1002/eem2.12001; 09

10.1002/eem2.12001.

[73] S. Pei and H.-M. Cheng, "The reduction of graphene oxide," vol. 50, ed, 2012, pp. 3210-3228.

[74] H.-J. Shin *et al.*, "Efficient Reduction of Graphite Oxide by Sodium Borohydride and Its Effect on Electrical Conductance," *Advanced Functional Materials,* vol. 19, no. 12, pp. 1987-1992, 2009, doi: 10.1002/adfm.200900167.

[75] V. H. Pham Viet Hung, "One-step synthesis of superior dispersion of chemically converted graphene in organic solvents," *Chem.Commun.,* vol. 46, no. 24, pp. 4375-7, 2010.

[76] S. Stankovich *et al.*, "Synthesis of graphene-based nanosheets via chemical reduction of exfoliated graphite oxide," vol. 45, ed, 2007, pp. 1558-1565.

[77] K. Chen *et al.*, "Hg(II) ion detection using thermally reduced graphene oxide decorated with functionalized gold nanoparticles," *Analytical Chemistry,* vol. 84, no. 9, pp. 4057-4062, 2012, doi: 10.1021/ac3000336.

[78] Z. Li, Y. Yao, Z. Lin, K.-S. Moon, W. Lin, and C. Wong, "Ultrafast, dry microwave synthesis of graphene sheets," *Journal of Materials Chemistry,* vol. 20, no. 23, p. 4781, 2010, doi: 10.1039/c0jm00168f.

[79] V. B. Mohan, R. Brown, K. Jayaraman, and D. Bhattacharyya, "Characterisation of reduced graphene oxide: Effects of reduction variables on electrical conductivity," *Materials Science & Engineering B,* vol. 193, pp. 49-60, 2015, doi: 10.1016/j.mseb.2014.11.002.

[80] D. Konios, M. M. Stylianakis, E. Stratakis, and E. Kymakis, "Dispersion behaviour of graphene oxide and reduced graphene oxide," *Journal of colloid and interface science,* vol. 430, pp. 108-112, 2014, doi: 10.1016/j.jcis.2014.05.033.

[81] Y. Wang *et al.*, "Reduced graphene oxide film with record-high conductivity and mobility," vol. 21, ed, 2018, pp. 186-192.

[82] C. Berger *et al.*, "Electronic confinement and coherence in patterned epitaxial graphene," *Science (New York, N.Y.),* vol. 312, no. 5777, pp. 1191-1196, 2006, doi: 10.1126/science.1125925.

[83] Q. Zhang, X. Liu, H. Meng, S. Liu, and C. Zhang, "Reduction pathway-dependent cytotoxicity of reduced graphene oxide," *Environmental Science: Nano,* vol. 5, no. 6, pp. 1361-1371, 2018, doi: 10.1039/C8EN00242H.

[84] Y. C. Shin *et al.*, "RGD peptide and graphene oxide co-functionalized PLGA nanofiber scaffolds for vascular tissue engineering," *Regenerative Biomaterials,* vol. 4, no. 3, pp. 159-166, 2017, doi: 10.1093/rb/rbx001.

[85] S.-R. Ryoo, Y.-K. Kim, M.-H. Kim, and D.-H. Min, "Behaviors of NIH-3T3 fibroblasts on graphene/carbon nanotubes: proliferation, focal adhesion, and gene transfection studies," *ACS nano,* vol. 4, no. 11, pp. 6587-6598, 2010, doi: 10.1021/nn1018279.

[86] S. Park *et al.*, "Biocompatible, robust free-standing paper composed of a TWEEN/graphene composite," *Advanced Materials (Deerfield Beach, Fla.),* vol. 22, no. 15, pp. 1736-1740, 2010, doi: 10.1002/adma.200903611.

[87] A. Mihic *et al.*, "A Conductive Polymer Hydrogel Supports Cell Electrical Signaling and Improves Cardiac Function

After Implantation into Myocardial Infarct," *Circulation,* vol. 132, no. 8, pp. 772-784, 2015, doi: 10.1161/CIRCULATIONAHA.114.014937.

[88] Y. Wu, L. Wang, B. Guo, and P. X. Ma, "Interwoven Aligned Conductive Nanofiber Yarn/Hydrogel Composite Scaffolds for Engineered 3D Cardiac Anisotropy," *ACS nano,* vol. 11, no. 6, pp. 5646-5659, 2017, doi: 10.1021/acsnano.7b01062.

[89] T.-J. Lee *et al.*, "Graphene enhances the cardiomyogenic differentiation of human embryonic stem cells," vol. 452, ed, 2014, pp. 174-180.

[90] A. Sasidharan *et al.*, "Hemocompatibility and macrophage response of pristine and functionalized graphene," *Small (Weinheim an Der Bergstrasse, Germany),* vol. 8, no. 8, pp. 1251-1263, 2012, doi: 10.1002/smll.201102393.

[91] H. Yue *et al.*, "The role of the lateral dimension of graphene oxide in the regulation of cellular responses," *Biomaterials,* vol. 33, no. 16, pp. 4013-4021, 2012, doi: 10.1016/j.biomaterials.2012.02.021.

[92] K. Wang *et al.*, *Biocompatibility of Graphene Oxide* (no. Book, Whole). 2010, pp. 1-8.

[93] C. Fu, T. Liu, L. Li, H. Liu, Q. Liang, and X. Meng, "Effects of graphene oxide on the development of offspring mice in lactation period," *Biomaterials,* vol. 40, pp. 23-31, 2015, doi: 10.1016/j.biomaterials.2014.11.014.

[94] K. Srikanth, L. S. Sundar, E. Pereira, and A. C. Duarte, "Graphene oxide induces cytotoxicity and oxidative stress in bluegill sunfish cells," *Journal of applied toxicology : JAT,* vol. 38, no. 4, p. 504, 2018, doi: 10.1002/jat.3557.

[95] M. Lv *et al.*, "Non-covalent functionalized graphene oxide (GO) adsorbent with an organic gelator for co-adsorption of dye, endocrine-disruptor, pharmaceutical and metal ion," vol. 349, ed, 2018, pp. 791-799.

[96] B. Li *et al.*, "Influence of polyethylene glycol coating on biodistribution and toxicity of nanoscale graphene oxide in mice after intravenous injection," *International journal of nanomedicine,* vol. 9, pp. 4697-4707, 2014, doi: 10.2147/IJN.S66591.

[97] K. Wang *et al.*, "Biocompatibility of Graphene Oxide," *Nanoscale Research Letters,* vol. 6, no. 1, p. 8, 2011, doi: 10.1007/s11671-010-9751-6.

[98] K. Yang, J. Wan, S. Zhang, Y. Zhang, S.-T. Lee, and Z. Liu, "In vivo pharmacokinetics, long-term biodistribution, and toxicology of PEGylated graphene in mice," *ACS nano,* vol. 5, no. 1, pp. 516-522, 2011, doi: 10.1021/nn1024303.

[99] S. Liang *et al.*, "In vivo pharmacokinetics, transfer and clearance study of graphene oxide by La/Ce dual elemental labelling method," *NanoImpact,* vol. 17, p. 100213, 2020/01/01/ 2020, doi: https://doi.org/10.1016/j.impact.2020.100213.

[100] S. Mullick Chowdhury, G. Lalwani, K. Zhang, J. Y. Yang, K. Neville, and B. Sitharaman, "Cell specific cytotoxicity and uptake of graphene nanoribbons," (in eng), *Biomaterials,* vol. 34, no. 1, pp. 283-93, Jan 2013, doi: 10.1016/j.biomaterials.2012.09.057.

[101] R. Geetha Bai, K. Muthoosamy, S. Manickam, and A. Hilal-Alnaqbi, "Graphene-based 3D scaffolds in tissue engineering: fabrication, applications, and future scope in liver tissue engineering," *International Journal of Nanomedicine,* vol. 14, pp. 5753-5783, 2019, doi: 10.2147/IJN.S192779.

[102] S. K. Singh *et al.*, "Thrombus Inducing Property of Atomically Thin Graphene Oxide Sheets," *ACS nano,* vol. 5, no. 6, pp. 4987-4996, 2011, doi: 10.1021/nn201092p.

[103] P. Yang *et al.*, "Bovine Serum Albumin-Coated Graphene Oxide for Effective Adsorption of Uranium(VI) from Aqueous Solutions," *Industrial & Engineering Chemistry Research,* vol. 56, no. 13, pp. 3588-3598, 2017, doi: 10.1021/acs.iecr.6b04532.

[104] C. Fu *et al.*, "Enhanced cell proliferation and osteogenic differentiation in electrospun PLGA/hydroxyapatite nanofibre scaffolds incorporated with graphene oxide," *PloS one,* vol. 12, no.

11, p. e0188352, 2017, doi: 10.1371/journal.pone.0188352.

[105] W. Guo *et al.*, "Construction of a 3D rGO–collagen hybrid scaffold for enhancement of the neural differentiation of mesenchymal stem cells," *Nanoscale,* vol. 8, no. 4, pp. 1897-1904, 2016, doi: 10.1039/C5NR06602F.

[106] K. S. Novoselov, V. I. Fal'ko, L. Colombo, P. R. Gellert, M. G. Schwab, and K. Kim, "A roadmap for graphene," *Nature,* vol. 490, no. 7419, p. 192, 2012, doi: 10.1038/nature11458.

[107] W. Hu *et al.*, "Protein corona-mediated mitigation of cytotoxicity of graphene oxide," *ACS nano,* vol. 5, no. 5, pp. 3693-3700, 2011, doi: 10.1021/nn200021j.

[108] Y. He *et al.*, "Alginate/graphene oxide fibers with enhanced mechanical strength prepared by wet spinning," *Carbohydrate Polymers,* vol. 88, pp. 1100–1108, 04/15 2012, doi: 10.1016/j.carbpol.2012.01.071.

[109] S. Kang *et al.*, "Covalent conjugation of mechanically stiff graphene oxide flakes to three-dimensional collagen scaffolds for osteogenic differentiation of human mesenchymal stem cells," vol. 83, ed, 2015, pp. 162-172.

[110] L. Jiang *et al.*, "Preparation of an Electrically Conductive Graphene Oxide/Chitosan Scaffold for Cardiac Tissue Engineering," *Applied Biochemistry and Biotechnology,* 2019, doi: 10.1007/s12010-019-02967-6.

[111] A. Raslan *et al.*, "BSA- and Elastin-Coated GO, but Not Collagen-Coated GO, Enhance the Biological Performance of Alginate Hydrogels," *Pharmaceutics,* vol. 12, no. 6, 2020, doi: 10.3390/pharmaceutics12060543.

[112] Z. Liu, J. T. Robinson, X. Sun, and H. Dai, "PEGylated nanographene oxide for delivery of water-insoluble cancer drugs," *Journal of the American Chemical Society,* vol. 130, no. 33, pp. 10876-10877, 2008, doi: 10.1021/ja803688x.

[113] X. Xu *et al.*, "Study on the interaction of graphene oxide-silver nanocomposites with bovine serum albumin and the formation of nanoparticle-protein corona," *International Journal of Biological Macromolecules,* 2018, doi: 10.1016/j.ijbiomac.2018.05.043.

[114] H. Zhou and H. H. K. Xu, "The fast release of stem cells from alginate-fibrin microbeads in injectable scaffolds for bone tissue engineering," *Biomaterials,* vol. 32, no. 30, pp. 7503-7513, 2011, doi: 10.1016/j.biomaterials.2011.06.045.

[115] A. Hermenean *et al.*, "Chitosan-Graphene Oxide 3D scaffolds as Promising Tools for Bone Regeneration in Critical-Size Mouse Calvarial Defects," *Scientific Reports,* vol. 7, no. 1, pp. 1-12, 2017, doi: 10.1038/s41598-017-16599-5.

[116] A. González-Mayorga *et al.*, "Favorable Biological Responses of Neural Cells and Tissue Interacting with Graphene Oxide Microfibers," vol. 2, ed: Figshare, 2017, pp. 8253-8263.

[117] W. Guo *et al.*, "Self-Powered Electrical Stimulation for Enhancing Neural Differentiation of Mesenchymal Stem Cells on Graphene–Poly(3,4-ethylenedioxythiophene) Hybrid Microfibers," *ACS Nano,* vol. 10, no. 5, pp. 5086-5095, 2016, doi: 10.1021/acsnano.6b00200.

[118] W. Guo, J. Qiu, J. Liu, and H. Liu, "Graphene microfiber as a scaffold for regulation of neural stem cells differentiation," *Scientific reports,* vol. 7, no. 1, pp. 5678-8, 2017, doi: 10.1038/s41598-017-06051-z.

[119] K. Kostarelos, M. Vincent, C. Hebert, and J. A. Garrido, "Graphene in the Design and Engineering of Next-Generation Neural Interfaces," *Advanced Materials (Deerfield Beach, Fla.),* vol. 29, no. 42, 2017, doi: 10.1002/adma.201700909.

[120] J. Fu *et al.*, "Reduced Graphene Oxide Incorporated Acellular Dermal Composite Scaffold Enables Efficient Local Delivery of Mesenchymal Stem Cells for Accelerating Diabetic Wound Healing," *ACS Biomaterials Science & Engineering,* vol. 5, no. 8, pp. 4054-4066, 2019, doi: 10.1021/acsbiomaterials.9b00485.

[121] O. Akhavan, E. Ghaderi, E. Abouei, S. Hatamie, and E. Ghasemi, "Accelerated differentiation of neural stem cells into neurons on ginseng-reduced graphene

oxide sheets," vol. 66, ed, 2014, pp. 395-406.

[122] Z. Ge *et al.*, "Graphene Family Nanomaterials: Properties and Potential Applications in Dentistry," vol. 2020, ed: Hindawi, 2018.

[123] M. Duran, A. C. M. Luzo, J. G. de Souza, W. J. Favaro, P. Garcia, and N. Duran, "Graphene Oxide as Scaffolds for Stem Cells: An Overview," *Current Molecular Medicine,* vol. 17, no. 9, pp. 619-626, 2017, doi: 10.2174/1566524018666180308111915.

[124] J. Kim *et al.*, "Enhanced osteogenic commitment of murine mesenchymal stem cells on graphene oxide substrate," *Biomaterials Research,* vol. 22, 2018, doi: 10.1186/s40824-017-0112-8.

[125] S. R. Shin *et al.*, "Reduced Graphene Oxide-GelMA Hybrid Hydrogels as Scaffolds for Cardiac Tissue Engineering," *Small (Weinheim an Der Bergstrasse, Germany),* vol. 12, no. 27, pp. 3677-3689, 2016, doi: 10.1002/smll.201600178.

[126] D. R. Dreyer, S. Park, C. W. Bielawski, and R. S. Ruoff, "The chemistry of graphene oxide," *Chemical Society Reviews,* vol. 39, no. 1, pp. 228-24, 2009, doi: 10.1039/b917103g.

[127] O. Akhavan, E. Ghaderi, and A. Akhavan, "Size-dependent genotoxicity of graphene nanoplatelets in human stem cells," *Biomaterials,* vol. 33, no. 32, pp. 8017-8025, 2012, doi: 10.1016/j.biomaterials.2012.07.040.

[128] I. Chowdhury, N. D. Mansukhani, L. M. Guiney, M. C. Hersam, and D. Bouchard, "Aggregation and Stability of Reduced Graphene Oxide: Complex Roles of Divalent Cations, pH, and Natural Organic Matter," *Environmental science & technology,* vol. 49, no. 18, pp. 10886-10893, 2015, doi: 10.1021/acs.est.5b01866.

[129] A. Gholampour, M. Valizadeh Kiamahalleh, D. N. H. Tran, T. Ozbakkaloglu, and D. Losic, "From Graphene Oxide to Reduced Graphene Oxide: Impact on the Physiochemical and Mechanical Properties of Graphene–Cement Composites," *ACS applied materials & interfaces,* vol. 9, no. 49, pp. 43275-43286, 2017, doi: 10.1021/acsami.7b16736.

[130] L. Ken-Hsuan, L. Yu-Shen, W. M. Christopher, and L. H. Christy, "Cytotoxicity of graphene oxide and graphene in human erythrocytes and skin fibroblasts," *ACS applied materials & interfaces,* vol. 3, no. 7, pp. 2607-2615, 2011, doi: 10.1021/am200428v.

[131] Y. Chang *et al.*, "In vitro toxicity evaluation of graphene oxide on A549 cells," *Toxicology Letters,* vol. 200, no. 3, pp. 201-210, 2011, doi: 10.1016/j.toxlet.2010.11.016.

[132] L. Ou *et al.*, "Toxicity of graphene-family nanoparticles: a general review of the origins and mechanisms," *Particle and Fibre Toxicology,* vol. 13, no. 1, p. 57, 2016, doi: 10.1186/s12989-016-0168-y.

[133] S. K. Misra, P. Kondaiah, S. Bhattacharya, and C. N. R. Rao, "Graphene as a nanocarrier for tamoxifen induces apoptosis in transformed cancer cell lines of different origins," *Small (Weinheim an Der Bergstrasse, Germany),* vol. 8, no. 1, pp. 131-143, 2012, doi: 10.1002/smll.201101640.

[134] N. Chatterjee, H.-J. Eom, and J. Choi, "A systems toxicology approach to the surface functionality control of graphene-cell interactions," *Biomaterials,* vol. 35, no. 4, pp. 1109-1127, 2014, doi: 10.1016/j.biomaterials.2013.09.108.

[135] S. Zhang, K. Yang, L. Feng, and Z. Liu, "In vitro and in vivo behaviors of dextran functionalized graphene," vol. 49, ed, 2011, pp. 4040-4049.

[136] R. T. M. D. J. G.Vijayakumar, "Adsorption, Kinetic, Equilibrium and Thermodynamic studies on the removal of basic dye Rhodamine-B from aqueous solution by the use of natural adsorbent perlite," vol. 3, no. 2028-2508, pp. 157-170, 2012.

[137] B. D. Ossonon and D. Bélanger, "Synthesis and characterization of sulfophenyl-functionalized reduced graphene oxide sheets," *RSC Advances,* vol. 7, no. 44, pp. 27224-27234, 2017, doi: 10.1039/C6RA28311J.

[138] L. Li, D. Xu, and Z. Pei, "Kinetics and thermodynamics studies for bisphenol S adsorption on reduced graphene oxide," *RSC Advances,* vol. 6, no. 65, pp. 60145-60151, 2016, doi: 10.1039/C6RA10607B.

[139] A. Yang, Y. Zhu, and C. P. Huang, "Facile preparation and adsorption performance of graphene oxide-manganese oxide composite for uranium," *Scientific Reports,* vol. 8, no. 1, p. 9058, 2018, doi: 10.1038/s41598-018-27111-y.

Chapter 2

Conclusions

1. By Raman spectroscopy and FTIR, we have confirmed the formation of protein coating layers on the GO and rGO surfaces. The formation of such coating layers would occur through the π–π interactions between the benzene ring from the proteins and the C=C from GO and rGO.
2. Adsorption of low molecular weight and highly hydrophilic proteins, such as BSA and elastin, is more favorable for GO. In contrast, rGO is more effective for adsorbing hydrophobic proteins such as collagen.
3. The adsorption of the three studied proteins by GO and rGO fitted to the Langmuir model, suggesting that the adsorption process occurs on the surface in an homogeneous manner. These proteins cover the finite number of adsorption sites from the surface of the GO and rGO platelets as a monolayer, without transmigration along the plane of the surface and without interactions between the adsorbed proteins. In addition, GO and rGO nanoparticles would have two adsorption sites for each protein, fitting the pseudo-second-order model.
4. The adsorption of proteins to GO surfaces is an endothermic reaction, which suggests a non-spontaneous adsorption process. On the other hand, the adsorption of BSA and elastin to rGO surfaces is an exothermic reaction, while the adsorption of collagen is endothermic.
5. The adsorption of the studied proteins into GO and rGO surfaces altered the electrochemical activity of these materials, decreasing their impedance and specific capacitance, which would improve GO and rGO biocompatibility.
6. The *in vitro* studies showed a higher increase cell viability of C2C12-EPO myoblasts, as well as EPO release when cells were embedded in alginate hydrogels containing GO nanoparticles covered by a BSA- or elastin-biocorona, in comparison to GO covered by collagen. The hydrophilicity of the adsorbed proteins might have play an essential role in the biocompatibility of protein-coated GO. Perhaps by attracting cells via π-π interactions, thereby increasing the number of cells adhering and proliferating on these matrices.
7. Retention of EPO and insulin was dramatically decreased when GO, and rGO were coated with BSA, elastin, and collagen, precluding their clinical translation.
8. Mainly BSA- and elastin-coated GO hybrid alginate hydrogels could act a promising scaffolds for improving the viability and functionality of embedded cells.

Chapter 3

Appendices

1- Raslan A, Saenz-del-Burgo L, Ciriza J, Pedraz JL. *Graphene oxide and reduced graphene oxide-based scaffolds in regenerative medicine.* Int J Pharm. 2020 Apr 30;580.119226. doi. 10.1016/j.ijpharm.2020.119226. (Appendix 1)

2- Raslan A, Saenz-del-Burgo L, Espona-Noguera A, Ochoa de Retana AM, Sanjuán ML, Cañibano-Hernández A, Gálvez-Martín P, Ciriza J, Pedraz JL. *BSA- and elastin-coated GO, but not collagen-coated GO, enhance the biological performance of alginate hydrogels.* Pharmaceutics. 2020 Jun 11;12(6).543. doi.10.3390/pharmaceutics12060543. (Appendix 2)

3- Raslan, A., Ciriza, J., Ochoa de Retana, A.M., Sanjuán, M.L., Toprak, M.S., Galvez-Martin, P., Saenz-del-Burgo, L., Pedraz, J.L. *Modulation of conductivity of alginate hydrogels containing reduced graphene oxide through the addition of proteins.* Pharmaceutics 2021, 13, 1473. https.//doi.org/10.3390/pharmaceutics13091473. (Appendix 3)

Appendix 1

Graphene oxide and reduced graphene oxide-based scaffolds in regenerative medicine

International Journal of Pharmaceutics, Volume 580, (2020), 119226.

IF 5.875 (2020)

CATEGORY: PHARMACOLOGY & PHARMACY

Rank 37/276 (Q1)

Graphene oxide and reduced graphene oxide-based scaffolds in regenerative medicine

Ahmed Raslan, Laura Saenz del Burgo, Jesús Ciriza, Jose Luis Pedraz

NanoBioCel Group, Laboratory of Pharmacy and Pharmaceutical Technology, Faculty of Pharmacy, University of the Basque Country UPV/EHU, Vitoria-Gasteiz 01006, Spain

Biomedical Research Networking Center in Bioengineering, Biomaterials, and Nanomedicine, CIBER-BBN, Spain

Abstract.

There is a vast and rapid increase in the applications of graphene oxide (GO) and reduced graphene oxide (rGO) in the biomedical field, including drug delivery, bio-sensing, and diagnostic tools. Among all the applications, the GO and rGO-based scaffolds are a very promising system that have attracted attention because of their great clinical projection in tissue regeneration therapies. Both GO and rGO have shown a strong impact on the proliferation and differentiation of implemented stem cells, but still need to overcome several challenges, such as cytotoxicity, biodistribution, biotransformation or immune response. However, there are still controversial hypothesises regarding the mechanisms involved in these issues that should be clarified in order to improve the applications of these compounds. 3D-scaffolds can help in solving some of those limitations when moving into preclinical studies in regenerative medicine. In this review, we will describe the application of GO and rGO within 3D scaffolds in bone, cardiac and neural regenerative medicine after analyzing the aforementioned challenges.

Keywords. Graphene oxide, Reduced graphene oxide, Regenerative medicine, Tissue engineering, 3D scaffolds.

1. Introduction

Graphene is an extraordinary material formed by a single-thick layer of sp2 hybridized carbon atoms arranged in a honeycomb lattice (He and Fang, 2016, Novoselov et al., 2012, Mohan et al., 2015, Safron and Arnold, 2011, Park and Ruoff, 2009). Graphene exhibits excellent electrochemical properties, such as high thermal conductivity (above 3000 $W\,m\,K^{-1}$), a million times higher capacity than copper and low redox potential (−0.5 V–1.2) (Casero et al., 2012, Molina et al., 2013, Sharma et al., 2016, Rose et al., 2015, Morkvenaite-Vilkonciene et al., 2015). Moreover, this material shows optical absorption in the infrared limit, complete impermeability to any gas, a high surface area (2630 m^2/g) (Bai et al., 2011) and strong mechanical strength (about 1100 GPa) (Graphene Oxide, 2018), providing the material with excellent properties that have increased its applications in various fields including electronics or biomedicine (Mohan et al., 2018).

Other derivative forms from graphene have been investigated in the last decade taking advantage of its future perspectives, being one of most studied, graphene oxide (GO) and its reduction, the reduced graphene oxide (rGO). These materials have been researched and developed for their applications in the field of electronics, optics, sensors, and filtration (Molina et al., 2013, Sharma et al., 2016, Rose et al., 2015). However, due to the ability to modulate their characteristics, it seems that graphene derivatives could have a high impact also in the area of biomedicine, including the development of drug delivery systems, applications in gene therapy or in the improvement of contrast substances for diagnostic images (Bai et al., 2011, Graphene Oxide, 2018, Mohan et al., 2018, Dreyer et al., 2009). In this review, we will describe the properties of GO and rGO, the challenges for their future application in biomedicine and the current studies in regenerative medicine and tissue engineering within 3D scaffolds.

2. GO physical chemical properties

The production of GO is based on the oxidation of graphite in acidic medium following Hummers and Offemann methods (Mohan et al., 2018, Bradder et al., 2011, Suk et al., 2010, Konkena and Vasudevan, 2012, Park et al., 2009). Briefly, among different modified methods, the GO production consists on dispersing flake graphites, oxidants such as $KMnO_4$ and K_2FeO_4 and a stabilizer, like boric acid, in a concentrated sulfuric acid solution for 1.5 h at under 5 C in agitation, next, more deeply oxidizing with $KMnO_4$.

When oxidation is completed, the product is slowly hydrolyzed with deionized water at 95 °C and held for 15 min, getting a brown suspension that indicates an absolute exfoliation of intercalated graphite oxide. Residual oxidants and intermediates to soluble sulfate from this product are reduced with H_2O_2 and washed several times with HCl and water (see Fig. 1).

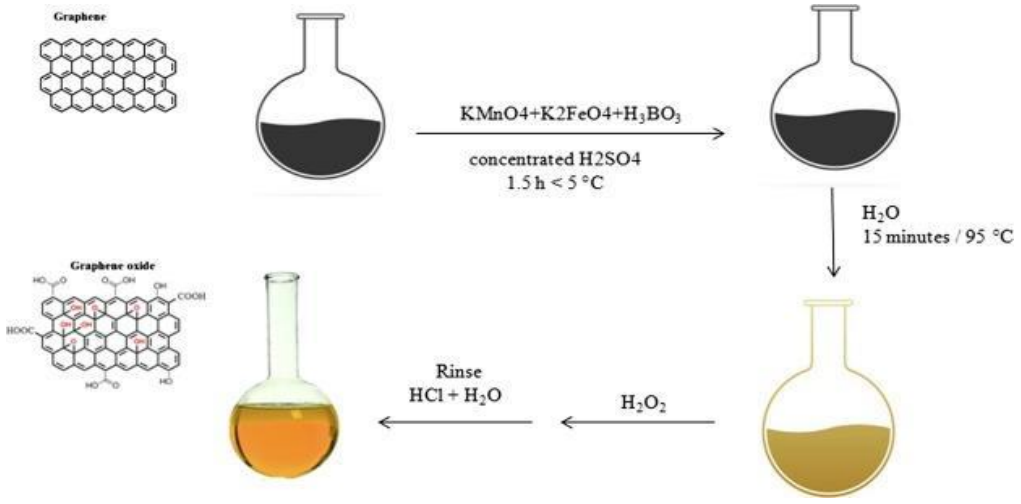

Fig. 1. Modified hummer method for GO synthesis from graphene.

GO is an electrically insulating material due to its disrupted sp2 bonding networks, but it can act as a semiconductor, depending on the degree of oxidation (Dreyer et al., 2009). Moreover, GO shows a high specific surface area (890 $m^2\ g^{-1}$) (Bradder et al., 2011) and mechanical strength (Young's modulus of ~1.0 and breaking strength of ~130 GPa) (Suk et al., 2010), being lows cost to escalate its production. The oxidation of graphene to GO increases the hydrophilicity of the surface, creating abundant functional groups, such as hydroxyl and epoxy groups on the basal plane, with slight amounts of carboxyl, carbonyl, phenol, lactone, and quinone (Mohan et al., 2018), clearly observed by FT-IR spectroscopy (He and Fang, 2016, Park and Ruoff, 2009, Sharma et al., 2016, Zhang et al., 2011, Liu et al., 2008). The presence of these oxygenated groups changes dramatically GO properties, facilitating the formation of stable dispersion in aqueous media and other polar solvents (Graphene Oxide, 2018, Konkena and Vasudevan, 2012, Park et al., 2009), and allows biochemical and bio-conjugation reactions occurring both at its basal plane and its edges (Park and Ruoff, 2009). These reactions facilitate the functionalization of GO surface with proteins, antibodies and DNA fragments (Zhang

et al., 2011, Liu et al., 2008), providing a wide number of biological applications to GO (Sharma et al., 2016, Chung et al., 2013).

GO also shows a high adsorption capacity for proteins and antibodies. On this regard, adsorbed proteins in GO have shown an increment in protection against proteolysis (Interaction of Graphene Oxide with Proteins and Applications of their Conjugates, 2017, Interaction of Graphene Oxide with Proteins and Applications of their Conjugates, 2017, Yan et al., 2014), providing an effective platform for protein delivery (Yang et al., 2017) or bio-sensors with GO functionalized with antibodies (Šimšíková, 2016, Lee et al., 2011). The mechanism for protein interaction with GO surface varies depending on the GO morphology, hydrophobicity (Interaction of Graphene Oxide with Proteins and Applications of their Conjugates, 2017) and the type of adsorbed protein (Interaction of Graphene Oxide with Proteins and Applications of their Conjugates, 2017). Thus, on one hand, it has been shown that adsorption behavior of GO would change from a Freundlich-type to a Langmuir-type adsorption as the oxidation degree (OD) increases (Yan et al., 2014), exponentially uptaking for example, methylene blue with the increase of OD. On the other hand, regarding the type of protein, the polypeptide can be adsorbed on the GO surface via hydrophobic interaction, Van der Waals forces, electrostatic interactions and hydrogen bonds (Emadi et al., 2017, Xu et al., 2018, Lv et al., 2018). Due to the SP^2 hybridization of GO; proteins adsorption on GO surface mostly occurs via hydrophobic-hydrophobic interaction (Kuchlyan et al., 2015), interacting the hydrophobic protein side with the hydrophobic carbon lattice (Šimšíková, 2016 Mar). For example, the adsorption of BSA on GO surface is attributed to hydrophobic interactions, which are electron density and protein molecule geometry dependent (Lee et al., 2011, Simsikova and Sikola, 2017). However, the low molecular weight heparin with a low electron density shows a decreased hydrophobic interaction (Lee et al., 2011). Also, the interaction between graphene oxide and other molecules can be attributed to van der Waals interactions (Amieva et al., 2016), but these interactions are weakened by the oxygenated moieties formed during the oxidation process (Stankovich et al., 2007). Even weakened, this non-covalent bonding enables the use of GO flakes as vehicles for hydrophobic drugs or nanocomposites formation between graphene and polymers that can be further bound to proteins (Hassan et al., 2014). However, the electrostatic interactions are the most observable on GO (Interaction of Graphene Oxide with Proteins and Applications of their Conjugates, 2017). In fact, GO sorption enhancement at $pH < 6.0$ is due to electrostatic attractions between negatively charged GO and positively charged compounds, since at

increased pH, more oxygen-containing functional groups on GO are deprotonated becoming GO more negatively charged and generating stable aqueous suspension through the electrostatic repulsion among the negatively charged GO particles (Yu et al., 2016). Thus, for example, electrostatic interactions contribute to the higher adsorption capacity of nitrobenzene (View Journal, 2018). Moreover, Cu(ii) and Pb(i) is highly adsorbed in acidic solution through the negative surface charge of GO and the electrostatic interactions between the metal ions and GO nanosheets (Sitko et al., 2003). Hydrogen bonding interactions have been also described in GO, showing how the adsorption of nitrogen oxides on GO is stronger than on graphene due to the formation of hydrogen bonds OH···O (N) between –OH and nitrogen oxides among others (Tang and Cao, 2011). Finally, it should be mention that due to the abundant π electrons on the basal plane of the GO surface, the π–π stacking interactions can also occur (Lv et al., 2018), as described for the individual hexagonal cells of the GO basal planes and the glucose oxidase (Interaction of Graphene Oxide with Proteins and Applications of their Conjugates, 2017).

GO shows also the possibility for covalent conjugation on its surface with substances such as proteins. Through covalent conjugation, the binding strength between GO and the protein is enhanced, maximizing their stability against heat, pH, organic solvents, and storage conditions (Oliveira et al., 2015). However, the covalent conjugation of proteins on the GO surface may cause an alteration in proteins structure, leading to decrease the protein functionality or enzymatic activity (Carrier-bound Immobilized Enzymes. Principles, 2019), avoiding it by suitable cross-linking molecules between protein and GO. These cross-linking molecules are usually adsorbed to GO through hydrophobic and π-π interactions, next binding covalently the protein, such bovine serum albumin (BSA) linked to GO by diimide-activated amidation (Shen et al., 2010). All the aforementioned described GO surface properties help to improve cell attachment and adhesion, with cell proliferation enhancement in cell cultures when GO is added (Agarwal et al., 2010, Advances, 2016, Nayak et al., 2011, Park et al., 2010, Ryoo et al., 2010, Shin et al., 2017), with higher potential when its surface is modified (Hassan et al., 2014).

3. rGO physical chemical properties

rGO is formed by the reduction of GO (Raidongia et al., 2014). Depending on the procedure for rGO production, its properties can vary, being important to select the most adequate method among those described (Zhang et al., 2018) (Table 1). Chemical reduction of GO by chemical agents is the most frequently used technique for rGO synthesis (Pei and Cheng, 2012), being often used inorganic agents such as $NaBH_4$ (Shin et al., 2009) or organic, such as phenyl hydrazine (Pham et al., 2010), hydrazine hydrate (Stankovich et al., 2007) or hydroxylamine (Stankovich et al., 2007). However, reducing agents are toxic (Zhao et al., 2012), producing a final rGO product with low carbon-to-oxygen ratio (C/O) (Pei and Cheng, 2012, Zhang et al., 2018), and poor quality powder of rGO sheets (Zhang et al., 2018). Therefore, high-quality rGO producing methods are also employed, such as thermal reduction where GO is reduced thermally under vacuum in an inert, or reducing atmosphere (Baradaran et al., 2014), at a temperature range between 300 °C and 2000 °C (Pei and Cheng, 2012, Wang et al., 2008). Other methods employ microwave heating where rGO is done by solid-state reduction of dry GO in a microwave oven (1000 W, 2.45 GHz) (Li et al., 2010). Finally, photothermal-reduction of GO can be done with direct laser beam at wavelengths under 390 nm (energy > 3.2 eV) (Lazauskas et al., 2018).

Table 1. Advantages and disadvantages among the rGo synthesis methods.

rGO synthesis method	Advantages	Disadvantages
Chemical reduction	applicable, easy and economical methods	toxicity of reducing agents Low carbon-to-oxygen ratio Poor quality product
Thermal-reduction	High reduction degrees than chemical reduction Restore of sp2 carbon domains Improved electrical properties	unsuitable for mass production carried out at very high temperatures. Economically not efficient. Thermal rGO is highly toxic
Microwave-Reduction	Larger specific surface area Higher electrical conductivity Discharge and charge capacities	the re-oxidation of the graphite structure caused by an extended exposure to MW radiation in air
Photo-reduction	less impurity. large scale production possibiliy of nanopatterning C/O atomic ratio increased Enhanced electrical conductivity	low reduction degree high cytotoxicity. require the help of chemical reduction process

As result of GO reduction process, dramatic changes on surface properties are quantified in rGO, involving significant variations in the structural properties, mechanical strength, stability, dispersability and reactivity of rGO (Park et al., 2009, Mohan et al., 2015, Konios et al., 2014, Azizighannad and Mitra, 2018). Thus, the elimination of most oxygen-containing functional groups from GO partially restores the SP^2 structure (Zhang et al., 2018), therefore enhancing rGO conductivity by several orders of magnitude (Zhang et al., 2018), reaching excellent electrical conductivity of 6300 S cm^{-1} and a high mobility of 320 cm^2 V^{-1} s^{-1} (Wang et al., 2018), and providing applicability of rGO in numerous fields, including electronics (Berger et al., 2006, Berger, 2004) energy storage and conversion devices, such as supercapacitors (Purkait et al., 2018) or chemical sensors and biosensors (Chen et al., 2012, Lu et al., 2011). However, compared to graphene, rGO still contains residual oxygen and structural defects originated in the chemical oxidation synthesis of GO, avoiding to reach the high conductivity shown by graphene. These defects and vacancies within the SP^2 carbon lattice are very difficult to be restored by the chemical reduction to obtain rGO (Zhang et al., 2018). Moreover, rGO surface area is enhanced after reduction (theoretically 2630 m^2/g for single-layer graphene), showing a strong mechanical strength, with average elastic modulus ~32 GPa and fracture strength of ~120 MPa (Dikin et al., 2007, Pokharel and Lee, 2014). The oxygen containing groups have also implications on the stability, dispersibility and aggregation in aqueous solutions and the chemical properties (Azizighannad and Mitra, 2018). For example, three GO partially reduced 1 h (rGO-1 h), 2 h (rGO-2 h) and 5 h (rGO-5 h) show that stability of rGO in water decreases with the degree of reduction on its functional groups, showing some suspension with rGO-1 h and rGO-2 h, but complete precipitation for rGO-5 h (Chowdhury et al., 2015)). Moreover, when comparing gradually reduced r-GO containing different levels of oxygen (from 31 to 9% oxygen), dispersibility behaviour was gradually decreased to nearly zero for r-GO with 9% oxygen, decreasing the dispersibility after sonication from 8 to 2.5 µg/ml. In this study, hydrophobicity index, measured as the octanol water partition coefficient, decreased from −3.89 to 5.2% when oxygen content dropped from 49 to 9%. The colloidal behavior was also affected depending the degree of reduction, decreasing the critical coagulation concentration (CCC) from 28 to 15 in presence of 0.5 mmole/l NaCl and from 6 to 2 in presence of 0.5 mmol/l MgCl (Azizighannad and Mitra, 2018). Regarding the reactivity, due to the elimination of oxygenated functional groups on rGO, the main adsorption mechanism is π-π interaction, but other adsorption mechanisms, such as hydrophobic interaction, Van der Waals and electrostatic interaction, pore-filling should not be excluded (Peng et al.,

2016). Thus, π–π interaction between rGO and 1-naphthol has shown to be useful in the removal of nanphthol from water (Royal Society, 2014). Hydrophobic interactions participate for the antibacterial activity of this 2D nanomaterial, promoting the destruction of bacteria's membrane (Tan et al., 2019). Moreover, hydrophobic interactions between rGO sheets and heparin backbones lead to the effective conjugation between rGO and heparin. Van der Waals interactions with aromatic molecules, such as benzene, through the rGO defects and oxygen containing functional groups have been also described (Hassan et al., 2014). Binding of graphene to polymers via dispersion forces is only marginally affected by low defects densities, a conjecture supported by a simple model that predicts a substantial decrease of van der Waals binding for defect densities exceeding roughly 15% (Hassan et al., 2014). Finally, regarding electrostatic interactions between the amylopectin-reduced graphene oxide (AP-rGO) composite and the positively charged hemoglobin have shown to provide an additional contribution to the adsorption of protein.

(Zhang et al., 2015), similarly to the favorable adsorption of methylene blue (MB, cationic) and methyl orange (MO, anionic) dyes with rGO (Minitha et al., 2017).

4. Challenges of using GO and rGO in biomedicine.

Scaffolds are structures able to support living cells and to create a suitable microenvironment that enables cells to grow and maintain themselves. These scaffolds represent excellent properties including, high level of porosity, allowing the passage of nutrients and oxygen into the system for maintaining the cells, as well as, the possibility to release the waste products and therapeutic products secreted by the cells. Moreover, these scaffolds provide protection for embedded cells from the external environment, such as high molecular weight immunoglobulins and immune system cells, when they are implanted in vivo (Paredes Juárez et al., 2014).

In recent years, incorporating the field of nanotechnology has shown to improve the properties of a huge number of materials. GO and rGO, for instance, seems to be very promising for being applied in scaffolds, supporting living cells and creating suitable microenvironment. However, several challenges with GO and rGO need to be overcome before these scaffolds can be used in clinic. Here, we summarized some of those challenges (Table 2).

Table 2. Challenges of using GO and rGO in biomedicine.

Challenges	Features	How to solve
Cytotoxicity.	Affecting on mitochondrial activity and the cell membrane integrity. (Zhang et al., 2010) Decreasing cell adhesion, metabolic activity (Wang et al., 2011 Dec) Inducing cell apoptosis (Wang et al., 2011 Dec)	Lower dose (up to 50 μg/mL) Small lateral sizes between (50–200 nm) Pre-coating layer such as BSA, FBS, PEG dextran or chitosan Inclusion 3D scaffold
Biodistribution and clearance	Long term retention in lung, liver, spleen and bone marrow (Ou et al., 2016, Zhang et al., 2011) Hard to be eliminated (Li et al., 2013 Apr) Induction of inflammatory, cell infiltration, granuloma pulmonary and edema in the lungs (Ou et al., 2016, Zhang et al., 2011)	Small lateral size (50–200 nm) Applying pre coating layer such as BSA, FBS , PEG or dextran Inclusion 3D scaffold
Biotransformation	Aggregating of GO (Bao et al., 2011) Changing lateral size and their interaction with the targeted cells (Qi et al., 2018)	Inclusion of GO within pre-coat Inclusion 3D scaffold
Immune response	Inflammatory response and chronic injury in gastrointestinal tract, respiratory tract, the central nervous system and blood components (Wen et al., 2015 Oct) macrophages necrotic cell death (Lee et al., 2018 Dec) prevents lipopolysaccharide (LPS) to induce interleukin 6 (IL-6) (Lategan et al., 2018)	Pre coating layer such as BSA, FBS, PEG, dextran Inclusion 3D scaffold

4.1. Cytotoxicity

Several factors have been outlined for being responsible for GO cytotoxicity, including dose, lateral size and surface charge (Misra et al., 2012, Jastrzębska et al., 2012). The studies carried out to date regarding the cytotoxity from these carbon-derived materials are contradictory (Feng and Liu, 2011, Yan et al., 2011). Some studies report no effects of these materials on cell behavior at certain doses (Sasidharan et al., 2012 Apr, Yue et al., 2012 Jun), while others show that can induce cellular damage (Singh et al., 2012 Mar, Hu et al., 2010). GO cytotoxicity seems to be dose dependent since GO dose less than 50 μg/mL exhibits higher biocompatibility with no evident cytotoxicity (Misra et al., 2012, Chang et al., 2011, Mittal et al., 2016–12-21;6.). For example, GO prepared by a modified Hummers method at doses lower than 20 μg/mL did not show toxicity on human fibroblast cells, while doses higher to 50 μg/mL did, decreasing cell adhesion, inducing cell apoptosis and showing presence of the carbon material within lysosomes, mitochondria, endoplasm and the cell nucleus. When studied in vivo, low doses of this modified Hummer method-GO at the range of 0.1–0.25 mg did not show significant toxicity in mice, while higher doses did (Wang et al., 2011). Similarly, GO at

20 µg/mL dose exhibited no evident cytotoxicity on the A549 (Chang et al., 2011) and the metabolic activity of neuronal PC12 cells was decreased in a dose-dependent manner after one day of the incubation with GO, being affected the mitochondrial activity and the cell membrane integrity, but always showing cytotoxicity even at low concentrations (Zhang et al., 2010). But this dose cytotoxicity dependence changes with different cell types since, the impact of GO on the human neuroblastoma SH-SY5Y cell line show no cytotoxicity up to 80 µg/mL GO concentration, observing a dose and time dependent viability reduction at higher concentrations (Lv et al., 2012). However, GO dose higher than 50 µg/mL exhibited lower biocompatibility and high cytotoxicity (Lv et al., 2012). Other studies have shown how GO induces cytotoxicity and oxidative stress in BF-2 cells, in a dose and time-dependent manner from low concentrations of GO (40 µg/ml) and 24 h of incubation (Srikanth et al., 2018), being the size of the GO particles another factor inducing the mitochondrial generation of ROS (Oxidative Stress, 2016). In our group, we have observed a dose depending cytotoxicity when GO was encapsulated in alginate with myoblast cells at higher GO concentration to 50 µg/ml (Ciriza et al., 2015, Saenz del Burgo et al., 2017 Mar, Ciriza et al., 2018). When rGO has been evaluated, even lower doses induce time and dose dependent apoptosis and mediate cell death (Zhang et al., 2018, Palejwala et al., 2016).

Another factor inducing cytotoxicity is the GO lateral size. Comparing GO, thermally reduced GO (TRGO) and chemically reduced GO (CRGO), significantly differing in their lateral size and functional groups density, on phenotypically different human lung cells; bronchial epithelial cells (BEAS-2B) and alveolar epithelial cells (A549), demonstrated that cytotoxicity depended on the reduced lateral size and the density of the functional groups, being more toxic TRGO and GO than CRGO (Mittal et al., 2016–12-21;6., Mittal et al., 2016). GO small particles have shown high toxicity, due to their small size and sharp edges, easily penetrating the cell membrane and entering to the cytoplasm, and consequently causing cell membrane damage and leakage of cytoplasmic contents (Mittal et al., 2016). However, small GO particles are easily cleared, due to their small size particle that allows them to penetrate through the renal glomeruli and being rapidly removed (Li et al., 2014). GO sheets larger than 200 nm are less toxic since they cannot penetrate the cell membrane (Mittal et al., 2016), are highly retained in different body organs, causing long term side effects (Ou et al., 2016). In fact, the uptake mechanisms are different depending on GO lateral size. Thus, large particles are phagocytosed, while smaller particles enter the cell through clathrin-mediated endocytosis in C_2C_{12} myoblasts

(Mu et al., 2012). In the case of macrophages, GO uptake is also size dependent (Russier et al., 2013), being the small GO particles, with lateral sizes between 50 and 350 nm, simply internalized, while the large GO particles, with lateral size between 750 and 1300 nm, adhered on their plasma membranes, and consequently causing the activation of toll-like receptor (TRL), nuclear factor NF-κB pathways and pro-inflammatory cytokines (Ma et al., 2015). When comparing both GO sizes (89 and 277 nm), large GO particles showed more toxicity than small particles, particularly at a longer incubation time (Gregorio Mendes et al., 2015). Therefore, the designing of GO particle should be in optimal size, not being able to penetrate the cell membrane and being easily cleared and removed from the body organs.

GO surface charge has also a strong impact on the internalization and cell uptake (Wang et al., 2013). GO uptake, was negligible in non-phagocyte cells, due to the strong electrostatic repulsion between the negatively charged GO and the cell membrane (Yue et al., 2012). However, the negatively charged nanoparticles can be internalized into non-phagocytic cells through the attachment to available cationic sites on the cell membrane (Chatterjee et al., 2014). The interaction between GO and the cell membrane can cause morphological changes and significant lysis, such as haemolysis of red blood cells (RBCs), due to the strong electrostatic interactions between the negatively charged oxygen groups on the GO surface and positively charged phosphatidylcholine lipids on the RBC external membrane (Liao et al., 2011). On this regard, the negative GO surface charge have shown to induce platelet activation and aggregation compared to rGO functionalized with amine groups (rGO –NH2) which charge could not induce any significant effect at the same doses (Singh et al., 2012).

In this sense, there are a limited number of contradictory reports available that compare the toxicity of GO with rGO, (Zhang et al., 2018, Liao et al., 2011). Some publications report that rGO is less toxic than GO (Palejwala et al., 2016, Tabish et al., 2017), while others indicate that rGO could cause more membrane disruption and oxidative stress than GO (Zhang et al., 2018). The reduction techniques could have a strong impact on the cytotoxicity of rGO. Thus, the light irradiated reduction of GO led to an enormous increase in the generation of free radicals and oxidative stress (Zhang et al., 2018), and the thermal rGO was able to induce more cytotoxicity effects, due to its small size, which facilitates its cellular uptake (Zhang et al., 2018). More studies comparing should be done comparing both compounds to clarify their cytotoxicity.

4.2. Biodistribution and clearance.

GO is highly stable in water solutions thanks to the affinity of the oxygenated functional groups on its surface of the pristine Graphene (Zhou and Bongiorno, 2013). Due to its high chemical stability, GO can be retained inside the body. In fact, injectable GO is highly retained in different body organs, such as lung, liver, spleen and bone marrow (Ou et al., 2016, Zhang et al., 2011), while functionalized GO, such as GO-PEG, is mainly retained in the liver and spleen. In lungs, GO is hard to be eliminated, inducing inflammatory, cell infiltration, granuloma formation and pulmonary edema in the lungs (Ou et al., 2016, Zhang et al., 2011). The clearance of GO from these body organs occurs by the renal and fecal excretion (Yang et al., 2011). For example, the injection of mice with 0.4 mg of GO exhibited high cytotoxicity, such as lung granuloma formation, mainly found in lung, liver, spleen, and kidney, resulting in mice death, since GO could not be cleared by the kidney (Wang et al., 2010). However, compared with other graphene derivatives, GO shows a long blood circulation time (half-time 5.3 ± 1.2 h), and limited absorption in the reticuloendothelial system (Zhang et al., 2011). The clearance of GO, examined by radioisotopes and morphological observation in mice, indicated that the presence of GO in bladder gradually increases within 1 h after treatments, detecting the maximum GO concentration in urine after 6 h. Small lateral sizes of GO diffused easily through the alveolar–capillary barrier into the blood, being quickly eliminated by the kidney, while GO retained in lung was clear 3 months after treatments (Li et al., 2013). Different mechanisms can explain GO clearance depending on GO particles size and surface modification. Thus, GO sheets larger than 200 nm are retained by splenic physical filtration (Ou et al., 2016), while small particles have the capacity to penetrate the renal tubules into the urine, being rapidly removed without evident toxicity (Li et al., 2014). The modification of GO surface, such as GO-PEG or GO-dextran (GO-DEX), facilitates the accumulation of GO into the reticuloendothelial system (RES) of liver and spleen, without showing short-term toxicity (Yang et al., 2013, Zhang et al., 2011). In vivo studies comparing the retention of GO and GO-PEG showed that GO particles are mainly retained in liver and spleen, and partially in lung, due to the aggregation of GO particles after reacting with lung fluids, while PEG coating improves the biocompatibility of GO, decreasing its retention in liver, lung, and spleen. However, both GO and GO-PEG were detected after 3 months of injection (Li et al., 2014). In addition, PEG coating significantly reduced the early weight loss caused by acute tissue injuries such as the injury of liver, lung, and kidney, as well as, chronic hepatic and lung fibrosis (Li et al., 2014).The

adsorption by the lateral size-dependent interaction of GO of plasma proteins, such as albumin, fibrinogen or globulin, also affects its bio-distribution (Yue et al., 2012 Jun, Aggarwal et al., 2009), showing for example, higher adsorption capacity with albumin than with fibrinogen (Kenry et al., 2016). In vivo, this adsorption facilitates the clearance from bloodstream, allowing the store of GO throughout most of the organs within 48 h. This retention occurs mainly in lungs, liver and spleen with a very low amount in brain, heart and bone. This high-level accumulation of GO in lungs, liver and spleen suggests that the rapid uptake of GO is intercepted by the mononuclear phagocytes in the reticuloendothelial system (Zhang et al., 2011). All the aforementioned issues with GO biodistribution could be solved by the inclusion of GO in a hydrogel that would retain it within the 3D scaffold, not allowing its biodistribution along the body.

4.3. Biotransformation

Due to the higher chemical reactivity, GO can undergo seriously biotransformation and may alter its physicochemical properties and consequently hinder its biomedical applications. For instance, GO is highly reactive against biological fluids inside the lung (Qi et al., 2018). Thus, GO undergoes a strong biotransformation when the impact of GO with the salts from Gamble's solution and artificial lysosomal fluids (ALF), two synthetic biological media simulating lung fluid. Fluids from lungs showed a strong potential to reduce GO, modifying its epoxy and carbonyl groups to phenolic groups, therefore, leading to significant alterations on Gamble's solution, enhancing the layer-by-layer aggregation of GO, causing the precipitation of GO and decreasing its interaction with cells, while large GO aggregates adhered to the plasma membrane without cellular absorption. In-vivo studies on mice corroborated the morphological alterations of GO in a real lung microenvironment. This biotransformation of GO may significantly alter its inherent properties, therefore affecting its biosafety and clearance by immune cells which could cause long-term side effects (Qi et al., 2018).

Other surrounding conditions, such as the presence of enzymes or pH, can modify the properties of GO/rGO affecting the interaction between GO or rGO and the biological systems (Guarnieri et al., 2019). For instance, the enzymatic oxidation of a single layer of GO by horseradish peroxidase (HRP), showed that the presence of low concentrations of hydrogen peroxide (~40 μM) causes the formation of holes on its basal plane, failing when GO was chemically reduced (Kotchey et al., 2011). In addition, GO during simulated oral ingestion showed that GO particles are aggregated by interacting with digestive fluids

and the acidic pH environment from the stomach. However, no structural changes or degradation were detected, indicating that GO is not bio-transformed through oral uptake (Guarnieri et al., 2019).

The biotransformation of GO has a strong impact on their biological responses. Thus, bio transformed GO reduces human embryonic lung fibroblasts (HELFs) viability less than pristine GO, also inducing lower reactive oxygen species (ROS) levels (Hu et al., 2017). Also, bio transformed GO can be formed by adsorbing bio molecules on its surface, forming what it is known as bio-corona. The formation of bio-corona on the GO surface increases the stability of GO in salt solutions, modifying also its biocompatibility and facilitating its clearance. For example, GO is able to adsorb IgG, enhancing its clearance from circulation after phagocytosis by macrophages, resulting in lower circulation time (Hu et al., 2017). Biotransformed GO, such as Gamble-GO or ALF-GO, also have shown stronger interaction with macrophages than pristine GO (Qi et al., 2018). An alternative to prevent GO biotransformation could be its encapsulation within 3D scaffolds based in hydrogels.

4.4. Immune response. Several authors have outlined the ability of GO to induce an inflammatory response and chronic injury through interfering with the normal physiological functions of important organs (Wen et al., 2015), including the respiratory tract, the central nervous system and blood components. In the respiratory tract, it was found that GO with high dose can create aggregations and that block pulmonary blood vessels, causing dyspnea (Li et al., 2014, Singh et al., 2011). In fact, GO can penetrate the alveolar-capillary barrier, causing the penetration of inflammatory cells to the lungs and inducing pro-inflammatory cytokines (Duch et al., 2011, Bengtson et al., 2017). Adverse outcomes are also found when high GO concentrations, between 1 and 2 mg/kg body weight, are administrated by intravenous injection, forming thrombi platelet (Li et al., 2014, Xu et al., 2016). Lower intravenous injection of GO (10 μg/mL) also causes an extensive increase of the pulmonary thromboembolism in mice. It is believed that this effect is based on the negative charge distribution of the GO surface, inducing a strong prothrombotic (Singh et al., 2011). However, rGO flakes have less charge density on its surface, therefore exhibiting less thrombogenic effects (Singh et al., 2011). Comparing the cytotoxicity induced by positively-charged rGO functionalized with amine groups (G-NH2) and GO, it was found that GO was able to induce platelet activation and aggregation, while G-NH2 did not induce any significant effects at the same doses (Singh

et al., 2012). In-vivo studies of thrombus formation in a thrombosis model with intravenous injections of GO (250 μg/kg body weight) and G-NH2 (250 μg/kg body weight) showed that G-NH2 didn't show the thrombotoxic property in histological samples from lungs (Singh et al., 2012). GO exposure can also activate an allergic pulmonary response. In vivo studies on a murine model of ovalbumin (OVA)-induced asthma, indicated that IL-4, IL-5, and IL-13 levels are reduced in broncho-alveolar lavage (BAL) fluid in GO-exposed mice, decreasing also the eosinophil accumulation and increasing the recruitment of macrophages in BAL fluid. Moreover, GO stimulated the production of OVA-specific IgG2a and down-regulated the levels of IgE and IgG1 (Shurin et al., 2014).

But GO and rGO have also shown adverse outcomes in other tissues. Thus, small size particles of GO has shown hemolytic activity, having its greatest activity at a concentration up to 75 μg/ml (de Sousa et al., 2018) (Sasidharan et al., 2012). On the other hand, in the central nervous system, rGO induces a transient disruption of the paracellular tightness of the blood-brain barrier (BBB) in the hippocampus, no improving even when rGO is functionalized with PEGylation (Oxidative Stress, 2016).

Several authors have outlined other effects of GO on the immune system cells, showing how GO provokes macrophages necrotic cell death, through activating Toll-like receptor 4 (TLR4) signaling (Guangbo et al., 2013). GO can also modulate the antigen-presenting cells including dendritic cells (DCs) (Lee et al., 2018 Dec) or can mediate iNKT cells through α-galactosylceramide (α-GalCer), by reducing the capacity of α-GalCer to activate the iNKT cell-mediated trans-activation after GO in vivo injection. It has been shown that TLR4 plays a key role in the induction of inflammatory response by GO, acting as a receptor. Infact, the absence of TLR4 partially enhanced the anti-inflammatory activity of GO against α-GalCer-elicited responses, implying negative effects of TLR4 signaling on the anti-infammatory properties of GO. In vivo studies, have shown how GO treatment significantly protected mice from α-GalCer-induced lethality and modulated iNKT cell responses (Lee et al., 2018). Moreover, in vitro, GO prevents lipopolysaccharide (LPS) to induce interleukin 6 (IL-6) synthesis and phytohaemmagglutinin (PHA) to induce the interferon gamma (IFNγ) synthesis by whole blood cell cultures in a dose-dependent manner from both RAW 264.7 cells and human whole blood cells at concentrations of 15.6 and 5 μg/mL, respectively. Moreover, GO, induces IL-10 synthesis by whole blood cell cultures, indicating that GO alters the immune system biomarkers (Lategan et al., 2018).

The modification of the GO surface can improve its biocompatibility, since functionalized GO, such as GO-BSA, GO-FBS, (GO-PEG), GO–dextran (GO–DEX) or the reduction of GO, exhibit less cytotoxicity than pristine GO and improves its biocompatibility (Saenz del Burgo et al., 2017 Mar, Ciriza et al., 2018, Zhang et al., 2011, Yang et al., 2013, Mittal et al., 2016).

5. Application of GO and rGO in 3D scaffolds for tissue engineering

Stem cells have the capacity for auto-renewal and the ability to differentiate into different functional cell types. This principle has been extended from the embryonic stem cells (ESCs), adult stem cells and pluripotent stem (IPS) cells (Nombela-Arrieta et al., 2011). The integration of stem cells in tissue engineering led to revolution re-generative medicine. The impact of GO on the differentiation of different stem cells has also been investigated, finding that GO and rGO have a strong impact on the differentiation of the stem cells. For example, in 2D cultures, the characteristic properties of the GO surface have a strong impact in terms of stem cells adhesion and the cell proliferation (Agarwal et al., 2010, Advances, 2016, Nayak et al., 2011, Park et al., 2010, Ryoo et al., 2010, Shin et al., 2017), promoting the differentiation of ESCs to cardiomyocytes (Mihic et al., 2015, Wu et al., 2017) and neurons (Palejwala et al., 2016, Akhavan et al., 2014), or the differentiation of mesenchymal stem cells (MSCs) to osteogenic lineages (Lee et al., 2014). Furthermore, GO suspension induces neuronal differentiation of neuroblastoma Sh-Sy5Y cells (Lv et al., 2012), whereas GO-doped poly (lactic-co-glycolic acid) (PLGA) nanofiber scaffolds, promote proliferation and osteogenic differentiation of the human mesenchymal stem cells (MSCs) (Luo et al., 2015 Mar). However, applications of GO and rGO in 3D scaffolds that closer mimic the natural microenvironment have not been deeply studied and could represent a good alternative for the translation of GO application in medicine. Several studies have been performed in bone, cardiac and nerve regeneration.

5.1. GO and rGO based scaffolds in bone regeneration

Calcium phosphates derivatives such as hydroxyapatite (HAp) and β-tricalcium phosphate (β-TCP) are well-known materials in designing the 3D scaffold for bone regeneration because of their excellent biocompatibility and osteoconductivity (Bashoor-Zadeh et al., 2011, Wang et al., 2010 Dec, Zhao et al., 2011 Dec, Turhani et al., 2005

Jul). However, hydroxyapatite (HAp) and β-tricalcium phosphate (β-TCP) cannot mediate the high rate of proliferation and differentiation for osteoblast cells (Turhani et al., 2005). Moreover, these ceramics materials lack the required mechanical strength and osteoconductivity. On this regard, various materials were conjugated to hydroxyapatite (HAp) and β-tricalcium phosphate (β-TCP) in order to improve the properties of the osteoconductive scaffold and accelerate the proliferation and differentiation of osteoblasts. For instance, bone morphogenetic protein-2 (BMP-2), was capable of differentiating the mesenchymal stem cells (MSCs) and preosteoblasts into osteoblasts and inducing the immigration of osteoblastic cells. However, BMP-2 lack stability due to its rapid degradation by proteinases (Wang et al., 1990). The integration of GO in 3D scaffold for bone regeneration led to a revolution in bone regeneration, due to the capacity of GO to induce the cell proliferation, cell viability, the migration and differentiation of the mesenchymal stem cells (Fu et al., 2017). GO has excellent mechanical properties, providing the osteoconductive scaffold with the required mechanical strength. Moreover, the integration of GO with hydroxyapatite (HAp), facilitates the functionality of hydroxyapatite with different growth factors such as BMP-2. In fact, GO can increase the stability of adsorbed proteins, such as BMP-2 (Fu et al., 2017).

GO improves also the surface properties of PLGA/HA scaffolds, mediating the high degree of adhesion, proliferation and osteogenesis differentiation of MC3T3-E1 cells on the GO-PLGA/HA surface. The integration of GO-BMP-2 within PLGA/HA scaffolds has shown an excellent bioactivity, supporting the adhesion, proliferation, and osteogenic differentiation of MC3T3-E1 cells (Fu et al., 2017). Moreover, the immobilization of BMP-2 via GO decreased the growth factor consumption and provided long-term osteoinductive effects (Fu et al., 2017).

The conjugation of GO with other type of scaffolds has also shown benefits in the differentiation of stem cells in osteogenic cells. Thus, in collagen scaffolds conjugated with GO, the mechanical properties of the collagen scaffolds are improved, promoting the osteogenic differentiation of human MSCs (Kang et al., 2015). In chitosan scaffolds conjugated with GO, the presence of GO improved the alkaline phosphatase activity both in vitro and in vivo. GO-Chitosan was found to improve the differentiation of osteoprogenitor cells, increasing the expression of the bone morphogenetic protein (BMP) and Runx-2 (Fig. 2). The up-regulation of osteopontin and osteocalcin was noticed on the 8th week, overexpressing on 18th week, showing that GO-Chitosan matrix could

be a promising tool for the reconstruction of large bone defects, without using exogenous growth factors (Hermenean et al., 2017).

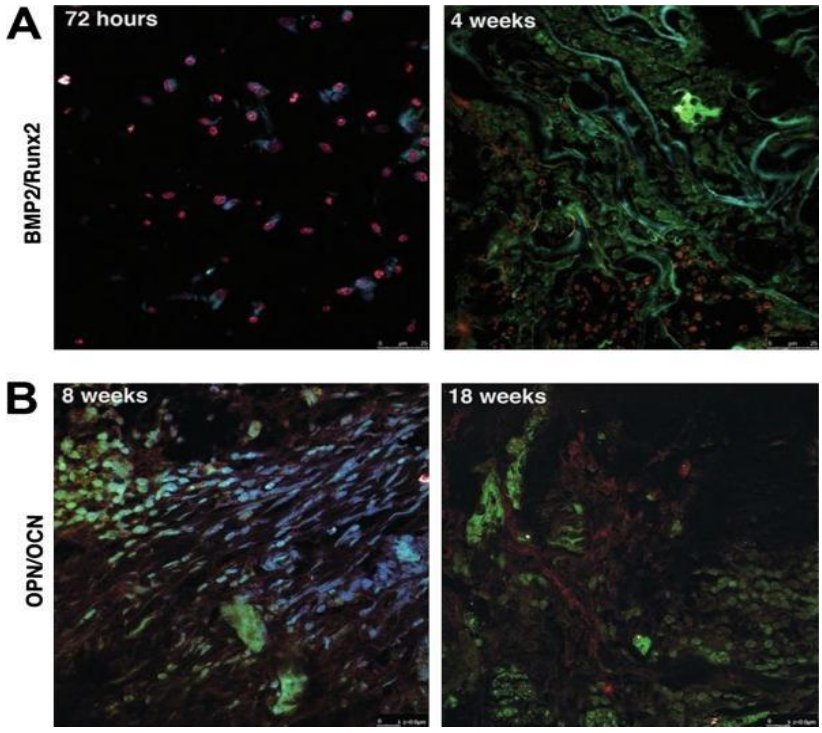

Fig. 2. Immunohistochemical expression of differentiated MSCs within CHT/GO 3.0 wt% after implantation stimulates early and late osteogenesis markers. (A) BMP-2 and Runx-2 at 72 h and 4 weeks post-implantation; (B) OPN and OCN at 8 and 18 weeks post-implantation (Hermenean et al., 2017).

The integration of rGO has also created an advance in osteoconductive scaffolds (Lee et al., 2015). For example, the elastic modulus and fracture toughness of hydroxyapatite-rGO composites are improved when increasing rGO percentage in the matrixes, inducing in vitro osteoblast adhesion and proliferation of human osteoblast cell lines (Baradaran et al., 2014). Similarly, rGO/Hydroxyapatite matrixes are able to enhance the osteogenesis of MC3T3-E1 preosteoblasts, inducing new bone formation, promoting the spontaneous osteodifferentiation (Lee et al., 2015). It can be envisioned that both GO and rGO combined with 3D scaffolds have potential application in the future bone regenerative medicine.

5.2. GO and rGO based scaffolds in cardiac regeneration

Due to myocardial infarction, the nonconductive nature of injured tissue can cause a ventricular dysfunction by low electrical conductivity of the cardiomyocytes in the injured heart tissue (Ruschitzka et al., 2013). In order to restore impulse propagation, there is a need for conductive biomaterial that can synchronize contraction, and restore ventricular

function through electrically connecting isolated cardiomyocytes with the intact tissue, allowing them to improve heart function (Rane and Christman, 2011). Moreover, these biomaterials must provide structural support and the electrical connection between the injured and healthy tissue myocardium (Mihic et al., 2015). For example, chitosan is a biodegradable and biocompatible material that has shown to induce the interconnectivity of cells (Zhang et al., 2014) and improve the cardiac function (Rabbani et al., 2017). Chitosan scaffolds (CS) are able to mimic extracellular matrix-like microenvironment, supportting cardiac cell functions. However, CS scaffold leaks the appropriate electrical connectivity (Mihic et al., 2015), which could be attained by incorporating other materials, such as GO or rGO, that modulate its surface properties. GO has shown to improve the mechanical properties of scaffolds containing cardiac cells, as well as the electrical conductivity of the cardiomycocytes cultures on GO based scaffolds, while enhancing cell attachment, the expression of cardiac-specific markers and improving the functionality of cardiac scaffolds through inducing cell-cell connection and supporting the re-stored of synchronous contractile activity in the scaffolds (Ciriza et al., 2015, Saenz del Burgo et al., 2017 Mar, Park et al., 2015, Jiang et al., 2019).

For example, chitosan- GO, a conductive scaffold with electrical conductivity and porous structure, has shown excellent properties, such as an appropriate swelling, porosity and high conductivity (0.134 S/m), closed to the native cardiac tissue conductivity environment. Chitosan (CS)/GO scaffolds improved in vitro cell viability, cell adhesion, intercellular network formation of cardiac H9C2 cells line. Moreover, cardiac-specific gene and protein expression related with muscle conduction of electrical signals involved in muscle contraction and electrical coupling, such as Connexin-43 or cardiac troponins (cTnT) (Jiang et al., 2019) was upregulated. Although the mechanism of CS/GO conductive scaffold to increase the capacity of cardiac tissue regeneration remains unclear, it has been suggested that the conductivity of these scaffolds has the ability to induce cell alignment, elongation functional maturation, and anisotropy of myocardial cell between different layers (Wu et al., 2017). Moreover, it has been hypothesized that GO improves the cardiac repair by enhancing secretion of reparative paracrine factors and reduced apoptosis of cardiac tissue (Park et al., 2015). Other authors have suggested GO could improve the conductivity of the scaffolds to create suitable signal conduction between the cells and the scaffolds, increasing the extracellular matrix that would continue participating in the transmission of electrical signals among cells, and between cells and scaffolds, forming a benign cycle (Jiang et al., 2019).

rGO has been also incorporated into gelatin methacryloyl (GelMA) hybrid hydrogels, showing a enhancement in electrical conductivity and mechanical properties. Cardiac progenitor cells cultured on this hydrogels improved viability, proliferation and maturation, with stronger contractility and faster spontaeous beating rate, showing that rGO-GelMA cultures had well-defined and more uniaxially aligned sarcomeric structures with homogeneously distributed Cx-43, compared pristine GelMA (Fig. 3). Similarly to bone regenerative medicine, it seems that GO and rGO combined with 3D scaffolds could represent a good alternative in cardiac regenerative medicine. (Shin et al., 2016).

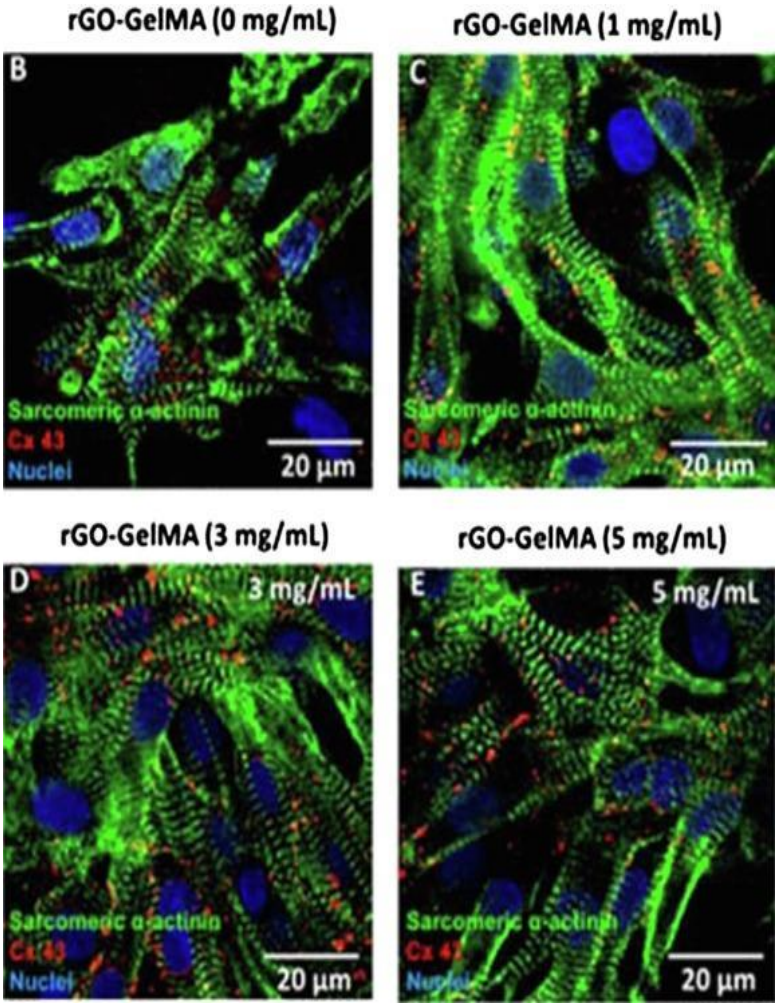

Fig. 3. Images of cardiomyocytes immunostained for sarcomeric α-actinin (green) and connexin 43 (red) after 8 days of culture on pristine GelMA and rGO-GelMA hydrogels at different concentrations of rGO. (B) 0 mg mL^{-1}, (C) 1 mg mL^{-1}, (D) 3 mg mL^{-1}, (E) 5 mg mL^{-1}. Note. nucleus (blue). (Shin et al., 2016 Jul). (For interpretation of the references to colour in this figure legend, the reader is referred to the web version of this article.)

5.3. GO and rGO based scaffolds in neural regeneration

Stem-cell-based therapies represent a promising therapy with a great potential for nerve regeneration, taking advantage of the self-renewal and differentiation capabilities of stem cells (Prabhakaran et al., 2009, Guo et al., 2017). Scaffold for neural tissue engineering should mimic the natural extracellular matrix (ECM) with suitable mechanical properties, biocompatibility, conductivity, and porosity, as well as, cell adhesion and migration (Subramanian et al., 2009). However, natural and synthetic polymers cannot comply all these requirements and make hard to regulate the morphology of the newly generated nerve (Leong et al., 1985). Since neural cells and their activities are electrical-dependent (Akhavan et al., 2014), the electrical properties of GO and rGO can offer an excellent advantage for neuronal stimulation (Wang et al., 2018).

For example, the incorporation of GO with poly (L-lactic-co-glycolic acid) PLGA improves its mechanical properties and mediates at the cell–material and cell–cell interfaces, initiating adhesion, growth, and neuronal differentiation of neuro stem cells (NSCs) on PLGA/GO scaffold. GO is able to increase the binding of insulin-like growth factor 1 (IGF-1) to the scaffold surface, resulting in the improvement of the viability, proliferation, and differentiation of NSCs. (Serrano et al., 2018). Moreover, the electrical stimulation combined with PLGA/GO membrane enhances NSC proliferation and neuronal differentiation on the material surface and promotes significant neurite elongation (Fig. 4) (Fu et al., 2019). In scaffolds of GO/aligned PLLA nanofibrous Schwann and rat pheochromocytoma 12 (PC12) cells improve their proliferation directing the cytoskeleton along the nanofibers more than aligned PLLA without GO nanofibrous scaffolds. PC12 cells also promoted differentiation and neurite growth along the nanofibrous alignment without nerve growth factor (NGF) in GO/aligned PLLA nanofibrous, indicating that GO combined with this scaffold shows better performance in nerve regeneration (Zhang et al., 2016).

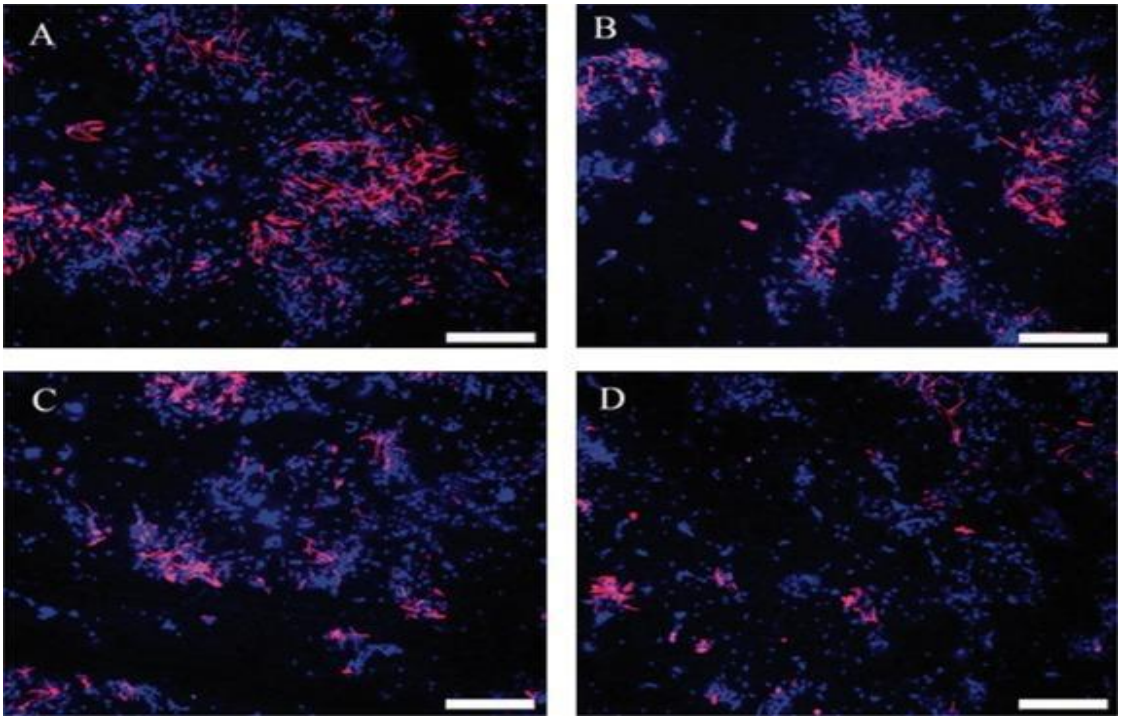

Fig. 4. Immunofluorescence of NSC differentiated into astrocytes scaffold of (A) PLGA, (B) PLGA/GO, C) PLGA + electrical stimulation and (D) PLGA/GO + electrical stimulation. Notes. GFAP (red) and DAPI (blue). Scale bar. 200 μm (Fu et al., 2019). (For interpretation of the references to colour in this figure legend, the reader is referred to the web version of this article.)

On regard of rGO, rat bone-marrow-derived mesenchymal stem cells (MSCs) cultured rGO on the surface of the porcine acellular dermal matrix (PADM) incorporating rGO showed better proliferation, up-regulated the Nestin, Tuj1 and MAP2 protein and gene expression after differentiation. Moreover, rGO integration on the surface of PADM channels, enhanced the conductivity of the scaffold (Guo et al., 2016). MSCs were also tested on rGO–poly(3,4-ethylenedioxythiophene) (rGOPEDOT) scaffolds stimulated with a triboelectric nanogenerator (TENG) providing an output of 300 V and 30 μA. The hybrid scaffold showed electrical conductivity strong mechanically and in vitro MSCs were differentiated into into neural cells, improving the expression of neural-specific proteins and gene expressions (Guo et al., 2016). Other studies with human neural stem cells (hNSCs) cultured on ginseng-rGO sheets showed that differentiation of hNSCs cells into neurons was accelerated due to its higher affinity for electron transfer, as well as, its higher biocompatibility (Akhavan et al., 2014). NSCs cultured on rGO microfibers, prepared through a capillary hydrothermal method have shown also good attachment, proliferation and regulation of NSCs differentiation to form a condensed neural network surrounding the microfiber thanks to the flexible, mechanically strength, surface porosity, biodegradability, and biocompatibility of the rGO microfibers. When coated with neural

adhesive molecules (poly-l-lysine and N-cadherin), these microfibers behave as supportive substrates of highly interconnected cultures composed of neurons and glial cells for up to 21 days, identifying synaptic contacts close to rGO. Interestingly, the colonization by meningeal fibroblasts is dramatically hindered by N-cadherin coating. In vivo studies reveal the feasible implantation of these rGO microfibers as a guidance platform in the injured rat spinal cord, without evident signs of subacute local toxicity. These positive findings boost further investigation at longer implantation times to prove the utility of these substrates as components of advanced therapies for enhancing repair in the damaged central neural tissue including the injured spinal cord (González-Mayorga et al., 2017). These finding shows the great potential of rGO matrixes as promising scaffold for neural tissue engineering (NTE) in nerve regeneration application (Guo et al., 2017).

6. Advantages and drawbacks of GO and rGO -based 3D scaffolds in tissue engineering

Compared to the other porous scaffolds, the GO and rGO 3D-based scaffolds have a strong impact on the proliferation and differentiation of the stem cells used for developing new tissues, such asbone, heart and neurons. The unique characteristics of GO and rGO-based 3D scaffolds enhance the cell proliferation and differentiation by improving cell–cell or cell–scaffold interactions through different cellular signals (chemical or electrical signals) (Geetha Bai et al., 2019), due to their extraordinary chemical and physical properties, their high surface area, excellent mechanical properties, electrical properties, high biocompatibility, cell adhesion and cell proliferation (Agarwal et al., 2010, Advances, 2016, Nayak et al., 2011, Park et al., 2010, Ryoo et al., 2010, Shin et al., 2017). Thus, the incorporation of GO and rGO into the scaffolds represent advantages, such as improving the hydrophilicity of the scaffold, providing the required mechanical strength, improving protein adsorption and stability, improving cell adhesion, proliferation or enhanceing electrical properties of the scaffolds (Park and Ruoff, 2009, Casero et al., 2012, Molina et al., 2013, Sharma et al., 2016, Rose et al., 2015, Morkvenaite-Vilkonciene et al., 2015). In fact, the integration of GO within the scaffold matrix improves the hydrophilicity of the scaffold and the stability of the growth factors adsorbed on those carbon derivatives. For example, the hydrophilicity of PLGA/HA scaffold is significantly improved when GO is integrated within the matrix, giving a water contact angle of 76.4 ± 4.6° in GO-PLGA/HA matrixes, compared to PLGA

and PLGA/HA matrixes, with 102.4 ± 8.4° and 91.4 ± 5.9° water contact angles respectively (Fu et al., 2017). Another advantage is the excellent mechanical properties of GO and rGO- based scaffolds (Novoselov et al., 2012, Huang et al., 2011, Kuila et al., 2011). In fact, alginate scaffolds, which lack mechanical strength, improve their mechanical strength by adding GO within the scaffolds (Ege et al., 2017). Moreover, the incorporation of GO to collagen scaffolds improve its mechanical strength, with the elastic moduli of 14.6 ± 2.8 kPa, 18.8 ± 2.2 kPa, 17.8 ± 1.9 kPa, and 38.7 ± 2.8 kPa for collagen, 1-ethyl-3-(3-dimethylaminopropyl) carbodiimide hydrochloride (EDC) + Collagen, GO + Collagen, and GO-collagen scaffolds, respectively, and promoting the osteogenic differentiation of human MSCs (Kang et al., 2015). Similarly, GO has shown to improve the mechanical properties of scaffolds containing cardiac cells (Norahan et al., 2019). On regard of rGO, its incorporation into gelatin methacryloyl (GelMA) hybrid hydrogels shows an enhancement in mechanical properties (Shin et al., 2016). Likewise, rGO microfibers, prepared through a capillary hydrothermal method, have shown good mechanical strength, surface porosity and biodegradability (Guo et al., 2017).

The electrical conductivity of GO and rGO- based scaffolds has been also extensively studied, being a particular property very important in cardiac culture and neural cell culture. It have been suggested that rGO and GO can improve the conductivity of the scaffolds, therefore creating a suitable signal conduction between cells and scaffolds (Jiang et al., 2019). For example, GO is able to enhance the electrical conductivity of the cardiomycocytes cultures on chitosan (CS)/GO scaffolds (Jiang et al., 2019), similarly to rGO integration on the surface of PADM channels (Guo et al., 2016). Interestingly, MSCs were tested on rGO–poly(3,4-ethylenedioxythiophene) (rGOPEDOT) scaffolds and stimulated with a triboelectric nanogenerator (TENG), providing an output of 300 V and 30 μA, a high electrical conductivity (Guo et al., 2016).

Moreover, the addition of GO or rGO improves the functionality of scaffolds. Due to their high protein adsorption and specific surface area, GO and rGO facilitate the bio-conjugation with proteins, antibodies and DNA fragments within scaffolds (Yang et al., 2017, Simsikova and Sikola, 2017), protecting the adsorbed proteins on GO or rGO against proteolysis (Yan et al., 2014, Simsikova and Sikola, 2017). For example, BMP-2 immobilized in GO-incorporated in PLGA/HA microcarriers improves the cell adhesion and osteogenic diferentiation of MC3T3-E1 cells, due to a higher bioactivity of the BMP-2 delivered by GO-PLGA/HA microcarriers (Fu et al., 2017). But in terms of cell adhesion

and proliferation, GO and rGO also improve these properties when they are included within scaffold matrixes. Thus, the fast adsorption of protein through the π–π interaction between GO and rGO aromatic sides provides a biocompatible environment for cells to adhere and proliferate (Fu et al., 2017). In conclusion, the high chemical stability, biocompatibility and low production cost presents to GO and rGO as an excellent platform to deliver proteins and antibodies, as well to promote cell proliferation, adhesion and differentiation.

But GO and rGO are not all advantages, presenting several drawbacks. In fact, the lack of clarity and inconsistency regarding cytotoxicity, biodistribution, biotransformation or immune response of both compounds remains as an important concern. Up till now, there is a large variation in the physical properties of prepared GO or rGO from different methods or different laboratories, affecting their aforementioned properties. Therefore, finding distinct chemical structures of GO and rGO will determine the future of GO and rGO and their applications in tissue engineering. Regarding GO and rGO cytotoxicity, many factors could be involved including dose, lateral size, and surface charge (Misra et al., 2012, Jastrzębska et al., 2012). For example, doses higher than 50 μg/mL exhibit a high cytotoxicity, decreasing cell adhesion, inducing cell apoptosis and showing presence of the carbon material within lysosomes, mitochondria, endoplasm and the cell nucleus (Wang et al., 2011). The small lateral size particles also increase the cytotoxicity as they easily penetrate cell membrane, well described with rGO particles. Similarly, high density of surface charges seems to promote GO and rGO toxicity. Biodistribution, is another important drawback of these carbon derivatives, since they can be retained inside the body for long time in different body organs, such as lung, liver, spleen and bone marrow (Ou et al., 2016, Zhang et al., 2011), even when applying a pre-coating layer on their surface that slightly decrease their retaining time. Moreover, the high chemical reactivity of GO and rGO can undergo potentially dangerous biotransformation that may change their physicochemical properties, and consequently affect its biomedical applications. It was found that GO is highly reactive against biological fluids such as lung fluids (Qi et al., 2018) and blood plasma (Hu et al., 2017). The biotransformed GO can be formed by adsorbing biomolecules on its surface, forming what it is known as bio-corona. However, this drawback may be advantageous in some cases. For example, the viability of human embryonic lung fibroblasts (HELFs) exposed to bio transformed GO compared to other materials induces lower levels of reactive oxygen species (ROS) (Hu et al., 2017). Finally, inflammatory response and chronic injury against GO and rGO, interfering with normal

physiological functions of important organs, including the respiratory tract, the central nervous system and blood components should be considered as another important bottleneck of this materials (Lv et al., 2018). Another drawback of these scaffolds is higher adsorbability from GO and rGO, due to their higher surface activity and that may affect the scaffolds efficiency. For example, the integration of the GO within alginate-erythropoietin secreting C_2C_{12} myoblasts microcapsules reduce the release of erytrhopoietin (Ciriza et al., 2015). However, pre-coating GO and rGO with FBS or BSA restored the relase of the protein (Saenz del Burgo et al., 2017). But, so far, the cytotoxicity from GO and rGO remains the fundamental drawback of GO and rGO-based 3D scaffolds.

7. Future perspective

The unique properties that GO and rGO have induced in tissue engineering such as strong mechanical strength, high proliferation and differentiation rate show them as very promising tools in the biomedical field in future. However, the leak of clarity and inconsistency regarding cytotoxicity, biodistribution, biotransformation or immune response of both compounds remains as an important concern. Up till now, there are not a distinct chemical structures for the prepared GO or rGO. Currently, there is a large variation in the physical properties of prepared GO or rGO from different methods or different laboratories. These variations affect their cytotoxicity, biodistribution, biotransformation or immune response. Therefore, finding distinct chemical structures of GO and rGO will determine the future of GO and rGO and their applications in tissue engineering. Specific particle size and surface modification of GO and rGO surface should also increase their biocompatibility and reduced their related problems such as cytotoxicity, biodistribution, biotransformation or immune response. Interestingly, integration of GO and rGO within 3D-scaffold matrices could solve this issues.

3D matrixes have great importance in tissue engineering due to its high biocompatibility and its high porosity. However, scaffolds are normally formed from inert polymers and they are unable to develop interactions with the cells, since inherently, they lack cellular adhesion (Safron and Arnold, 2011). The modification of the surface of the scaffolds in order to create more bio- mimic support for the cells can overcome this challenge. In this sense, the modification of these scaffolds through the incorporation of other materials has attracted great interest. On this regard GO and rGO have been incorporated in 3D matrixes to provide bio-mimetic support. Graphene and its derivatives seem to be very

suitable candidates for improving scaffolds surface properties and their mechanical strength, partly due to their excellent mechanical properties (Novoselov et al., 2012, Huang et al., 2011, Kuila et al., 2011). In fact, these materials can help to reinforce the physical characteristics of different materials, such as hydroxyapatite (HAp) and β-tricalcium phosphate (β-TCP). These materials have been developed and researched for their application in biomedicine, due to their extraordinary chemical and physical properties including, high surface area, excellent mechanical properties, super electrical properties, high biocompatibility, cell adhesion and the cell proliferation (Agarwal et al., 2010, Advances, 2016, Nayak et al., 2011, Park et al., 2010, Ryoo et al., 2010, Shin et al., 2017). Although, challenges such as cytotoxicity, biodistribution, biotransformation and immune response remain as concerns for GO and rGO in future tissue engineering applications, their inclusion into scaffolds seems to solve these issues. In fact, it seems that both materials, GO and rGO, combined with 3D matrixes could have a high impact also in the area of tissue engineering, including the development of bones scaffold, cardiac scaffolds and scaffolds for neural regeneration. So far, the integration of GO and rGO within scaffold matrices has shown to improve stem cells adhesion and proliferation (Agarwal et al., 2010, Advances, 2016, Nayak et al., 2011, Park et al., 2010, Ryoo et al., 2010, Shin et al., 2017), promoting the differentiation of MSCs into osteogenic lineages (Lee et al., 2014) and ESCs into cardiomyocytes (Mihic et al., 2015, Wu et al., 2017) or neurons (Palejwala et al., 2016, Akhavan et al., 2014).

Declaration of Competing Interest

The authors declare that they have no known competing financial interests or personal relationships that could have appeared to influence the work reported in this paper.

Acknowledgments

This study was financially supported by the University of the Basque Country UPV/EHU and the Basque Country Government (Grupos Consolidados, No ref. IT907-16). Authors also wish to thank the intellectual and technical assistance from the ICTS “NANBIOSIS”, more specifically by the Drug Formulation Unit (U10) of the CIBER in Bioengineering, Biomaterials & Nanomedicine (CIBER-BBN) at the University of Basque Country (UPV/EHU).

Declaration of Interest Statement

The authors report no conflicts of interest.

References

RSC Advances [Internet]. London. RSC Publishing; 2016 [updated -06-09]. Available from. http.//pubs.rsc.org/en/content/articlelanding/2016/ra/c6ra07414f.

Agarwal, S., Zhou, X., Ye, F., He, Q., Chen, G.C.K., Soo, J., et al., 2010. Interfacing live cells with nanocarbon substrates. Langmuir 26(4), 2244–2247.

Aggarwal, P., Hall, J.B., McLeland, C.B., Dobrovolskaia, M.A., McNeil, S.E., 2009.

Nanoparticle interaction with plasma proteins as it relates to particle biodistribution, biocompatibility and therapeutic efficacy. Adv. Drug Deliv. Rev. 61 (6), 428–437.

Akhavan, O., Ghaderi, E., Abouei, E., Hatamie, S., Ghasemi, E., 2014. Accelerated dif-

ferentiation of neural stem cells into neurons on ginseng-reduced graphene oxide sheets. Carbon 66, 395–406.

Amieva, E.J., López-Barroso, J., Martínez-Hernández, A.L., Velasco-Santos, C., 2016.

Graphene-based materials functionalization with natural polymeric biomolecules. Recent Advances in Graphene Research. 2016 -10-12.

Azizighannad, S., Mitra, S., 2018. Stepwise reduction of graphene oxide (GO) and its effects on chemical and colloidal properties. Sci. Rep. 10083.

Azizighannad, S., Mitra, S., 2018. Stepwise reduction of graphene oxide (GO) and its

effects on chemical and colloidal properties. Sci. Rep. 8 (1), 1–8.

Bai, H., Li, C., Shi, G., 2011. Functional composite materials based on chemically con- verted graphene. Adv. Mater. 1089–1115.

Bao, H., Pan, Y., Ping, Y., Sahoo, N.G., Wu, T., Li,

L., et al., 2011. Chitosan-functionalized graphene

oxide as a nanocarrier for drug and gene delivery.

Small. 7 (11),

1569–1578.

Baradaran, S., Moghaddam, E., Basirun, W.J., Mehrali, M., Sookhakian, M., Hamdi, M., et al., 2014. Mechanical properties and biomedical applications of a nanotube hydroxyapatite-reduced graphene oxide composite. Carbon 69, 32–45.

Bashoor-Zadeh, M., Baroud, G., Bohner, M., 2011. Simulation of the in vivo resorption rate of β-tricalcium phosphate bone graft substitutes implanted in a sheep model. Biomaterials 32 (27), 6362–6373.

Bengtson, Stefan, Knudsen, Kristina B., Kyjovska, Zdenka O., Berthing, Trine, Skaug, Vidar, Levin, Marcus, et al., 2017. Differences in inflammation and acute phase re- sponse but similar genotoxicity in mice following pulmonary exposure to graphene oxide and reduced graphene oxide. PloS one. 12(6), e0178355.

Berger, C., et al., 2004. No title. J. Phys. Chem. 108 (52), 19912.

Berger, C., Song, Z., Li, X., Wu, X., Brown, N., Naud, C., et al., 2006. Electronic con- finement and coherence in patterned epitaxial graphene. Science 312(5777), 1191–1196.

Bradder, P., Ling, S.K., Wang, S., Liu, S., 2011. Dye adsorption on layered graphite oxide.

J. Chem. Eng. Data 56(1), 138–141.

Carrier-bound Immobilized Enzymes. Principles, Application and Design [Internet]. [cited Mar 26, 2019]. Available from. <https.//www.wiley.com/en-us/Carrier

+bound+Immobilized+Enzymes%3A+Principles%2C+Application+and

+Design-p-9783527312320>.

Casero, E., Parra-Alfambra, A.M., Petit-Domínguez, M.D., Pariente, F., Lorenzo, E., Alonso, C., 2012. Differentiation between graphene oxide and reduced graphene by electrochemical impedance spectroscopy (EIS). Electrochem. Commun. 20, 63–66.

Chang, Y., Yang, S., Liu, J., Dong, E., Wang, Y., Cao, A., et al., In vitro toxicity evaluation of graphene oxide on A549 cells. Toxicol Lett., 200(3), 201–210.

Chatterjee, N., Eom, H., Choi, J., 2014 Jan. A systems toxicology approach to the surface functionality control of graphene-cell interactions. Biomaterials 35 (4), 1109–1127.

Chen, K., Lu, G., Chang, J., Mao, S., Yu, K., Cui, S., et al., 2012. Hg(II) ion detection using thermally reduced graphene oxide decorated with functionalized gold nanoparticles.

Anal Chem., 84(9), 4057–4062.

Chowdhury, I., Mansukhani, N.D., Guiney, L.M., Hersam, M.C., Bouchard, D., 2015. Aggregation and Stability of Reduced Graphene Oxide. Complex Roles of Divalent Cations, pH, and Natural Organic Matter. Environmental science & technology 49(18), 10886–10893.

Chung, C., Kim, Y., Shin, D., Ryoo, S., Hong, B.H., Min, D., 2013. Biomedical applications

of graphene and graphene oxide. Acc Chem Res., 46(10), 2211–2224.

Ciriza, J., Saenz del Burgo, L., Virumbrales-Muñoz, M., Ochoa, I., Fernandez, L.J., Orive, G., et al., 2015. Graphene oxide increases the viability of C2C12 myoblasts microencapsulated in alginate. Int. J. Pharm. 493(1-2), 260–270.

Ciriza, J., Saenz del Burgo, L., Gurruchaga, H., Borras, F.E., Franquesa, M., Orive, G., et al., 2018. Graphene oxide enhances alginate encapsulated cells viability and functionality while not affecting the foreign body response. Drug Deliv. 25(1), 1147–1160.

Ciriza, J., Saenz Del Burgo, L., Gurruchaga, H., Borras, F.E., Franquesa, M., Orive, G.,

et al., 2018. Graphene oxide enhances alginate encapsulated cells viability and functionality while not affecting the foreign body response. Drug Deliv. 25 (1), 1147–1160.

de Sousa, M., Martins, C.H.Z., Franqui, L.S., Fonseca, L.C., Delite, F.S., Lanzoni, E.M., et al., 2018. Covalent functionalization of graphene oxide with d-mannose. evaluating the hemolytic effect and protein corona formation. J. Mater. Chem. B 6 (18), 2803–2812.

Dikin, D.A., Stankovich, S., Zimney, E.J., Piner, R.D., Dommett, G.H.B., Evmenenko, G., et al., 2007. Preparation and characterization of graphene oxide paper. Nature 448(7152), 457–460.

Dreyer, D.R., Park, S., Bielawski, C.W., Ruoff, R.S., 2009. The chemistry of graphene oxide. Chem. Soc. Rev., 39(1), 228–24.

Duch, Matthew C., Scott Budinger, G.R., Liang, Yu Teng, Soberanes, Saul, Urich, Daniela, Chiarella, Sergio E., et al., 2011. Minimizing oxidation and stable nanoscale disper- sion improves the biocompatibility of graphene in the lung. Nano Lett. 11(12), 5201–5207.

Ege, D., Kamali, A.R., Boccaccini, A.R., 2017. Graphene oxide/polymer-based biomater-

ials. Adv. Eng.Mater. 19 (12), 1700627.

Emadi, F., Amini, A., Gholami, A., Ghasemi, Y., 2017. Functionalized graphene oxide with chitosan for protein nanocarriers to protect against enzymatic cleavage and retain collagenase activity. Scientific Reports 7(1), 42258.

Feng, L., Liu, Z., 2011. Graphene in biomedicine. opportunities and challenges.
Nanomedicine (Lond). 6 (2), 317–324.
Fu, C., Bai, H., Zhu, J., Niu, Z., Wang, Y., Li, J., et al., 2017. Enhanced cell proliferation and osteogenic differentiation in electrospun PLGA/hydroxyapatite nanofibre scaf- folds incorporated with graphene oxide. PLoS ONE 12 (11), e0188352.
Fu, C., Pan, S., Ma, Y., Kong, W., Qi, Z., Yang, X., 2019. Effect of electrical stimulation
combined with graphene-oxide-based membranes on neural stem cell proliferation and differentiation. Artificial Cells Nanomed. Biotechnol. 47(1), 1867–1876.
Fu, C., Yang, X., Tan, S., Song, L., 2017. Enhancing cell proliferation and osteogenic differentiation of MC3T3-E1 pre-osteoblasts by BMP-2 delivery in graphene oxide-incorporated PLGA/HA biodegradable microcarriers. Sci. Rep. 7 (1), 12549.
Fu, C., Yang, X., Tan, S., Song, L., 2017 Dec. Enhancing cell proliferation and osteogenic
differentiation of MC3T3-E1 pre-osteoblasts by BMP-2 delivery in graphene oxide- incorporated PLGA/HA biodegradable microcarriers. Sci. Rep. 7 (1), 1.
Geetha Bai, R., Muthoosamy, K., Manickam, S., Hilal-Alnaqbi, A., 2019. Graphene-based 3D scaffolds in tissue engineering. fabrication, applications, and future scope in liver tissue engineering. Int. J. Nanomed. 14 5753–5783.
González-Mayorga, A., López-Dolado, E., Gutiérrez, M.C., Collazos-Castro, J.E., Ferrer,
M.L., Monte, F.D., et al., 2017. Favorable biological responses of neural cells and tissue interacting with graphene oxide microfibers. ACS Omega. 2 (11), 8253–8263.
Graphene Oxide. Preparation, Functionalization, and Electrochemical Applications [Internet] [cited Sep 7, 2018]. Available from. https.//pubs.acs.org/doi/ipdf/10. 1021/cr300115g.
Gregorio Mendes, R., Koch, B., Bachmatiuk, A., Ma, X., Sanchez, S., Damm, C., et al., 2015. A size dependent evaluation of the cytotoxicity and uptake of nanographene oxide. J. Mater. Chem. B 3 (12), 2522–2529.
Guangbo Qu, Sijin Liu, Shuping Zhang, Lei Wang, Xiaoyan Wang, Bingbing Sun, et al.,
2013. Graphene oxide induces toll-like receptor 4 (TLR4)-dependent necrosis in macrophages. ACS Nano 7(7), 5732–5745.
Guarnieri, D., Sanchez-Moreno, P., Castillo, Antonio Esau Del Rio, Bonaccorso, F., Gatto,
F., Bardi, G., et al., 2019. Biotransformation and biological impact of graphene and graphene oxide during simulated oral ingestion.
Guarnieri, D., Sanchez-Moreno, P., Castillo, Antonio Esau, Rio, Del, Bonaccorso, F., Gatto, F., Bardi, G., et al., 2019 Mar. Biotransformation and biological impact of graphene and graphene oxide during simulated oral ingestion. Small. 14(24), 1800227.
Guo, W., Qiu, J., Liu, J., Liu, H., 2017. Graphene microfiber as a scaffold for regulation of neural stem cells differentiation. Scientific Reports 7(1), 5678–5678.
Guo, W., Wang, S., Yu, X., Qiu, J., Li, J., Tang, W., et al., 2016. Construction of a 3D rGO–collagen hybrid scaffold for enhancement of the neural differentiation of me- senchymal stem cells. Nanoscale. 8 (4), 1897–1904.
Guo, W., Zhang, X., Yu, X., Wang, S., Qiu, J., Tang, W., et al., 2016. Self-powered elec- trical stimulation for enhancing neural differentiation of mesenchymal stem cells on
graphene–poly(3,4-ethylenedioxythiophene) hybrid microfibers. ACS Nano 10 (5), 5086–5095.
Hassan, M., Walter, M., Moseler, M., 2014. Interactions of polymers with reduced gra- phene oxide. van der Waals binding energies of benzene on graphene with defects. Phys Chem Chem Phys., 16(1), 33–37.
Hassan, M., Walter, M., Moseler, M., 2014. Interactions of polymers with reduced gra- phene oxide. van der Waals binding energies of benzene on graphene with defects. Phys. Chem. Chem. Phys. 16 (1), 33–37.
He, J., Fang, L., 2016. Controllable synthesis of reduced graphene oxide. Curr. Appl Phys.
16 (9), 1152–1158.
Hermenean, A., Codreanu, A., Herman, H., Balta, C., Rosu, M., Mihali, C.V., et al., 2017 Dec. Chitosan-graphene oxide 3D scaffolds as promising tools for bone regeneration in critical-size mouse calvarial defects. Sci. Rep. 7 (1), 1–12.
Hu, W., Peng, C., Luo, W., Lv, M., Li, X., Li, D., et al., 2010. Graphene-based antibacterial
paper. ACS Nano 4(7), 4317–4723.
Hu, X., Li, D., Mu, L., 2017. Biotransformation of graphene oxide nanosheets in blood plasma affects their interactions with cells. Environ Sci. Nano. 4 (7), 1569–1578.
Huang, X., Yin, Z., Wu, S., Qi, X., He, Q., Zhang, Q., et al., 2011. Graphene-based ma- terials. synthesis, characterization, properties, and applications. Small. 7(14), 1876–1902.
Interaction of Graphene Oxide with Proteins and Applications of their Conjugates. J.
Nanomedi. Res. 5(2).
Jastrzębska, A., Kurtycz, P., Olszyna, A., 2012 Dec. Recent advances in graphene family materials toxicity investigations. J. Nanopart Res. 14 (12), 1–21.
Jiang, L., Chen, D., Wang, Z., Zhang, Z., Xia, Y., Xue, H., et al., 2019. Preparation of an electrically conductive graphene oxide/chitosan scaffold for cardiac tissue

engineering. Appl. Biochem. Biotechnol.
Kang, S., Park, J.B., Lee, T., Ryu, S., Bhang, S.H., La, W., et al., 2015. Covalent con- jugation of mechanically stiff graphene oxide flakes to three-dimensional collagen scaffolds for osteogenic differentiation of human mesenchymal stem cells. Carbon 83, 162–172.
Kenry, N., Loh, K.P., Lim, C.T., 2016. Molecular interactions of graphene oxide with human blood plasma proteins. Nanoscale. 8(17), 9425–9441.
Konios, D., Stylianakis, M.M., Stratakis, E., Kymakis, E., 2014. Dispersion behaviour of graphene oxide and reduced graphene oxide. J. Colloid Interface Sci. 430, 108–112.
Konkena, B., Vasudevan, S., 2012. Understanding aqueous dispersibility of graphene oxide and reduced graphene oxide through pKa measurements. J. Phys. Chem. Lett. 3(7), 867.
Kotchey, G.P., Allen, B.L., Vedala, H., Yanamala, N., Kapralov, A.A., Tyurina, Y.Y., et al., 2011 Mar. The enzymatic oxidation of graphene oxide. ACS Nano 5(3), 2098–2108.
Kuchlyan, J., Kundu, N., Banik, D., Roy, A., Sarkar, N., 2015. Spectroscopy and fluores- cence lifetime imaging microscopy to probe the interaction of bovine serum albumin
with graphene oxide. Langmuir. the ACS Journal of Surfaces and Colloids 31(51), 13793–13801.
Kuila, T., Bose, S., Khanra, P., Mishra, A.K., Kim, N.H., Lee, J.H., 2011. Recent advances
in graphene-based biosensors. Biosens Bioelectron. 26(12), 4637–4648.
Lategan, K., Alghadi, H., Bayati, M., de Cortalezzi, M.F., Pool, E., 2018. Effects of gra- phene oxide nanoparticles on the immune system biomarkers produced by RAW 264. 7 and human whole blood cell cultures. Nanomaterials (Basel, Switzerland) 8(2), 125.

Lazauskas, A., Marcinauskas, L., Andrulevicius, M., 2018. Photothermal reduction of
thick graphene oxide multilayer films via direct laser writing. morphology, structural and chemical properties. Superlatt. Microstruct. 122, 36–45.
Lee, D.Y., Khatun, Z., Lee, J., Lee, Y., In, I., 2011. Blood compatible graphene/heparin conjugate through noncovalent chemistry. Biomacromolecules, 12(2), 336–341.
Lee, J.H., Shin, Y.C., Lee, S., Jin, O.S., Kang, S.H., Hong, S.W., et al., 2015. Enhanced osteogenesis by reduced graphene oxide/hydroxyapatite nanocomposites. Scientific Reports. 5(1), 18833.
Lee, T., Park, S., Bhang, S.H., Yoon, J., Jo, I., Jeong, G., et al., 2014. Graphene enhances the cardiomyogenic differentiation of human embryonic stem cells. Biochem.
Biophys. Res. Commun. 452 (1), 174–180.
Lee, S.W., Park, H.J., Van Kaer, L., Hong, S., Hong, S., 2018. Graphene oxide polarizes iNKT cells for production of TGFβ and attenuates inflammation in an iNKT cell- mediated sepsis model. Sci. Rep. 8 (1), 1–12.
Leong, K.W., Brott, B.C., Langer, R., 1985. Bioerodible polyanhydrides as drug-carrier
matrices. I. Characterization, degradation, and release characteristics. J. Biomed. Mater. Res. 19 (8), 941–955.
Li, Bo, Yang, Jianzhong, Huang, Qing, Zhang, Yi, Peng, Cheng, Zhang, Yujie, et al., 2013.
Biodistribution and pulmonary toxicity of intratracheally instilled graphene oxide in mice. NPG Asia Materials 5(4), e44.
Li, Z., Yao, Y., Lin, Z., Moon, K., Lin, W., Wong, C., 2010. Ultrafast, dry microwave synthesis of graphene sheets. J. Mater. Chem. 20 (23), 4781.
Li, B., Zhang, X., Yang, J., Zhang, Y., Li, W., Fan, C., et al., 2014. Influence of polyethylene glycol coating on biodistribution and toxicity of nanoscale graphene oxide in mice after intravenous injection. Int. J. Nanomed. 9, 4697–4707.
Liao, Ken-Hsuan, Lin, Yu-Shen, Macosko, Christopher W., Haynes, Christy L., 2011.
Cytotoxicity of graphene oxide and graphene in human erythrocytes and skin fibro- blasts. ACS Appl Mater Interfaces 3(7), 2607–2615.
Liu, Z., Robinson, J.T., Sun, X., Dai, H., 2008. PEGylated nanographene oxide for delivery of water-insoluble cancer drugs. J. Am. Chem. Soc. 130(33), 10876–7.
Lu, G., Park, S., Yu, K., Ruoff, R.S., Ocola, L.E., Rosenmann, D., et al., 2011. Toward practical gas sensing with highly reduced graphene oxide. a new signal processing method to circumvent run-to-run and device-to-device variations. ACS Nano. 5(2), 1154–1164.
Luo, Y., Shen, H., Fang, Y., Cao, Y., Huang, J., Zhang, M., et al., 2015 Mar. Enhanced proliferation and osteogenic differentiation of mesenchymal stem cells on graphene oxide-incorporated electrospun poly(lactic-co-glycolic acid) nanofibrous mats. ACS Appl Mater Interfaces. 7(11), 6331–6339.
Lv, M., Zhang, Y., Liang, L., Wei, M., Hu, W., Li, X., et al., 2012. Effect of graphene oxide
on undifferentiated and retinoic acid-differentiated SH-SY5Y cells line. Nanoscale 4(13), 3861–3866.
Lv, M., Yan, L., Liu, C., Su, C., Zhou, Q., Zhang, X., et al., 2018. Non-covalent functio-
nalized graphene oxide (GO) adsorbent with an organic gelator for co-adsorption of dye, endocrine-disruptor, pharmaceutical and metal ion. Chem. Eng. J. 349, 791–799.
Ma, J., Liu, R., Wang, X., Liu, Q., Chen, Y., Valle, R.P., et al., 2015. Crucial role of lateral
size for graphene oxide in activating macrophages and stimulating pro-inflammatory responses in cells and animals. ACS Nano. 9(10), 10498–10515.
Mihic, A., Cui, Z., Wu, J., Vlacic, G., Miyagi, Y., Li, S., et al., 2015. A conductive polymer
hydrogel supports cell electrical signaling and improves cardiac function after im- plantation into myocardial infarct. Circulation. 132(8).772–784.
Minitha, C.R., Murugan, L., Jeyachandran, Y., Senthilkumar, L., Rt, R., 2017. Adsorption behaviour of reduced graphene oxide towards cationic and anionic dyes. co-action of electrostatic and π – π interactions.
Misra, S.K., Kondaiah, P., Bhattacharya, S., Rao, C.N.R., 2012. Graphene as a nanocarrier for tamoxifen induces apoptosis in transformed cancer cell lines of different origins. Small, 8(1), 131–143.
Mittal, Sandeep, Kumar, Veeresh, Dhiman, Nitesh, Singh Chauhan, Lalit Kumar, Pasricha,
Renu, Pandey, Alok Kumar, 2016. Physico-chemical properties based differential toxicity of graphene oxide/reduced graphene oxide in human lung cells mediated through oxidative stress. Scientific Reports. 6(1), 39548.
Mittal, S., Kumar, V., Dhiman, N., Chauhan, L.K.S., Pasricha, R., Pandey, A.K., 2016.. Physico-chemical properties based differential toxicity of graphene oxide/reduced
graphene oxide in human lung cells mediated through oxidative stress. Sci. Rep. 39548.
Mohan, V.B., Brown, R., Jayaraman, K., Bhattacharyya, D., 2015. Characterisation of reduced graphene oxide. effects of reduction variables on electrical conductivity. Mater. Sci. Eng. B 193, 49–60.
Mohan, V.B., Lau, K., Hui, D., Bhattacharyya, D., 2018. Graphene-based materials and their composites. a review on production, applications and product limitations.
Compos. B Eng. 142, 200–220.
Molina, J., Fernández, J., Inés, J.C., del Río, A.I., Bonastre, J., Cases, F., 2013.
Electrochemical characterization of reduced graphene oxide-coated polyester fabrics. Electrochim. Acta 93, 44–52.
Morkvenaite-Vilkonciene, I., Genys, P., Ramanaviciene, A., Ramanavicius, A., 2015.
Scanning electrochemical impedance microscopy for investigation of glucose oxidase catalyzed reaction. Colloids Surf., B 126, 598–602.
Mu, Q., Su, G., Li, L., Gilbertson, B.O., Yu, L.H., Zhang, Q., et al., 2012. Size-dependent cell uptake of protein-coated graphene oxide nanosheets. ACS Appl. Mater Interfaces 4 (4), 2259–2266.
Nayak, T.R., Andersen, H., Makam, V.S., Khaw, C., Bae, S., Xu, X., et al., 2011. Graphene for controlled and accelerated osteogenic differentiation of human mesenchymal stem cells. ACS Nano, 5(6), 4670–4678.
Nombela-Arrieta, C., Ritz, J., Silberstein, L.E., 2011. The elusive nature and function of mesenchymal stem cells. Nat. Rev. Mol. Cell Biol. 12 (2), 126–131.
Norahan, M.H., Amroon, M., Ghahremanzadeh, R., Mahmoodi, M., Baheiraei, N., 2019.
Electroactive graphene oxide-incorporated collagen assisting vascularization for cardiac tissue engineering. J. Biomed. Mater. Res. Part A 107 (1), 204–219.
K.S. Novoselov, V.I. Fal'ko, L. Colombo, P.R. Gellert, M.G. Schwab, K. Kim, 2012. A roadmap for graphene. Nature 11, 490(7419).192.
Oliveira, S.F., Bisker, G., Bakh, N.A., Gibbs, S.L., Landry, M.P., Strano, M.S., 2015. Protein
functionalized carbon nanomaterials for biomedical applications. Carbon 95, 767–779.

Ou, L., Song, B., Liang, H., Liu, J., Feng, X., Deng, B., et al., 2016. Toxicity of graphene-
family nanoparticles. a general review of the origins and mechanisms. Part Fibre Toxicol. 13(1), 57.
Oxidative Stress and Mitochondrial Activation as the Main Mechanisms Underlying Graphene Toxicity against Human Cancer Cells [Internet]. Hindawi; 2016 [cited Sep 13, 2018]. Available from. https.//www.hindawi.com/journals/omcl/2016/5851035/.
Palejwala, A.H., Fridley, J.S., Mata, J.A., Samuel, E.L.G., Luerssen, T.G., Perlaky, L., et al.,
2016. Biocompatibility of reduced graphene oxide nanoscaffolds following acute spinal cord injury in rats. Surg. Neurol Int 8-23;7.
Paredes Juárez, G.A., Spasojevic, M., Faas, M.M., de Vos, P., 2014. Immunological and
technical considerations in application of alginate-based microencapsulation systems. Front. Bioeng. Biotechnol.
Park, S., An, J., Jung, I., Piner, R.D., An, S.J., Li, X., et al., 2009. Colloidal suspensions of highly reduced graphene oxide in a wide variety of organic solvents. Nano Lett. 9(4), 1593–1597.
Park, J., Kim, B., Han, J., Oh, J., Park, S., Ryu, S., et al., 2015. Graphene oxide flakes as a cellular adhesive. prevention of reactive oxygen species mediated death of implanted
cells for cardiac repair. ACS Nano. 9(5), 4987–4999.
Park, S., Ruoff, R.S., 2009. Chemical methods for the production of graphenes. Nat.
Nanotechnol. 4 (4), 217–224.
Park, S., Mohanty, N., Suk, J.W., Nagaraja, A., An, J., Piner, R.D., et al., 2010.
Biocompatible, robust free-standing paper composed of a TWEEN/graphene compo- site. Adv Mater Weinheim 22(15), 1736–1740.
Pei, S., Cheng, H., 2012. The reduction of graphene oxide. Carbon 50 (9), 3210–3228.
Peng, B., Chen, L., Que, C., Yang, K., Deng, F., Deng, X., et al., 2016. Adsorption of antibiotics on graphene and biochar in aqueous solutions induced by π-π interactions. Scientific Reports. 6(1), 31920.
Pham Viet Hung, V.H., 2010. One-step synthesis of superior dispersion of chemically converted graphene in organic solvents. Chem.Commun. 46(24), 4375–7.
Pokharel, P., Lee, D.S., 2014. Thermal and mechanical properties of reduced graphene oxide/polyurethane nanocomposite. J. Nanosci. Nanotechnol. 14 (8), 5718–5721.
Prabhakaran, M.P., Venugopal, J.R., Ramakrishna, S., 2009. Mesenchymal stem cell differentiation to neuronal cells on electrospun nanofibrous substrates for nerve tissue engineering. Biomaterials 30 (28), 4996–5003.
Purkait, T., Singh, G., Kumar, D., Singh, M., Dey, R.S., 2018. High-performance flexible supercapacitors based on electrochemically tailored three-dimensional reduced graphene oxide networks. Scientific Reports. 8(1), 640–613.
Qi, Yu, Liu, Yun, Xia, Tian, Xu, An, Liu, Sijin, Chen, Wei, 2018. The biotransformation of
graphene oxide in lung fluids significantly alters its inherent properties and bioac- tivities toward immune cells. NPG Asia Mater. 10(5), 385–396.
Rabbani, S., Soleimani, M., Imani, M., Sahebjam, M., Ghiaseddin, A., Nassiri, S.M., et al.,
2017. Regenerating heart using a novel compound and human wharton jelly me- senchymal stem cells. Arch. Med. Res. 48 (3), 228–237.
Raidongia, K., Tan, A.T.L., Huang, J., 2014. Chapter 14 – graphene oxide. some new insights into an old material. Carbon Nanotubes and Graphene (Second Edition), 341–374.
Rane, A.A., Christman, K.L., 2011. Biomaterials for the treatment of myocardial infarc- tion. a 5-year update. J. Am. Coll. Cardiol. 58 (25), 2615–2629.
Rose, A., Raghavan, N., Thangavel, S., Uma Maheswari, B., Nair, D.P., Venugopal, G., 2015. Investigation of cyclic voltammetry of graphene oxide/polyaniline/poly- vinylidene fluoride nanofibers prepared via electrospinning. Mater. Sci. Semicond. Process. 31, 281–286.
Royal Society of Chemistry (Great Britain). RSC Adv. 4(93), 51624–51631.
Ruschitzka, F., Abraham, W.T., Singh, J.P., Bax, J.J., Borer, J.S., Brugada, J., et al., 2013. Cardiac-resynchronization therapy in heart failure with a narrow QRS complex. N
Engl. J. Med. 369 (15), 1395–1405.
Russier, J., Treossi, E., Scarsi, A., Perrozzi, F., Dumortier, H., Ottaviano, L., et al., 2013.
Evidencing the mask effect of graphene oxide. a comparative study on primary human and murine phagocytic cells. Nanoscale 5(22).11234–11247.
Ryoo, S., Kim, Y., Kim, M., Min, D., 2010. Behaviors of NIH-3T3 fibroblasts on graphene/ carbon nanotubes. proliferation, focal adhesion, and gene transfection studies. ACS Nano., 4(11), 6587–6598.
Saenz del Burgo, L., Ciriza, J., Acarregui, A., Gurruchaga, H., Blanco, F.J., Orive, G., et al., 2017 Mar. Hybrid alginate–protein-coated graphene oxide microcapsules enhance the functionality of erythropoietin secreting C2C12 myoblasts. Mol. Pharm. 14(3), 885–898.
Safron, N.S., Arnold, M.S., 2011. Characterization of conduction mechanisms relevant to
device performance in nanoperforated graphene. Int J Hi Spe Ele Syst 20(03), 697–706.
Sasidharan, A., Panchakarla, L.S., Sadanandan, A.R., Ashokan, A., Chandran, P., Girish, C.M., et al., 2012 Apr. Hemocompatibility and macrophage response of pristine and functionalized graphene. Small. 8(8), 1251–1263.
Serrano, M.C., Feito, M.J., González-Mayorga, A., Diez-Orejas, R., Matesanz, M.C., Portolés, M.T., 2018. Response of macrophages and neural cells in contact with re-
duced graphene oxide microfibers. Biomater. Sci. 6(11), 2987–2997.
Sharma, D., Kanchi, S., Sabela, M.I., Bisetty, K., 2016. Insight into the biosensing of graphene oxide. present and future prospects. Arabian J. Chem. 9 (2), 238–261.
Shen, J., Shi, M., Yan, B., Ma, H., Li, N., Hu, Y., et al., 2010. Covalent attaching protein to graphene oxide via diimide-activated amidation. Colloids Surf B Biointerfaces 81(2),
434–438.
Shin, H., Kim, K.K., Benayad, A., Yoon, S., Park, H.K., Jung, I., et al., 2009. Efficient reduction of graphite oxide by sodium borohydride and its effect on electrical con- ductance. Adv. Funct. Mater. 19(12), 1987–1992.
Shin, Y.C., Kim, J., Kim, S.E., Song, S., Hong, S.W., Oh, J., et al., 2017. RGD peptide and graphene oxide co-functionalized PLGA nanofiber scaffolds for vascular tissue en- gineering. Regenerative Biomater 4(3), 159–66.
Shin, S.R., Zihlmann, C., Akbari, M., Assawes, P., Cheung, L., Zhang, K., et al., 2016 Jul. Reduced graphene oxide-GelMA hybrid hydrogels as scaffolds for cardiac tissue engineering. Small 12 (27), 3677–3689.
Shurin, M.R., Yanamala, N., Kisin, E.R., Tkach, A.V., Shurin, G.V., Murray, A.R., et al.,
2014 Jun. Graphene oxide attenuates Th2-type immune responses, but augments airway remodeling and hyperresponsiveness in a murine model of asthma. ACS Nano 8(6), 5585–5599.

Šimšíková, M., 2016. Interaction of graphene oxide with albumins. Effect of size, pH, and temperature. Arch Biochem Biophys. 593, 69–79.
Simsikova, M., Sikola, T., 2017. Interaction of graphene oxide with proteins and appli-
cations of their conjugates. J. Nanomed. Res., 5(2), 1–0.
Singh, S.K., Singh, M.K., Nayak, M.K., Kumari, S., Shrivastava, S., Grácio, J.J.A., et al., 2011. Thrombus inducing property of atomically thin graphene oxide sheets. ACS Nano 5(6), 4987–4996.
Singh, Sunil K., Singh, Manoj K., Kulkarni, Paresh P., Sonkar, Vijay K., Grácio, José J.A., 2012. Debabrata Dash. Amine-Modified Graphene. Thrombo-Protective Safer Alternative to Graphene Oxide for Biomedical Applications. ACS nano. 6(3), 2731–2740.
Singh, S.K., Singh, M.K., Kulkarni, P.P., Sonkar, V.K., Grácio, J.J.A., Dash, D., 2012 Mar.
Amine-modified graphene. thrombo-protective safer alternative to graphene oxide for biomedical applications. ACS Nano 6(3), 2731–2740.
Sitko, R., Turek, E., Zawisza, B., Malicka, E., Talik, E., Heimann, J,, et al., 2013.
Adsorption of divalent metal ions from aqueous solutions using graphene oxide. Dalton transactions (Cambridge, England . 2003), 42(16), 5682–5689.
Srikanth, K., Sundar, L.S., Pereira, E., Duarte, A.C., 2018 Apr. Graphene oxide induces cytotoxicity and oxidative stress in bluegill sunfish cells. J. Appl. Toxicol. 38 (4), 504–513.
Stankovich, S., Dikin, D.A., Piner, R.D., Kohlhaas, K.A., Kleinhammes, A., Jia, Y., et al., 2007. Synthesis of graphene-based nanosheets via chemical reduction of exfoliated
graphite oxide. Carbon 45 (7), 1558–1565.
Subramanian, A., Krishnan, U.M., Sethuraman, S., 2009. Development of biomaterial scaffold for nerve tissue engineering. Biomaterial mediated neural regeneration. J. Biomed. Sci. 16(1), 108.
Suk, J.W., Piner, R.D., An, J., Ruoff, R.S., 2010. Mechanical properties of monolayer
graphene oxide. ACS Nano, 4(11), 6557–6564.
Tabish, T., Pranjol, Z., Hayat, H., Rahat, A., Abdullah, T., L Whatmore, J., et al., 2017. In vitro toxic effects of reduced graphene oxide nanosheets on lung cancer cells.
Tan, K.H., Sattari, S., Beyranvand, S., Faghani, A., Ludwig, K., Schwibbert, K., et al., 2019.
Thermoresponsive amphiphilic functionalization of thermally reduced graphene oxide to study graphene/bacteria hydrophobic interactions. Langmuir 35 (13), 4736–4746.
Tang, S., Cao, Z., 2011. Adsorption of nitrogen oxides on graphene and graphene oxides. insights from density functional calculations. J. Chem. Phys., 134(4), 044710.
Turhani, D., Weissenböck, M., Watzinger, E., Yerit, K., Cvikl, B., Ewers, R., et al., 2005 Jul. Invitro study of adherent mandibular osteoblast-like cells on carrier materials. Int J Oral Maxillofac Surg. 34 (5), 543–550.
View Journal | View Issue. PAPER View Article Online. Environ Sci. Nano. 2018-10- 11;5(10).2357-67.
Wang, Y., Chen, Y., Lacey, S.D., Xu, L., Xie, H., Li, T., et al., 2018. Reduced graphene oxide film with record-high conductivity and mobility. Mater. Today 21 (2), 186–192.
Wang, X., Zhi, L., Müllen, K., 2008. Transparent, conductive graphene electrodes for dye- sensitized solar cells. Nano Lett. 8(1), 323–327.
Wang, K., Ruan, J., Song, H., Zhang, J., Wo, Y., Guo, S., et al., 2010. Biocompatibility of Graphene Oxide.
Wang, L., Fan, H., Zhang, Z., Lou, A., Pei, G., Jiang, S., et al., 2010 Dec. Osteogenesis and angiogenesis of tissue-engineered bone constructed by prevascularized β-tricalcium phosphate scaffold and mesenchymal stem cells. Biomaterials 31 (36), 9452–9461.
Wang, A., Pu, K., Dong, B., Liu, Y., Zhang, L., Zhang, Z., et al., 2013 Oct. Role of surface
charge and oxidative stress in cytotoxicity and genotoxicity of graphene oxide to- wards human lung fibroblast cells. J. Appl. Toxicol. 33 (10), 1156–1164.
Wang, E.A., Rosen, V., D'Alessandro, J.S., Bauduy, M., Cordes, P., Harada, T., et al., 1990
Mar. Recombinant human bone morphogenetic protein induces bone formation. Proc Natl Acad Sci USA 87 (6), 2220–2224.
Wang, K., Ruan, J., Song, H., Zhang, J., Wo, Y., Guo, S., et al., 2011 Dec. Biocompatibility of graphene oxide. Nanoscale Res Lett. 6 (1), 1–8.
Wen, K., Chen, Y., Chuang, C., Chang, H., Lee, C., Tai, N., 2015 Oct. Accumulation and
toxicity of intravenously-injected functionalized graphene oxide in mice. J. Appl. Toxicol. 35 (10), 1211–1218.
Wu, Y., Wang, L., Guo, B., Ma, P.X., 2017. Interwoven aligned conductive nanofiber yarn/ hydrogel composite scaffolds for engineered 3D cardiac anisotropy. ACS nano 11(6), 5646–5659.
Xu, M., Zhu, J., Wang, F., Xiong, Y., Wu, Y., Wang, Q., et al., 2016. Improved in vitro and in vivo biocompatibility of graphene oxide through surface modification. poly(acrylic
acid)-functionalization is superior to PEGylation. ACS Nano., 10(3), 3267–3281.
Xu, X., Mao, X., Wang, Y., Li, D., Du, Z., Wu, W., et al., 2018. Study on the interaction of graphene oxide–silver nanocomposites with bovine serum albumin and the formation of nanoparticle-protein corona. Int. J. Biol. Macromol.
Yan, H., Tao, X., Yang, Z., Li, K., Yang, H., Li, A., et al., 2014. Effects of the oxidation
degree of graphene oxide on the adsorption of methylene blue. J. Hazard Mater. 268, 191–198.
Yan, L., Zhao, F., Li, S., Hu, Z., Zhao, Y., 2011. Low-toxic and safe nanomaterials by surface-chemical design, carbon nanotubes, fullerenes, metallofullerenes, and gra- phenes. Nanoscale 3 (2), 362–382.
Yang, K., Wan, J., Zhang, S., Zhang, Y., Lee, S., Liu, Z., 2011. In vivo pharmacokinetics,
long-term biodistribution, and toxicology of PEGylated graphene in mice. ACS Nano. 5(1), 516–522.
Yang, P., Liu, Q., Liu, J., Zhang, H., Li, Z., Li, R., et al. Bovine Serum albumin-coated graphene oxide for effective adsorption of uranium(VI) from aqueous solutions. Ind Eng Chem Res. 56(13), 3588–3598.
Yang, K., Gong, H., Shi, X., Wan, J., Zhang, Y., Liu, Z., 2013. In vivo biodistribution and
toxicology of functionalized nano-graphene oxide in mice after oral and in- traperitoneal administration. Biomaterials 34 (11), 2787–2795.

Yu, S., Wang, X., Ai, Y., Liang, Y., Ji, Y., Li, J., et al., 2016. Spectroscopic and theoretical studies on the counterion effect of Cu(ii) ion and graphene oxide interaction with titanium dioxide. Environ Sci . Nano. 3 (6), 1361–1368. Zhang, X., Yin, J., Peng, C., Hu, W., Zhu, Z., Li, W., et al., 2011. Distribution and bio- compatibility studies of graphene oxide in mice after intravenous administration. Carbon 49 (3), 986–995.
Zhang, K., Zheng, H., Liang, S., Gao, C., 2016. Aligned PLLA nanofibrous scaffolds coated with graphene oxide for promoting neural cell growth. Acta Biomater. 37, 131–142.
Zhao, J., Liu, Y., Sun, W., Zhang, H., 2011 Dec. Amorphous calcium phosphate and its
application in dentistry. Chem. Cent. J. 5 (1), 1–7.

Zhao, G., Wen, T., Chen, C., Wang, X., 2012. Synthesis of graphene-based nanomaterials and their application in energy-related and environmental-related areas. RSC Adv. 2 (25), 9286.
Zhou, S., Bongiorno, A., 2013. Origin of the chemical and kinetic stability of graphene oxide. Sci. Rep. 3 (1), 2484.

Yue, H., Wei, W., Yue, Z., Wang, B., Luo, N., Gao, Y., et al., 2012 Jun. The role of the
3186.

lateral dimension of graphene oxide in the regulation of cellular responses. Biomaterials 33 (16), 4013–4021.
Zhang, Y., Ali, S.F., Dervishi, E., Xu, Y., Li, Z., Casciano, D., et al., 2010. Cytotoxicity
effects of graphene and single-wall carbon nanotubes in neural phaeochromocytoma- derived PC12 cells. ACS Nano. 4(6), 3181–

Appendix 2

BSA- and Elastin-Coated GO, but Not Collagen-Coated GO, Enhance the Biological Performance of Alginate Hydrogels

Pharmaceutics **2020**, *12*(6), 543.

IF 6.321 (2020)

CATEGORY: PHARMACOLOGY & PHARMACY

Rank 29/276 (Q1)

https://doi.org/10.3390/pharmaceutics12060543

BSA- and Elastin-Coated GO, but Not Collagen- Coated GO, Enhance the Biological Performance of Alginate Hydrogels

Ahmed Raslan 1,2,†,Laura Saenz del Burgo 1,2,†,Albert Espona-Noguera 1,2 ,Ana María Ochoa de Retana 3,María Luisa Sanjuán 4,Alberto Cañibano-Hernández 1,2 ,Patricia Gálvez-Martín 5 ,Jesús Ciriza 1,2,* andJose Luis Pedraz 1,2,*

[1] NanoBioCel Group, Laboratory of Pharmacy and Pharmaceutical Technology, Faculty of Pharmacy, University of the Basque Country UPV/EHU, 01006 Vitoria-Gasteiz, Spain; drrayad@gmail.com (A.R.); laura.saenzdelburgo@ehu.eus (L.S.d.B.); albertesponanoguera@gmail.com (A.E.-N.); albertocanibano@gmail.com (A.C.-H.)

[2] Biomedical Research Networking Center in Bioengineering, Biomaterials, and Nanomedicine,

CIBER-BBN, 28029 Madrid, Spain

[3] Department of Organic Chemistry I, Faculty of Pharmacy and Lascaray Research Center, University of the Basque Country (UPV/EHU), Paseo de la Universidad 7,

01006 Vitoria, Spain; anamaria.ochoaderetana@ehu.eus

[4] Instituto de Ciencia de Materiales de Aragón (Universidad de Zaragoza-CSIC), Facultad de Ciencias, 50009 Zaragoza, Spain; sanjuan@unizar.es

[5] R&D Human Health, Bioibérica S.A.U., 08029 Barcelona E-, Spain; pgalvez@bioiberica.com

***** Correspondence. jesus.ciriza@ehu.eus or jeciriza@gmail.com (J.C.); joseluis.pedraz@ehu.eus (J.L.P.);

Abstract.

The use of embedded cells within alginate matrices is a developing technique with great clinical applications in cell-based therapies. However, one feature that needs additional investigation is the improvement of alginate-cells viability, which could be achieved by integrating other materials with alginate to improve its surface properties. In recent years, the field of nanotechnology has shown the many properties of a huge number of materials. Graphene oxide (GO), for instance, seems to be a good choice for improving alginate cell viability and functionality. We previously observed that GO, coated with fetal bovine serum (FBS) within alginate hydrogels, improves the viability of embedded myoblasts. In the current research, we aim to study several proteins, specifically bovine serum albumin (BSA), type I collagen and elastin, to discern their impact on the previously observed improvement on embedded myoblasts within alginate hydrogels containing GO coated with FBS. Thus, we describe the mechanisms of the formation of BSA, collagen and elastin protein layers on the GO surface, showing a high adsorption by BSA and elastin, and a decreasing GO impedance and capacitance. Moreover, we described a better cell viability and protein release from embedded cells within hydrogels containing protein-coated GO. We conclude that these hybrid hydrogels could provide a step forward in regenerative medicine.

Keywords. graphene oxide; bovine serum albumin; type I collagen; elastin; alginate hydrogels; cell viability

1. Introduction

Hydrogels are 3D structures capable of supporting living cells and creating a suitable microenvironment that enables cells to maintain their viability. Hydrogels are characterized by excellent properties, such as having enough porosity to allow for the exchange of nutrients and oxygen inside, while releasing waste products and therapeutic proteins outside. Moreover, hydrogels provide protection to embedded cells from the immune system, avoiding their rejection [1] Alginate is the most popular natural biomaterial used in the performance of the aforementioned hydrogels for tissue engineering, due to its high biocompatibility and ease of performance. Alginate hydrogels have been extensively studied for wound healing, drug delivery, cell-based therapies and tissue engineering applications. Although alginate hydrogels retain a structure similar to the extracellular 3D structure [2,3] this inert polymer is unable to mimic interactions with cells, since it inherently lacks cellular adhesion [4]. Therefore, the modification of the alginate surface in order to create a closer bio-mimic support for embedded cells is desired.

In the last few years, the incorporation of nanotechnology into a huge number of materials has shown the improvement of their properties. Thus, for example, graphene oxide (GO), the most studied graphene derivative, has been incorporated into alginate matrices to provide bio-mimetic support, suggesting that is a suitable candidate for the improvement of alginate surface properties and mechanical strength, partly due to its excellent mechanical properties [5–7]. In fact, graphene and its derivates can reinforce the physical characteristics of different materials, such as thermoplastic polyurethane [8], hydroxyapatite (HAp) and β-tricalcium phosphate (β-TCP) [9]. GO has also been shown to be a good candidate in the development of drug delivery systems, gene therapy or in the improvement of contrast substances for diagnostic images [10–13].

GO is produced by the oxidation and exfoliation of natural graphite powder, using various oxidizing agents in a strong acid medium, this being the traditional synthesis method developed by Hummers and colleagues [14]. It shows unique properties, such as high specific surface area (890 $m^2\ g^{-1}$) [15] and mechanical strength (Young's modulus of ~1.0 and breaking strength of~130 GPa) [16]. Moreover, the oxidation procedure from graphene to generate GO, provides the material with a high

hydrophilicity. In fact, GO is formed by abundant oxygenated groups, such as hydroxyl and epoxy groups on the basal plane, with slight amounts of carboxyl, carbonyl, phenol, lactone and quinone [13], clearly observed by FT-IR spectroscopy [14–16]. These groups facilitate the formation of the stable dispersion of the graphene derivate in aqueous media and other polar solvents [17–19], also allowing biochemical and bio-conjugation reactions on its basal plane and edges [20]. These reactions facilitate the functionalization of the GO surface with proteins, antibodies and DNA fragments [21,22], providing a wide number of biological applications [23]. Moreover, GO can adsorb proteins and antibodies, providing them with stability against proteolysis [24,25], resulting in an effective platform for protein delivery [26] or biosensors [27,28]. Depending on GO morphology, hydrophobicity [25] and the type of adsorbed protein [25], physical or chemical adsorption on GO can be involved in the adsorption of those proteins. Physical adsorption includes hydrophobic interaction, Van der Waals forces, electrostatic interactions and hydrogen bonds [25,29,30]. Protein adsorption on the GO surface mostly occurs via hydrophobic–hydrophobic interactions through the sp2 hybridization of GO [31], with a high affinity for the hydrophobic carbon lattice from the hydrophobic domain of proteins [32]. Van der Waals forces also play an important role in the adsorption of hydrophobic drugs or nanocomposites [27], while electrostatic interactions are generated at lower pH than 6.0 [28]. Hydrogen bonds are particularly described in the adsorption of gases, such as nitrogen oxides, with the formation of hydrogen bonds OH···O (N), between –OH and nitrogen oxides [33]. Moreover, π–π stacking interactions have been described due to the abundant π electrons on the basal plane of the GO surface [30]. On the other hand, the chemical adsorption of proteins on GO provides stability to the proteins against heat, pH and organic solvents [34]. However, this interaction alters the protein structure, decreasing protein functionality or enzymatic activity [35]. However, current studies regarding cytotoxicity with graphene and its derivates are contradictory [36,37]. While some studies reported that GO has no effects on cell behavior at certain doses [38,39], others demonstrated that GO can induce cellular damage [40,41]. On one hand, some studies reported that GO has no effects on the behavior of cells [38,39], such as the high hemocompatibility of pristine and functionalized graphene, even at high concentrations, with red blood cells, platelets and plasma coagulation pathways, the mediation of the activation of cytokines, [38] or on the lack of cytotoxicity of GO at low doses in A549 cells [42]. On the other hand, other

studies have demonstrated that this material could induce cellular damage [40,41], such as mitochondrial toxicity and the cell membrane damage of neuronal PC12 cells in a dose-dependent manner with high cytotoxicity even at low concentrations [43] or the cytotoxicity and oxidative stress detected in BF-2 cells at low GO concentrations after 24 h of incubation [44,45]. However, another study demonstrated that low concentrations of GO (≤20 µg/mL) do not show toxicity on human fibroblast cells, while concentrations over 50 µg/mL decrease cell adhesion, induce cell apoptosis and show carbon material within the lysosomes, mitochondrion, endoplasm and cell nucleus [46]. We have also reported that concentrations between 25 and 50 µg/mL GO improve the viability, metabolic activity and membrane integrity of alginate encapsulated myoblasts [10,47,48]. Nevertheless, we also detected adsorption on the GO surface, precluding the release of the studied therapeutic protein, erythropoietin (EPO). We hypothesized that adsorption could occur probably via electrostatic interactions and the formation of hydrogen bonds with oxygenated groups from GO. In addition, the presence of surface defects on the GO surface could also act as active sites where the EPO molecules would be adsorbed. We were able to block the adsorption of EPO by previously incubating GO platelets with fetal bovine serum (FBS), which also further improved the viability of encapsulated cells.

Following our previous results, we aimed to discern a protein that could prevent the adsorption by GO, instead of using a complex mixture of unknown proteins, such as FBS, and describe and characterize which processes could be involved in the interaction between the selected proteins and GO platelets. Therefore, we have deeply characterized the interaction with three proteins—bovine serum albumin (BSA), type I collagen and elastin—next studying their biological outcomes for embedded myoblasts within alginate hydrogels in the presence of selected protein-coated GO platelets.

2. Materials and Methods

2.1 Materials

GO suspension was purchased from Graphenea (San Sebastián, Spain). In order to avoid the formation of aggregates, the suspension was diluted to 250 ug/mL in deionized water and sonicated for 1 h before use. BSA, collagen, calciu]m sulphate and mannitol were purchased from Sigma Aldrich (St. Louis, MO, USA). Elastin was provided by

Bioiberica (Barcelona, Spain). Ultrapure low-viscosity and high guluronic (LVG) sodium alginate was purchased from FMC Biopolymer (Sandvika, Norway). Glacial acetic acid was supplied by Panreac. FBS, L-glutamine, Dulbecco's phosphate-buffered saline (DPBS) and the antibiotic/antimycotic solution were purchased from Gibco. Trypsin-EDTA was purchased from Life Technologies (Carlsbad, CA, USA).

2.2 Characterization of GO-Protein Interactions

GO (250 µg/mL) was dispersed in either a BSA solution (900 µg/mL), collagen solution (315 µg/mL) or elastin solution (900 µg/mL). These mixtures were incubated for 2 h at 37 °C. Then, the samples were centrifuged at 14,000 rpm for 15 min and lyophilized in a lyobeta 15 Telstar. The GO and proteins alone were also analyzed in parallel. All of the samples were analyzed in triplicate. Thus, FT-IR spectroscopy measurements were performed with a BRUKER IFS 66/S Spectrometer (Bruker, Billerica, MA, USA), using 32 scans with a resolution of 4 (cm^{-1}) in 4000–400 cm^{-1} regions. The Raman spectrum was acquired using a Confocal Raman Imaging Alpha 300 M (Company WITEC) with a 532 nm laser (1 m W laser power, 50× microscope objective, an exposure time of 50 s, and four accumulations).

2.3 Adsorption Capacity Experiments

2.3.1 Effect of Initial Concentration

In order to study the effect of the initial concentration (C_0) of selected proteins on the GO adsorption capacity (qe), sequential protein concentrations from 0 to 2 mg/mL were incubated with a GO suspension (250 µg/mL) for 2 h at 37 °C. The resulting GO-protein suspensions were centrifuged at 14,000 rpm for 15 min. Then, the quantification of non-adsorbed protein was determined from the supernatant using a BCA kit (Thermo Fisher, Waltham, MA, USA). Absorbance was read at 562 nm on a M 200 TECAN Microplate reader (TECAN Trading AG, Männedorf, Switzerland). Each experiment was performed in triplicate. The percentages of adsorbed proteins were calculated according to Equation (1) and the adsorption capacity qe (µg/µg) was calculated using Equation (2).

$$\text{Adsorption capability (\%)} = \frac{(C0 - Ce) \times 00}{C0} \quad (1)$$

$$\text{Adsorption capacity } qe = \frac{(C0 - Ce) \times V}{W} \quad (2)$$

Where C_0 (µg/mL) and C_e (µg/mL) are the initial and final protein concentrations, respectively; V is the volume of the samples (0.1 mL) and W is the mass of GO (250 µg).

2.3.2 Adsorption Isotherms

Langmuir and Freundlich adsorption models were applied to study the adsorption isotherm.

The Langmuir equation is expressed as follows in Equations (3) and (4).

$$Ce/qe = Ce/qmax + 1/(qmax.\ KL) \quad (3)$$

$$RL = 1/(1 + KL \times C0) \quad (4)$$

where C_e (µg/mL) is the concentration of the adsorbed protein at equilibrium, qe is the adsorption capacity (ug/ug), q_{max} (µg/µg) is the maximum amount of protein absorbed per unit weight of GO, K_L (mL/µg) is the Langmuir constant related to the surface affinity for the protein, (C_0) is the initial protein concentration and R_L is the separation factor, which describes the essential characteristics of the Langmuir isotherm.

The Freundlich equation was expressed as follows in Equation (5).

$$\text{Log } qe = \log KF + 1/n \times \log Ce \quad (5)$$

where K_F and n are the Freundlich constant and intensity adsorption, respectively.

2.3 Kinetic Study of Protein Adsorption

GO (250 µg/mL) was dispersed in either a BSA solution (900 µg/mL), collagen solution (315 µg/mL) or elastin solution (900 µg/mL). These mixtures were incubated at 37 °C and the samples were centrifuged at 14,000 rpm for 10 min at 12,000 rpm after 0, 5, 10, 20, 30 and 80 min of incubation. The supernatants were collected for the quantification of the non-adsorbed proteins with the BCA kit (Thermo Fisher). The

results were analyzed using the pseudo-second-order model in order to clarify the nature of the adsorption phenomenon. This pseudo-second-order model is described by Equation (6) [49].

$$t/q_t = t/qe + 1/k_2 \times (q_e)^2 \quad (6)$$

Where q_e (µg/µg) and q_t (µg/µg) are the adsorption capacity at equilibrium and at selected times, respectively, t (min) is the time and k_2 (µg/µg.min^{-1}) is the rate constant of the pseudo-second-order adsorption. The intra-particle diffusion model was also used to find out the diffusion mechanism, denoted in Equation (7).

$$qt = Kp.t1/2 + C \quad (7)$$

Where qt is the amount of protein adsorbed at the equilibrium (µg/µg) at time t,C (µg/µg) refers to the intra-particle diffusion constant related to the thickness of the boundary layer and Kp is the intra-particle diffusion rate constant KP (µg/µg. min1/2) [50,51].

2.4 Thermodynamic Studies.

GO (250 µg/mL) was dispersed in either BSA solution (900 µg/mL), collagen solution (315 µg/mL) or elastin solution (900 µg/mL). These mixtures were incubated for 2 h at different temperatures (5 ◦C, 10 ◦C, 15 ◦C, 25 ◦C, 37 ◦C and 39 ◦C). Samples were centrifuged for 10 min at 12,000 rpm and the supernatants were collected for the quantification of the non-adsorbed proteins with the BCA kit (Thermo Fisher). The three basic thermodynamic parameters—Gibbs free energy change (∆G◦), entropy change (∆S◦) and enthalpy change (∆H◦) were calculated using the following Equations (8)–(11) [29,52].

$$Kd = qe/Ce \quad (8)$$

$$\Delta G = -RT \ln Kd \quad (9)$$

$$\text{Ln } Kd = -\Delta H/RT + \Delta S/R \quad (10)$$

$$\Delta G^\circ = \Delta H - T\Delta S \quad (11)$$

Where R is the gas constant (8.314 J/mol K), T is the absolute temperature (K), Kd is

the equilibrium constant, q_e (µg/µg) is the amount of protein adsorbed per mass unit of GO at equilibrium and C_e (µg/mL) is the equilibrium concentration of the proteins.

2.5 Electrochemical Study

First, sodium alginate solutions in combination with GO or GO-protein mixtures were prepared as follows. 1.87% (*w*/*v*) sodium alginate solutions were prepared in 1% mannitol and were then mixed with a GO suspension or mixtures of GO with the studied proteins at the aforementioned concentrations. With these reagents, the alginate hydrogels were elaborated. For this purpose, 2.7 mL of the previous solutions (alginate, alginate-GO and alginate-GO-proteins) were mixed with 60 µL of calcium sulphate 1.22 M and 240 µL of mannitol 1%, through two Luer Lock syringes (BS Syringe) connected with a Fluid Dispensing Connector (Braun), for 15 s. Then, the resulting mixtures were kept for gelification between two glass plates with a separation of 2 mm. The obtained hydrogels were cut into 14 mm diameter disks for electrochemical studies.

Electrochemical Impedance Spectroscopy (EIS) was conducted using a versa state-3 instrument (Princeton Applied research-USA), and a screen-printed electrode (Dropsens-Spain), based on carbon and a silver electrode for reference. The samples were immersed in 0.1 M PBS performing EIS measurements at room temperature, with a frequency range from 10^{-1} to 10^{3} Hz. Cyclic Voltammetry (CV) was performed to quantify the specific capacitance. The samples were immersed in 0.1 M PBS and CV measurements were carried out at the potential window of −0.5 to 0.2 V at various scan rates (100 mVs^{-1}). The specific capacitance was calculated from the CV curves according to the following Equation (12) [53].

$$C = Q/(2\ Vm) \quad (12)$$

Where C ($F \cdot g^{-1}$) is the specific capacitance, Q (C) is the average charge during the charging and discharging process, V (Volt) is the potential window and m (g) is the mass of the hydrogel disk.

2.6 In Vitro Cell Viability Studies

The biological effects of alginate hydrogels containing GO or GO with different

adsorbed proteins (BSA, collagen and elastin) were studied on murine C_2C_{12} myoblasts genetically engineered to secrete erythropoietin (C_2C_{12}-EPO). The cells were grown in Dulbecco's modified Eagle's medium (Gibco) supplemented with 10% FBS, 2 mM L-glutamine and 1% antibiotic/antimycotic solution (basal medium) at 37 ◦C in a humidified atmosphere containing 5% CO_2. The cells were passaged every 2–3 days. For the preparation of the C_2C_{12}-EPO containing hydrogels, the alginate, alginate-GO and alginate-GO-proteins (BSA, collagen or elastin) hydrogels were prepared as explained in Section2.6 under aseptic conditions, filtering all of the solutions through a 0.20 µm syringe filter (Millipore, MA, USA). The myoblasts were harvested with 0.25% trypsin-EDTA, centrifuged and mixed with the hydrogels at a 5×10^6 cells/mL cell density. Afterwards, the resulting mixtures were kept for gelling between two glass plates with 2 mm of thickness and disks were cut in aseptic conditions. The disks were cultured at 37 ◦C in a humidified atmosphere containing 5% CO_2 with basal medium.

For fluorescence microscopy viability imaging, the hydrogels were stained with the LIVE/DEAD® Viability/Cytotoxicity Kit (Invitrogen™) at different time points. The hydrogels were washed with DPBS and stained with 0.5 µM calcein AM and 0.5 µM ethidium homodimer. The samples were incubated at room temperature for 40 min, protected from light and observed under a Nikon TMS microscope (excitation/emission settings for calcein AM. 495/515 nm and for ethidium homodimer. 495/635 nm). At least three independent experiments were analyzed for each condition. For metabolic activity study, six disks from each condition were placed on 96-well plates, adding 100 µL of culture medium with 10 µL of Cell Counting Kit-8 solution (CCK-8, Sigma-Aldrich) per well. The plates were incubated inside a humidified chamber for 4 h at 37 ◦C. Then, the absorbance was read out on an Infinite M200 TECAN plate reader at 450 nm with a reference wavelength set at 650 nm. The secretion of EPO was also quantified from three disks/conditions. The disks were placed in 12-well plates adding 1 mL of the culture medium and collecting supernatants the next day. The amount of released EPO was quantified using the Quantikine IVD EPO ELISA kit (R&D Systems). All of the samples and standards were measured at least in triplicate.

2.7 EPO and Insulin Adsorption Blocking Study

We evaluated the capacity of BSA, collagen and elastin for avoiding the adsorption of other proteins to the GO particle surface, such as EPO and insulin. First, GO-BSA,

GO-collagen and GO-elastin mixtures were obtained as previously described in Section2.5. These mixtures were incubated overnight with either recombinant EPO (200 mIU/mL) or insulin (150 mIU/mL). Next, the samples were spun for 5 min at 12,000 rpm, and then the supernatants were collected. The non-adsorbed EPO and insulin was quantified with the ELISA kits, the Quantikine IVD-EPO ELISA kit (R&D Systems) and the Insulin ELISA Kit (Mercodia), respectively. The GO without adsorbed proteins was considered as a control. All of the samples and standards were measured in duplicate. Three independent experiments were analyzed for each condition.

Statistical Analysis

Statistical analysis was done with SPSS software, version 24.00, or GraphPad Prism 8.0 (GraphPad Inc., San Diego, CA, USA). The data are shown as mean ± standard deviation. Values with $p < 0.05$ were considered significant for comparison between groups after confirming normality and performing ANOVA and Tukey's post-hoc test for bivariate correlation. Pearson's correlation coefficient was used for continuous data and Spearman's for ordinal and nominal data.

3 Results and Discussion

In this experimental work, we studied how BSA, type I collagen and elastin, interact with the GO surface, analyzing their electrochemical characteristics after being embedded within alginate hydrogels. Next, we evaluated the biological impact of embedded C_2C_{12}-EPO cells within hybrid protein-coated GO particles with alginate hydrogels.

Raman Spectroscopy Shows the Functionalization of GO by BSA, Collagen and Elastin

The interactions between the studied proteins and GO were analyzed by Raman spectroscopy, obtaining the spectra of GO, BSA, collagen, elastin and the combinations of GO with each protein type, as shown in Figure1. The proteins were hardly detected after mixing with the GO due to the higher Raman activity of the GO compared to the proteins. In the GO spectrum, two prominent peaks, commonly observed in sp^2 graphite systems, corresponding to D (~1340 cm^{-1}) and G (~1600 cm^{-1}) bands, were clearly visible [54]. Moreover, the combination of 2D, D + G bands

and 2G bands at 2500 cm^{-1} and 3200 cm^{-1} were detected, with a wide band around 3500 cm^{-1}, maybe due to OH^- presence. More detailed analysis of the spectrum evidenced the presence of a band (I) at the low wavenumber side (1100–1250 cm^{-1}) of the D band, usually attributed to sp^3 bonds arising from broken sp^2rings or surface functionalization.

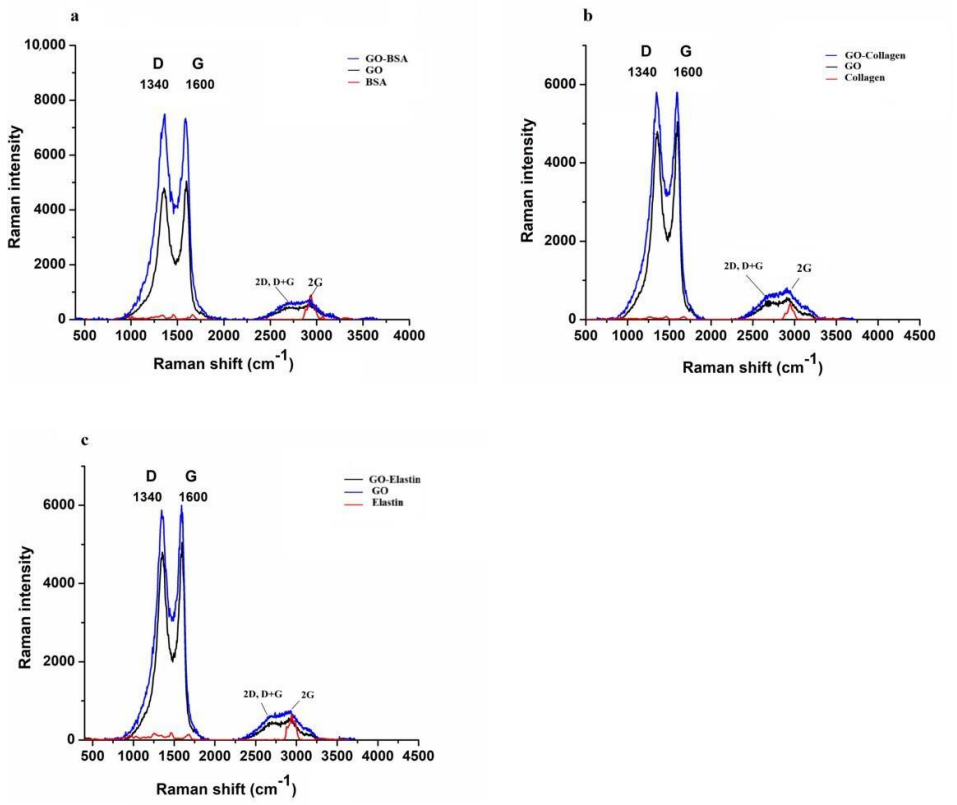

Figure 1. Raman spectrum of GO, BSA (**a**), collagen (**b**) and elastin (**c**), and the combination of each protein with GO.

Two components (G1 and G2) are required to fit the asymmetry of the G band. These excitations were present both in the GO and GO with protein spectra and were used to determine GO modifications after combining with protein. Detection at the same excitation wavelength (532 nm) did not show significant differences between the band wavenumbers of the GO and GO mixed with proteins, as shown in Table1. Similarly, no appreciable wavenumber di fferences were observed among the three proteins mixed with the GO.

However, interestingly, there was an evolution of the integrated band intensities comparing the GO and GO mixed with protein spectra. A constant D/G intensity ratio was observed for all of the proteins studied, within error, while the I/D ratio was enhanced after mixing the GO and proteins, shown in Table1, indicating an increment in the functionalization of GO.

Table 1. Raman spectroscopy data from the GO and protein-coated GO nanoparticles (proteins = BSA, collagen or elastin).

Wavenumbers (cm^{-1}) at 532 nm Excitation Wavelength	**GO**	**GO + Protein**
(I)	1245	1230–1250
(D)	1354	1352–1354
(G1)	1569	1530–1570
(G2)	1603	1595–1605
Band Intensity Ratio	**GO**	**GO + Protein**
I/D	0.25	0.45–0.48
D/(G1 + G2)	1.3	1.1–1.5
(D + I)/(G1 + G2)	1.7	1.6–2.2

3.2 FTIR Spectroscopy Indicates a Formation of a Bio-Corona on the GO Surface

In order to determine the adsorption of proteins on the GO surface, Fourier Transform Infrared Spectroscopy (FTIR) spectra from the GO of GO-proteins before and after the adsorption of the studied proteins were compared, as shown in Figure2. The GO spectrum showed broadband for H-bonded and an OH stretch at 3300 cm^{-1}, a C=C characteristic band at 1645 cm^{-1} and a C-O stretch at 1056 cm^{-1} [54]. However, when the studied proteins were adsorbed on the GO surface, bands from the GO and proteins were overlapped. Thus, the FTIR spectrum for protein-coated GO showed NHCO stretching vibrations at 1636–1639 cm^{-1}, characteristic of amide bonds from proteins and primary alcohol (C-OH stretch) at 1083–1089 cm^{-1}. The amide II band from BSA was shifted from 1523 cm^{-1} to 1541 cm^{-1} when adsorbed within the GO, while collagen shifted from 1544 cm^{-1} to 1559 cm^{-1} and elastin from 1538 cm^{-1} to 1552 cm^{-1}. Similarly, the amide III bands shifted from 1247 cm^{-1} to 1256 cm^{-1} with BSA, from 1250 cm^{-1} to 1244 cm^{-1} with collagen and from 1244 cm^{-1} to 1241 cm^{-1} with elastin. A peak at 1645 cm^{-1} in the GO spectrum, attributed to the aromatic C=C group of the sp^2 carbon atom structure, was detected. However, this peak was not detected after the

adsorption of the proteins, suggesting either the loss of the sp^2 structure or the formation of a bio-corona on the GO surface. These results would indicate that the formation of such bio-corona on the GO surface would occur through the π–π interactions between the benzene ring from the proteins and the C=C from GO [55,56]. Nevertheless, other interactions, such as hydrogen bonds, could participate in the bio-corona formation.

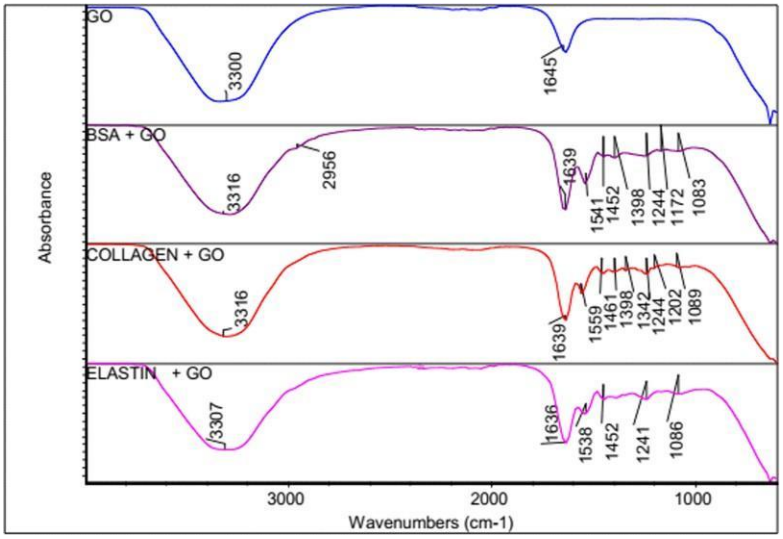

Figure 2. FTIR spectrum for GO, GO-BSA, GO-collagen and GO-elastin matrix.

3.3 Protein-GO Adsorption Capacity Is Related to the Protein Molecular Weight

The adsorption capacity of GO platelets was studied by exposing them to different initial concentrations of BSA, collagen and elastin. From the quantified data, it was clear that the adsorption capacity of GO increased when the initial concentration of the proteins was enhanced, as shown in Figure3. In fact, an increment in the initial protein concentration accelerated the di ffusion of more protein from the solution towards the GO particle surface, indicating that the initial adsorbed protein provides the needed driving force for overcoming the resistance to the mass transfer of the protein between the aqueous phase and the GO particles' solid phase [57]. However, this effect seems to be different among the three studied proteins. Thus, BSA-GO was the most affected interaction by the increment of the initial protein concentration, showing a q_e of 0.045 ug/ug at an initial BSA concentration of 112.5 µg/mL and a 5.9-times increment at an initial BSA concentration of up to 1000 µg/mL. The maximum BSA adsorption capacity

value on the GO surface was 0.332 ± 0.02 µg/µg. In contrast, collagen was the least affected in terms of GO surface adsorption when modifying the initial concentration, with the highest qe value at 0.092 ± 0.005 µg/µg.

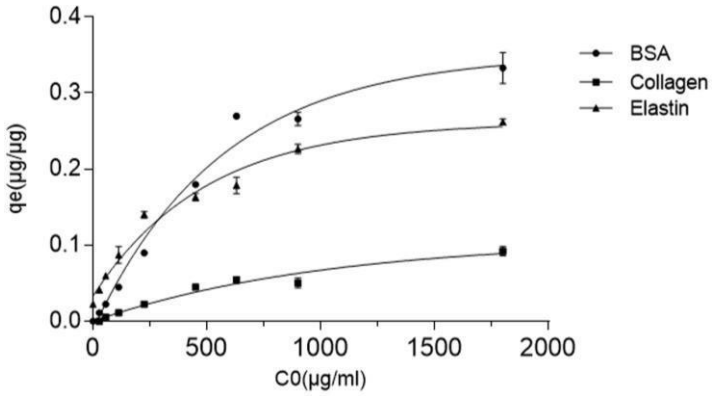

Figure 3. Effect on the GO adsorption capacity (qe) of the initial concentration (C0) of BSA, collagen and elastin at 37 °C after 2 h of incubation.

All of the studied protein-GO interactions reached a plateau, indicating that all of the active sites of the GO surface were occupied. Since BSA and elastin are small molecular weight proteins, with 66.5 KDa and 70 KDa, respectively, while collagen has 300 KDa, we consider that the theoretical Random Sequential Adsorption (RSA) model can explain this adsorption process. In the RSA model, adsorption is described as a stochastic process with particles successively placed onto a surface where other particles have already existed. According to the RSA model, proteins will be adsorbed if they are not overlapped with previously adsorbed proteins (steric repulsion) [58]. Based on this model, collagen would show higher steric repulsion than BSA or elastin, because higher molecular weight would have more chance of overlapping with other collagen molecules on the GO surface, reflecting in a lower adsorption capacity than BSA or collagen, as observed.

3.4 Proteins Are Adsorbed in GO Platelets as a Monolayer

Langmuir and Freundlich models were applied to the adsorption capacity experimental data at constant temperature to determine the adsorption performance on the GO surface from the studied proteins, as shown in Table2. Experimental data from the three proteins fitted to Langmuir model with a R^2 value between 0.97–0.99, suggesting

that the adsorption process occurs on the homogeneous surface. Moreover, the calculated q_{max} values from the three proteins are close to the q_e experimental results, indicating that this model describes the adsorption of the proteins in contact with the GO particles in suspension. Therefore, we can conclude that the three proteins cover the finite number of adsorption sites from the surface of the GO platelets as a monolayer, without transmigration along the plane of the surface [51] and without interactions between the adsorbed proteins along the surface [59]. Since, no good R^2 values were detected after applying the Freundlich model, we can discard the adsorption of an heterogeneous adsorbent with the formation of multiple layers of adsorbed proteins [52,60]. Separation factor values (R_L) below 1 indicated a favorable adsorption into the GO surface of the three studied proteins, with the indication of an interaction with BSA with a value close to zero [51].

Table 2. Parameters calculated from experimental data for Langmuir and Freundlich models. Notes. qe. amount of protein adsorbed per GO weight at equilibrium; qmax. maximum amount of protein adsorbed per GO weight; KL. Langmuir constant; RL. separation factor; n. adsorption intensity; KF. Freundlich constant.

	Langmuir Model						**Freundlich Model**		
	qe (µg/µg)	**qmax (µg/µg)**	**1/n**	**KL (mL/µg)**	**RL**	**R^2**	**N**	**KF**	**R^2**
BSA	0.332	0.330	0.057	0.009	0.99	0.050	22.030	0.225	0.750
Elastin	0.262	0.380	0.002	0.249	0.97	0.380	2.600	0.014	0.950
Collagen	0.122	0.071	0.023	0.044	0.97	0.200	4.780	0.019	0.700

3.5 Kinetic Study of the Protein Adsorption into GO Shows that Lower Molecular Weight Proteins Are Adsorbed Faster

Next, we studied the kinetics of the protein adsorption, detecting that the rate of adsorption rapidly increases after proteins and GO platelets are mixed, due to the high available number of active sites on the GO platelets surface, shown in Figure4a. The GO demonstrated a high capacity to adsorb the studied proteins on its surface and, ten minutes later when equilibrium state was reached, adsorption gradually slowed down since fewer sorption sites were available.

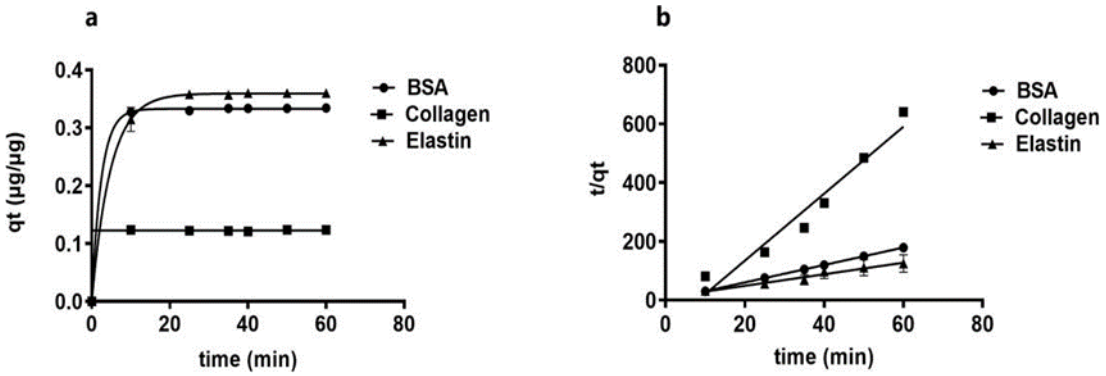

Figure 4. Kinetic study of protein adsorption and the GO adsorption capacity for BSA, collagen and elastin. (**a**) Representation of adsorption capacity (qt) over time. (**b**) Pseudo-second-order kinetic model.

To understand the nature of this process, both pseudo-first-order and pseudo-second-order kinetic models were applied. The experimental data did not fit on the pseudo-first order kinetic mode, indicating that adsorption does not occur between one protein and one sorption site on the GO solid surface. However, the data did fit onto the pseudo-second-order kinetic model, shown in Figure4b and Table3, suggesting that each protein can be adsorbed into two sorption sites on the GO platelets [56]. Among the three proteins, collagen showed the lowest affinity based on its q_t value, maybe due to its higher molecular weight (300 kDa), compared to BSA (66.5 kDa) and elastin (70 kDa) which increase steric repulsion forces, shown in Figure 4.

Table 3. Parameters calculated from the pseudo-second-order kinetic model.

	qe (µg/µg)	K2(µg/µg.min)	R^2	qt (µg/µg)
BSA	0.336	7.220	0.990	0.332
Collagen	0.362	12.860	0.990	0.123
Elastin	0.125	4.158	0.990	0.352

Next, to find the mechanism that fits the uptake of the protein into the GO surface, we applied the intra-particle diffusion model, a common study for material adsorption on solid adsorbents, such as GO, which would assume the adsorption process in three steps. the diffusion of molecules from the bulk solution to the external surface of GO particles; a diffusion through the internal surface of GO pores; a final adsorption into the internal sites of GO [44]. According to this model, elastin and BSA showed higher adsorption capacities (q_t) than collagen (I). However, the plot of q_t against $t^{1/2}$ was

linear, as shown in Figure5, indicating that the intra-particle di ffusion is not the unique process interposed in the GO adsorption of proteins, but film diffusion is also involved [50,61].

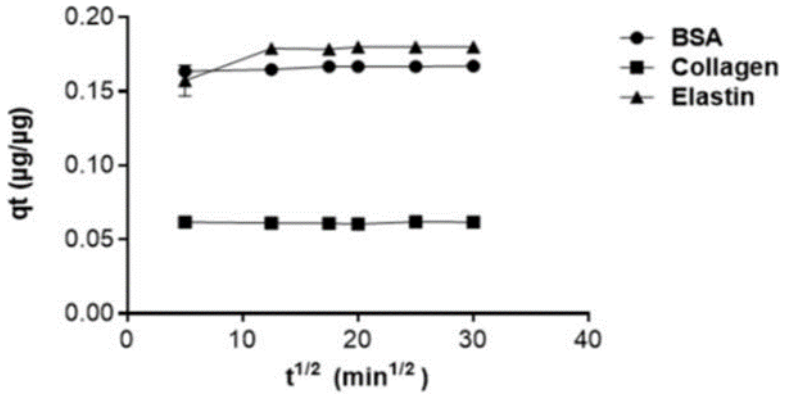

Figure 5. Intra-particle diffusion model plot.

Values calculated from the intra-particle diffusion model indicate that elastin and BSA have higher Kp (as the intra-particle diffusion rate is constant), than collagen, which is similar to C, the thickness of the boundary layer, shown in Table4. We consider that Kp and C provide an indication of the high affinity of BSA and elastin to the GO surface through the hydrophilic–hydrophilic interactions of the proteins to the carbon material. In contrast, interfering forces from the hydrophobic interaction with collagen, in addition to its high molecular weight, would be responsible of the lower Kp and C values.

Table 4. Parameters calculated from intra-particle diffusion model. Note. Kp, intra-particle diffusion rate constant; C, the thickness of the boundary layer.

	Kp (µg/µg.min$^{1/2}$)	C	R^2
BSA	0.00014	0.163	0.91
Collagen	1.15×10^{-5}	0.060	0.37
Elastin	0.00078	0.161	0.70

3.6 Protein Molecules Determine Thermodynamic Behavior in Their Adsorption by GO

We studied the effect of temperature on the protein adsorption into the GO platelets

surface, since a change in temperature could modify the protein adsorption into GO. Therefore, we analyzed the protein adsorption from 278 K to 315 K, and calculated the parameters ΔH◦, ΔS◦ and ΔG◦ with Equations (8)–(11), shown in Table5. We detected an increase in adsorption capacity with the increment of temperature, as shown in Figure6. The positive ΔH ◦ values indicate that the adsorption of proteins on the GO surface is endothermic, evidencing that the interaction of BSA with GO is weaker than collagen and elastin, as observed with its lower ΔH value [62]. Since adsorption is the sum of two steps, the endothermic hydration of the protein in the solution and the exothermic adsorption on the GO surface [53], the positive ΔH◦ values indicate that, in the protein adsorption on GO, hydration is the most predominant step.

Table 5. Thermodynamic parameters. Enthalpy change. ΔH◦; Entropy change. ΔS◦; Gibbs free energy change. ΔG◦ at 300 K.

	ΔH◦ (kJ/mol)	**ΔS◦ (kJ/mol.K)**	**ΔG◦ (kJ/mol)**	**R^2**	**ΔH◦ (kJ/mol)**
BSA	2.598	−0.057887	20.543	0.981	BSA
Elastin	16.270	−0.008881	19.031	0.779	Elastin
Collagen	17.363	−0.006935	19.513	0.935	Collagen

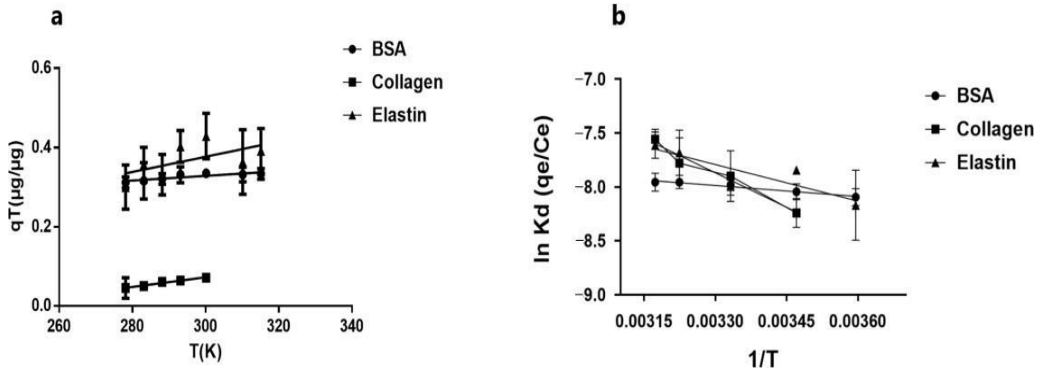

Figure 6. (**a**) Effect of temperature on adsorption capacity of BSA, collagen and elastin onto GO platelets surface. (**b**) van't Hoff plot. Kd. equilibrium constant; T. absolute temperature in K.

Entropy at this range of temperature for the three studied proteins was negative (ΔS◦< 0), indicating a decrease in randomness after the adsorption of the proteins into GO, in accordance with common protein behavior [1,51,60]. The highest ΔS◦ was detected in collagen while the lowest was in BSA, suggesting again that protein molecular weight plays an important role. Finally, the positive ΔG◦ values, characteristic of an endergonic reaction, suggest a non-spontaneous adsorption process of these proteins and an energy

barrier for proteins to diffuse from the solution to the GO surface, with a hydration shell around the proteins that could prevent its adsorption into GO. Moreover, the values below 40 KJ/mol indicated not a physisorption process [43,54,56], but a chemisorption process instead.

3.7 . Conductivity Is Improved after Coating GO with Proteins within Alginate Matrixes

GO is an electrically insulating material due to its disrupted sp^2 bonding networks, but it can act as a semiconductor, depending on the degree of oxidation [63], mediating as an electrochemical mediator in contact with cells. Therefore, we studied the electrochemical activity of protein coated-GO-hydrogels. We first determined the electrochemical impedance spectroscopy by measuring the phase impedance (Z) in the frequency range of 10^{-1}–10^3 Hz, as shown in Figure7. The data indicated an insulating /conducting behavior in the studied hydrogels.

We quantified the phase angles of Z from all the samples and represented them in Bode plots, shown in Figure7a. Although the data at the lowest frequencies could not be represented due to the noise caused by the high values of impedance, we could detect that the phase angle tended to decrease towards zero at the high-frequencies region, reaching close to 90 degrees at lower high-frequencies, shown in Figure7a. However slight modifications could be detected when GO or protein-coated GO was embedded in the alginate matrixes. We also quantified the impedances (Z_{im}) from the different samples and represented them in Nyquist plots, shown in Figure7b, detecting slight di fferences after embedding GO or coated-GO within alginate hydrogels. GO-alginate matrixes showed higher impedance than alginate hydrogels. However, although the presence of GO increased the impedance, protein-coating the GO decreased it, indicating an improvement in conductive behavior. The disrupted sp^2 bonding networks from GO provided an insulating behavior [63], but coating with proteins could

have led to the recovery of the sp^2 networks, improving its conductivity properties [64], and therefore, creating a suitable signal conduction between cells and the alginate matrix when used in vivo. In fact, conductivity, among other GO-containing scaffold properties, would help to overcome the limitations from metals and silicon implantable devices, providing safer and effective treatments for pathological conditions in the clinic,

particularly in the field of neurology or cardiology [65–67].

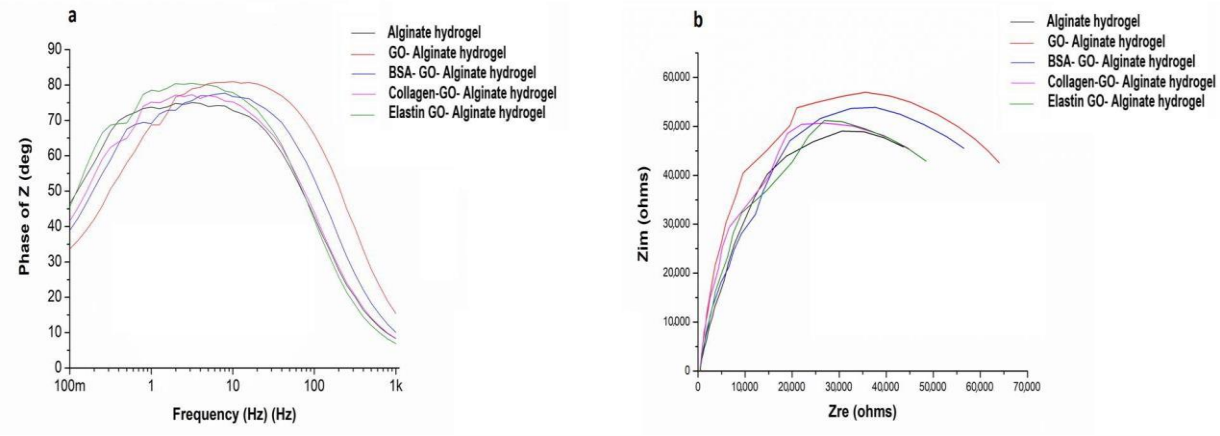

Figure 7. Electrochemical study from protein coated-GO alginate hydrogels compared to alginate hydrogels. (**a**) Bode plots, (phase angle Z vs. frequency from 10^{-1} to 10^{3} Hz. (**b**) Nyquist diagram, Zim vs. Zre (ohm).

3.8. Capacitance Is Reduced after GO Protein Coating.

We determined the capacitance (Z_{im}) of the protein-coated alginate hydrogels by cyclic voltammetry (CV) at scan rates of ±100 mV, in a potential window of −0.5 to 0.2 V, as shown in Figure 8.

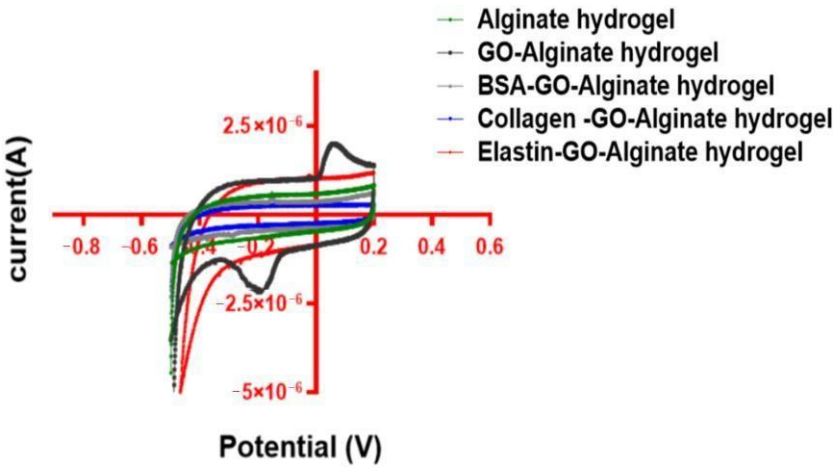

Figure 8. Voltammograms from protein-coated GO alginate and alginate hydrogels.

The calculated non-coated GO-alginate hydrogel capacitance was the highest among the

studied hydrogels (2.78×10^3 f/g), 5.64-times higher than alginate hydrogels (4.77×10^4 f/g). However, we detected a reduction in the capacitance of the protein-coated GO-alginate hybrid hydrogels compared to GO-alginate hydrogels. BSA-GO and collagen-GO containing hydrogels showed a value of 7.04×10^4 f/g and 4.98×10^4 f/g, smaller than the hydrogels containing elastin (2.47×10^3 f/g). This reduction in the GO capacitance after protein coating is in agreement with those observed in EIS measurements, indicating that there is an accelerated electron transfer evidenced by a decreased Z_{im}, lower phase shift and smaller impedance after the adsorption of proteins by GO sheets [68]. We consider that impedance decrease, in combination with observed capacitance measurements, indicate a slight improvement in the conductivity of protein-coated GO hybrid alginate hydrogels.

3.9. Collagen and Elastin Coated GO Improves Alginate Hydrogel-Embedded C_2C_{12} Cell Viability

The introduction of FBS-coated GO nanoparticles in the matrix of alginate-poly-L-lysine-alginate hydrogels has shown to enhance the viability of the encapsulated erythropoietin-releasing C_2C_{12} myoblasts (C_2C_{12}-EPO) [10,47,48], but if a sole protein could reproduce, this enhancement has not been discerned yet. Therefore, after characterizing the interaction between BSA, collagen or elastin with the GO surface, we generated alginate-based hydrogels containing protein-coated GO platelets to embed C_2C_{12}-EPO cells in order to study the in vitro outcomes from each protein-coated GO on a 3D model. Cell viability, assessed by confocal microscopy, showed that one day after embedding the cells, there were no differences among all the studied groups of hydrogels, with a similar number of live and dead cells, shown in Figure9. However, one week later, there was a noteworthy cell viability enhancement from hydrogels containing collagen- and elastin-coated GO particles, increasing even more the second week in the elastin-coated GO group, indicating that collagen, and especially elastin, are able to improve the viability of embedded C_2C_{12} cells within alginate hydrogels.

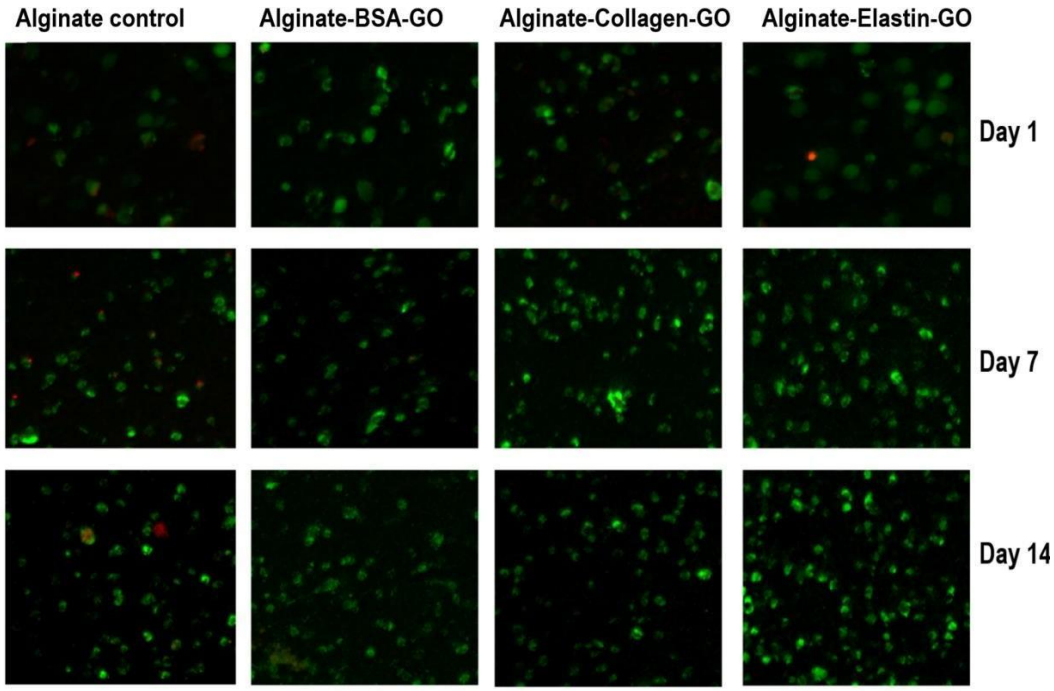

Figure 9. Fluorescence microscopy images, after calcein/ethidium staining for C2C12–EPO myoblasts incorporated within the modified alginate hydrogels based on GO-BSA, GO-collagen and GO-elastin matrices. Green. live cells. Red. dead cells. Scale bar. 100 µm.

Next, we complemented the imaging studies through the quantification of metabolic activity. On the first day, the metabolic activity of the embedded cells was low with all of the studied protein-coated GO, perhaps due to the high shear stress that cells suffer during hydrogel fabrication after 24 h, shown in Figure10. However, a significantly higher metabolic activity ($p < 0.001$) was already detected at this time point from the elastin-coated GO hydrogels. One and two weeks later, metabolic activity had increased over all of the hydrogels studied, showing only a statistically significant increment ($p < 0.01$) at two weeks in collagen-coated GO samples, as shown in Figure10.

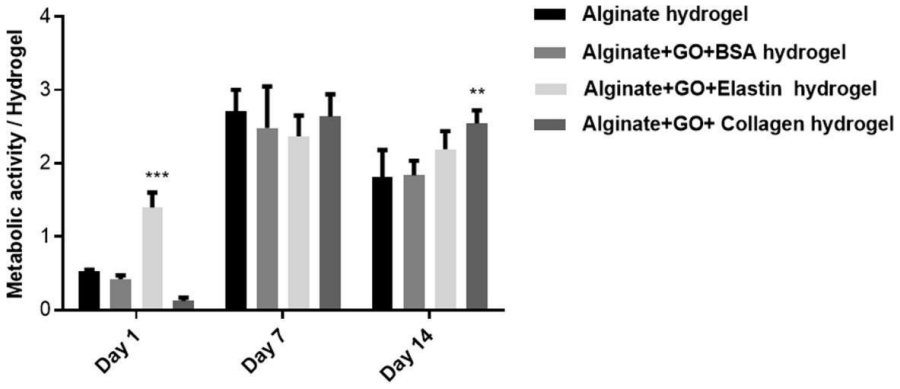

Figure 10. Metabolic activity of hybrid alginate-GO embedded C_2C_{12}-EPO myoblasts over two weeks. Note. **. $p < 0.01$; ***. $p < 0.001$ compared with cells encapsulated in alginate without GO.

3.10 . Protein Release by Embedded Cells Is Influenced by the Type of Protein-Coated GO.

Next we quantified if the different protein-coated GO platelets had any effect on the production and release of the therapeutic protein, EPO. The BSA-coated GO containing alginate hydrogel showed the highest EPO release among the analyzed groups, while the elastin group had a similar profile in comparison to the control and the collagen group released a lower amount, as shown in Figure11. These results were difficult to foresee, taking into account the viability results obtained with the calcein/ethidium staining, shown in Figure9. We expected that a higher cell viability would represent a higher release of the therapeutic protein EPO. In addition, the collagen-GO-alginate hydrogels did not show lower viability in comparison to the controls but released a lower amount of EPO. One possible explanation is that elastin and collagen proteins are not able to form a stable and uniform bio-corona around the GO platelets of the release protein before their use for hydrogel fabrication, therefore avoiding the GO-inherent adsorption of the released proteins. Thus, although cells could be producing high quatities of EPO, the therapeutic protein could be retained in the GO surface, avoiding its release.

In order to confirm this hypothesis, we studied the capacity of BSA, elastin and collagen to block the GO platelets surface and avoid the adherence or interaction of EPO, shown in Figure12a. Thus, the GO platelets were able to adsorb the 70% of the recombinant protein EPO when mixed and incubated in vitro. Interestingly, the BSA pre-coating of the GO nanoparticles was able to reduce this adsorption almost completely, which means that all of the EPO produced by the encapsulated C2C12 myoblast inside

the BSA-GO-alginate hydrogels should be released into the culture media. In contrast, collagen and elastin reduced the percentage of EPO adsorption, but not completely, suggesting that some of the therapeutic protein can be retained within the hydrogels adsorbed into the GO particles. These results would explain why the amount of therapeutic protein detected on the culture media was similar to the alginate control group, although higher levels of viability were detected from elastin-GO-alginate hybrid hydrogels. Thus, although cells in the elastin group would produce higher amounts of protein (39.71% more than the detected levels), we were not able to quantify this difference. Regarding collagen, it was only able to block 45.29% of the EPO protein, indicating that 54.71% of the produced EPO should be retained within the hydrogels, shown in Figure12a. However, even if we take into account this low blocking capacity, the amount of protein released by the cells on this hybrid hydrogel would be lower than in the BSA or elastin group. Therefore, we believe that another mechanism could be affecting the low protein release in collagen-coated GO hydrogels, such as the adsorption of EPO not only by the GO platelets, but also by collagen itself, since EPO has a tendency to cross-link soluble type IV collagen in vitro [69,70]

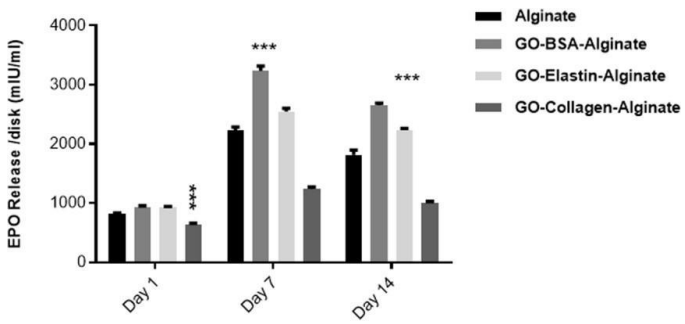

Figure 11. EPO production and release from C2C12-EPO myoblasts embedded in different hybrid protein-GO-alginate hydrogels. Note.; ***. $p < 0.001$ compared with cells embedded in alginate without GO.

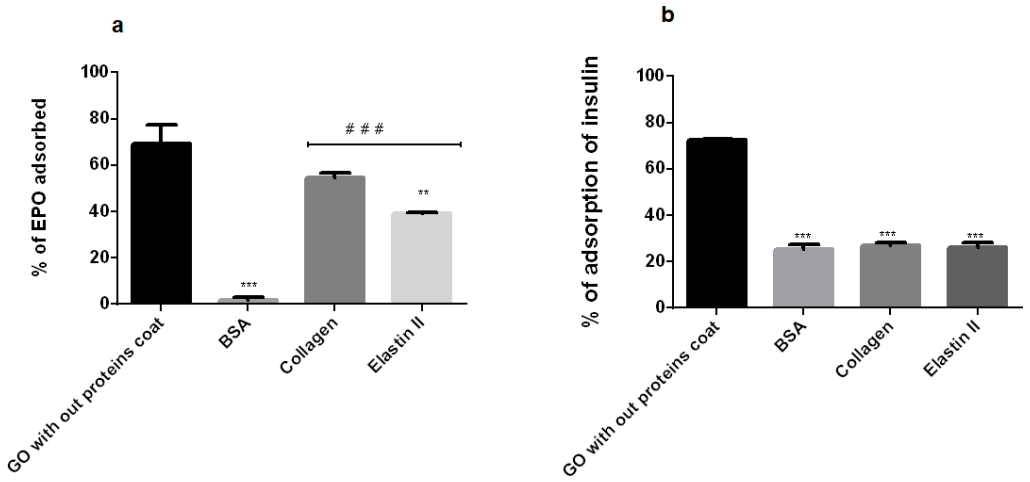

Figure 12. Percentage of (**a**) EPO and (**b**) insulin adsorbed by GO without coating, and BSA-, collagen- and elastin-coating. Incubation conditions. GO final concentration, 50 µg/mL; temperature, 37 ◦C; incubation time, 24 h. Note. $p < 0.01$; **. $p < 0.001$; *** compared with non-coated GO. ###. $p < 0.001$ compared to BSA coated-GO.

Aiming to establish if the blocking effect of the assayed three proteins has the same effect on different therapeutic proteins, we performed this study with insulin, since insulin producing cells in alginate microcapsules or hydrogels are a wide field of investigation for the treatment of type one diabetes mellitus [71,72]. Insulin showed a similar percentage of the adsorption of EPO to the GO surface, close to 70%. However, in contrast to EPO, the three studied proteins had the same blocking capacity in the interaction between the GO particles and insulin, reducing the adsorption of insulin into the GO surface by up to 60%, shown in Figure12b. Therefore, we hypothesized that the hydrophilic nature of BSA and elastin interferes with the hydrophobic nature of EPO [73], decreasing the affinity of EPO to be adsorbed on the GO surface, in contrast to the hydrophobic nature of collagen, which would interact with the therapeutic protein, reducing its ability to prevent the trapping of EPO on the GO surface. Regarding insulin, its small molecular weight (6 kD) and its high hydrophilic nature, could possibly compete with the studied proteins at the GO binding sites, replacing part of the coating protein, or being inserted into the void spaces between the adsorbed proteins.

4 Conclusions

We have confirmed the formation of protein layers on the GO surface by Raman spectroscopy and FTIR, studying BSA, collagen and elastin. To understand the mechanisms underlying the bio-corona formation, we have described how the protein–

GO adsorption capacity is related to the protein All these mechanisms would be reflected in better cell viability and EPO release in hydrogels based more on GO-BSA and GO-elastin, than on GO-collagen. However, the hydrophilic nature of the adsorbed protein would play an important role in the biocompatibility of protein-coated GO, perhaps by attracting cells via π–π interactions and boosting more cells to adhere and proliferate on these matrices. Finally, although cells could be producing high quantities of EPO within the hybrid hydrogels, the therapeutic protein is retained in the GO surface, preventing its release. This retention is dramatically observed in the collagen-coated GO hybrid hydrogels, precluding their clinical translation. Therefore, we conclude that BSA- or elastin-coated GO hybrid hydrogels could act as promising scaffolds for improving the viability and functionality of embedded cells.

Author Contributions. Conceptualization, J.C., L.S. and J.L.P.; methodology, A.R., A.E.-N. and A.C.-H.; software,

A.M.O.d.R. and M.L.S.; validation, J.C., L.S.d.B. and J.L.P.; formal analysis, A.R., J.C., L.S.d.B. and J.L.P.; investigation, A.R., J.C., L.S.d.P. and J.L.P.; resources, P.G.-M.; writing—original draft preparation, A.R.; writing—review and editing, J.C., L.S. and J.L.P.; visualization, A.R.; supervision, J.C., L.S.d.B. and J.L.P.; project administration, J.C., L.S.d.P. and J.L.P.; funding acquisition, J.L.P. All authors have read and agreed to the published version of the manuscript.

Funding. This research was funded by the University of the Basque Country UPV/EHU and the Basque Country Government (Grupos Consolidados, No ref. IT907-16).

Acknowledgments. The authors also wish to thank the intellectual and technical assistance provided by the ICTS “NANBIOSIS”, more specifically by the Drug Formulation Unit (U10) of the CIBER in Bioengineering, Biomaterials and Nanomedicine (CIBER-BBN) at the University of Basque Country (UPV/EHU).

Conflicts of Interest. The authors declare no conflict of interes

References

1. Paredes Juárez, G.A.; Spasojevic, M.; Faas, M.M.; de Vos, P. Immunological and technical considerations in application of alginate-based microencapsulation systems. Front. Bioeng. Biotechnol. 2014, 2, 106–126.
2. Lee, K.Y.; Mooney, D.J. Alginate. Properties and biomedical applications. Prog. Polym. Sci. 2012, 37, 106–126.
3. Orive, G.; De Castro, M.; Kong, H.; Hernández, R.M.A.; Ponce, S.; Mooney, D.J.; Pedraz, J.L. Bioactive cell-hydrogel microcapsules for cell-based drug delivery. J. Control. Release 2009, 135, 203–210.
4. Garate, A.; Ciriza, J.; Casado, J.G.; Blazquez, R.; Pedraz, J.L.; Orive, G.; Hernandez, R.M. Assessment of the Behavior of Mesenchymal Stem Cells Immobilized in Biomimetic Alginate Microcapsules. Mol. Pharm. 2015, 12, 3953–3962. [PubMed]
5. Huang, X.; Yin, Z.; Wu, S.; Qi, X.; He, Q.; Zhang, Q.; Yan, Q.; Boey, F.; Zhang, H. Graphene-based materials. Synthesis, characterization, properties, and applications. Small 2011, 7, 1876–1902.
6. Novoselov, K.S.; Fal'ko, V.I.; Colombo, L.; Gellert, P.R.; Schwab, M.G.; Kim, K. A roadmap for graphene. Nature 2012, 490, 192.
7. Kuila, T.; Bose, S.; Khanra, P.; Mishra, A.K.; Kim, N.H.; Lee, J.H. Recent advances in graphene-based biosensors. Biosens. Bioelectron. 2011, 26, 4637–4648.
8. Nguyen, D.A.; Lee, Y.R.; Raghu, A.V.; Jeong, H.M.; Shin, C.M.; Kim, B.K. Morphological and physical properties of a thermoplastic polyurethane reinforced with functionalized graphene sheet. Polym. Int. 2009, 58, 412–417.
9. Wang, L.; Fan, H.; Zhang, Z.; Lou, A.; Pei, G.; Jiang, S.; Mu, T.; Qin, J.; Chen, S.; Jin, D. Osteogenesis and angiogenesis of tissue-engineered bone constructed by prevascularized β-tricalcium phosphate scaffold and mesenchymal stem cells. Biomaterials 2010, 31, 9452–9461.
10. Ciriza, J.; Saenz del Burgo, L.; Virumbrales-Muñoz, M.; Ochoa, I.; Fernandez, L.J.; Orive, G.; Hernandez, R.M.; Pedraz, J.L. Graphene oxide increases the viability of C2C12 myoblasts microencapsulated in alginate. Int. J. Pharm. 2015, 493, 260–270.
11. Goenka, S.; Sant, V.; Sant, S. Graphene-based nanomaterials for drug delivery and tissue engineering. J. Control. Release 2014, 173, 75–88.
12. Liu, J.; Cui, L.; Losic, D. Graphene and graphene oxide as new nanocarriers for drug delivery applications. Acta Biomater. 2013, 9, 9243–9257. [PubMed]
13. Sun, X.; Liu, Z.; Welsher, K.; Robinson, J.; Goodwin, A.; Zaric, S.; Dai, H. Nano-graphene oxide for cellular imaging and drug delivery. Nano Res. 2008, 1, 203–212. [PubMed]
14. Li, J.; Zeng, X.; Ren, T.; van der Heide, E. The preparation of graphene oxide and its derivatives and their application in bio-tribological systems. Lubricants 2014, 2, 137–161.
15. Bradder, P.; Ling, S.K.; Wang, S.; Liu, S. Dye adsorption on layered graphite oxide. J. Chem. Eng. Data 2011, 56, 138–141.
16. Suk, J.W.; Piner, R.D.; An, J.; Ruoff, R.S. Mechanical properties of monolayer graphene oxide. ACS Nano 2010, 4, 6557–6564.
17. Konkena, B.; Vasudevan, S. Understanding aqueous dispersibility of graphene oxide and reduced graphene oxide through pKa measurements. J. Phys. Chem. Lett. 2012, 3, 867.
18. Park, S.; An, J.; Jung, I.; Piner, R.D.; An, S.J.; Li, X.; Velamakanni, A.; Ruoff, R.S. Colloidal suspensions of highly reduced graphene oxide in a wide variety of organic solvents. Nano Lett. 2009, 9, 1593–1597.
19. Anonymous. Graphene Oxide. Preparation, Functionalization, and Electrochemical Applications. Available online. https.//pubs.acs.org/doi/ipdf/10.1021/cr300115g (accessed on 7 September 2018).
20. Park, S.; Ruoff, R.S. Chemical methods for the production of graphenes. Nat. Nanotechnol. 2009, 4, 217–224.
21. Zhang, L.; Lu, Z.; Zhao, Q.; Huang, J.; Shen, H.; Zhang, Z. Enhanced chemotherapy efficacy by sequential delivery of siRNA and anticancer drugs using PEI-grafted graphene oxide. Small 2011, 7, 460–464.
22. Liu, Z.; Robinson, J.T.; Sun, X.; Dai, H. PEGylated nanographene oxide for delivery of water-insoluble cancer drugs. J. Am. Chem. Soc. 2008, 130, 10876–10877. [PubMed]
23. Chung, C.; Kim, Y.; Shin, D.; Ryoo, S.; Hong, B.H.; Min, D. Biomedical applications of graphene and graphene oxide. Acc. Chem. Res. 2013, 46, 2211–2224.
24. Simsikova, M.; Šikola, T. Interaction of graphene oxide with proteins and applications of their conjugates. J. Nanomed. Res. 2017, 5.
Emadi, F.; Amini, A.; Gholami, A.; Ghasemi, Y. Functionalized graphene oxide with chitosan for protein nanocarriers to protect against enzymatic cleavage and retain collagenase activity. Sci. Rep. 2017, 7, 42258.
25. Yang, P.; Liu, Q.; Liu, J.; Zhang, H.; Li, Z.; Li, R.; Liu, L.; Wang, J. Bovine serum albumin-coated graphene oxide for effective adsorption of uranium(VI) from aqueous solutions. Ind. Eng. Chem. Res. 2017, 56, 3588–3598.
26. Hassan, M.; Walter, M.; Moseler, M. Interactions of polymers with reduced graphene oxide. Van der Waals binding energies of benzene on graphene with defects. Phys. Chem. Chem. Phys. 2014, 16, 33–37. [PubMed]
27. Yu, S.; Wang, X.; Ai, Y.; Liang, Y.; Ji, Y.; Li, J.; Hayat, T.; Alsaedi, A.; Wang, X. Spectroscopic and theoretical studies on the counterion effect of Cu(ii) ion and graphene oxide interaction with titanium dioxide. Environ. Sci. Nano 2016, 3, 1361–1368.
28. Xu, X.; Mao, X.; Wang, Y.; Li, D.; Du, Z.; Wu, W.; Jiang, L.; Yang, J.; Li, J. Study on the interaction of graphene oxide-silver nanocomposites with bovine serum albumin and the formation of nanoparticle-protein corona. Int. J. Biol. Macromol. 2018, 116, 492–501.
29. Lv, M.; Yan, L.; Liu, C.; Su, C.; Zhou, Q.; Zhang, X.; Lan, Y.; Zheng, Y.; Lai, L.; Liu, X.; et al. Non-covalent functionalized graphene oxide (GO) adsorbent with an organic gelator for co-adsorption of dye, endocrine-disruptor, pharmaceutical and metal ion. Chem. Eng. J. 2018, 349, 791–799.
30. Kuchlyan, J.; Kundu, N.; Banik, D.; Roy, A.; Sarkar, N. Spectroscopy and fluorescence lifetime imaging microscopy to probe the interaction of bovine serum albumin with graphene oxide. Langmuir ACS J. Surf. Colloids 2015, 31, 13793–13801.
31. Šimšíková, M. Interaction of graphene oxide with albumins. Effect of size, pH, and temperature. Arch. Biochem. Biophys. 2016, 593, 69–79. [PubMed]
32. Tang, S.; Cao, Z. Adsorption of nitrogen oxides on graphene and graphene oxides. Insights from density functional calculations. J. Chem. Phys. 2011, 134, 044710. [PubMed]
33. Oliveira, S.F.; Bisker, G.; Bakh, N.A.; Gibbs, S.L.; Landry, M.P.; Strano, M.S. Protein functionalized carbon nanomaterials for biomedical applications. Carbon 2015, 95, 767–779.
34. Carrier-bound Immobilized Enzymes. Principles, Application and Design. Available online. https.//www.wiley.com/enus/Carrier+bound+Immobilized+Enzymes%3A+Principles%2C+Application+and+Design-p-9783527312320 (accessed on 26 March 2019).
35. Feng, L.; Liu, Z. Graphene in biomedicine. Opportunities and challenges. Nanomedicine (London) 2011, 6, 317–324. [PubMed]
36. Yan, L.; Zhao, F.; Li, S.; Hu, Z.; Zhao, Y. Low-toxic and safe nanomaterials by surface-chemical design, carbon nanotubes, fullerenes, metallofullerenes, and graphenes. Nanoscale 2011, 3, 362–382.
37. Sasidharan, A.; Panchakarla, L.S.; Sadanandan, A.R.; Ashokan, A.; Chandran, P.; Girish, C.M.; Menon, D.; Nair, S.V.; Rao, C.N.R.; Koyakutty, M. Hemocompatibility and macrophage response of pristine and functionalized graphene. Small 2012, 8, 1251–1263.

38. Yue, H.; Wei, W.; Yue, Z.; Wang, B.; Luo, N.; Gao, Y.; Ma, D.; Ma, G.; Su, Z. The role of the lateral dimension of graphene oxide in the regulation of cellular responses. Biomaterials 2012, 33, 4013–4021. [PubMed]
39. Singh, S.K.; Singh, M.K.; Kulkarni, P.P.; Sonkar, V.K.; Grácio, J.J.A.; Dash, D. Amine-modified graphene. Thrombo-protective safer alternative to graphene oxide for biomedical applications. ACS Nano 2012, 6, 2731–2740.
40. Hu, W.; Peng, C.; Luo, W.; Lv, M.; Li, X.; Li, D.; Huang, Q.; Fan, C. Graphene-based antibacterial paper. ACS Nano 2010, 4, 4317–4323.
41. Chang, Y.; Yang, S.; Liu, J.; Dong, E.; Wang, Y.; Cao, A.; Liu, Y.; Wang, H. In vitro toxicity evaluation of graphene oxide on A549 cells. Toxicol. Lett. 2011, 200, 201–210. [PubMed]
42. Zhang, Y.; Ali, S.F.; Dervishi, E.; Xu, Y.; Li, Z.; Casciano, D.; Biris, A.S. Cytotoxicity effects of graphene and single-wall carbon nanotubes in neural phaeochromocytoma-derived PC12 cells. ACS Nano 2010, 4, 3181–3186. [PubMed]
43. Srikanth, K.; Sundar, L.S.; Pereira, E.; Duarte, A.C. Graphene oxide induces cytotoxicity and oxidative stress in bluegill sunfish cells. J. Appl. Toxicol. 2018, 38, 504–513. [PubMed]
44. Raslan, A.; Saenz del Burgo, L.; Ciriza, J.; Luis Pedraz, J. Graphene oxide and reduced graphene oxide-based scaffolds in regenerative medicine. Int. J. Pharm. 2020, 580, 119–226. [PubMed]
45. Wang, K.; Ruan, J.; Song, H.; Zhang, J.; Wo, Y.; Guo, S.; Cui, D. Biocompatibility of graphene oxide. Nanoscale Res. Lett. 2011, 6, 1–8.
46. Ciriza, J.; Saenz Del Burgo, L.; Gurruchaga, H.; Borras, F.E.; Franquesa, M.; Orive, G.; Hernández, R.M.; Pedraz, J.L. Graphene oxide enhances alginate encapsulated cells viability and functionality while not affecting the foreign body response. Drug Deliv. 2018, 25, 1147–1160.
47. Saenz del Burgo, L.; Ciriza, J.; Acarregui, A.; Gurruchaga, H.; Blanco, F.J.; Orive, G.; Hernández, R.M.; Pedraz, J.L. Hybrid alginate–protein-coated graphene oxide microcapsules enhance the functionality of erythropoietin secreting C2C12 myoblasts. Mol. Pharm. 2017, 14, 885–898.
48. Simonin, J. On the comparison of pseudo-first order and pseudo-second order rate laws in the modeling of adsorption kinetics. Chem. Eng. J. 2016, 300, 254–263.
49. Fierro, V.; Torné-Fernández, V.; Montané, D.; Celzard, A. Adsorption of phenol onto activated carbons having different textural and surface properties. Microporous Mesoporous Mater. 2008, 111, 276–284.
50. Nuengmatcha, P.; Mahachai, R.; Chanthai, S. Adsorption capacity of the as-synthetic graphene oxide for the removal of alizarin red S dye from aqueous solution. Orient. J. Chem. 2016, 32, 1399–1410.
51. Ahmad, M.A.; Ahmad Puad, N.A.; Bello, O.S. Kinetic, equilibrium and thermodynamic studies of synthetic dye removal using pomegranate peel activated carbon prepared by microwave-induced KOH activation. Water Resour. Ind. 2014, 6, 18–35.
52. Hong, F.; Yue, B.; Hirao, N.; Liu, Z.; Chen, B. Significant improvement in Mn2O3 transition metal oxide electrical conductivity via high pressure. Sci. Rep. 2017, 7, 44078. [PubMed]
53. Hu, X.; Li, D.; Mu, L. Biotransformation of graphene oxide nanosheets in blood plasma affects their interactions with cells. Environ. Sci. Nano 2017, 4, 1569–1578.
54. Peng, B.; Chen, L.; Que, C.; Yang, K.; Deng, F.; Deng, X.; Shi, G.; Xu, G.; Wu, M. Adsorption of antibiotics on graphene and biochar in aqueous solutions induced by π-π interactions. Sci. Rep. 2016, 6, 31920. [PubMed]
55. Yuan, X.; Wei, Y.; Chen, S.; Wang, P.; Liu, L. Bio-based graphene/sodium alginate aerogels for strain sensor. RSC Adv. 2016, 6, 64056–64064.
56. Sarfert, F.T.; Etzel, M.R. Mass transfer limitations in protein separations using ion-exchange membranes. J. Chromatogr. A 1997, 764, 3–20.
57. Manzi, B.M.; Werner, M.; Ivanova, E.P.; Crawford, R.J.; Baulin, V.A. Simulations of protein adsorption on nanostructured surfaces. Sci. Rep. 2019, 9, 1–13.
58. Foo, K.Y.; Hameed, B.H. Insights into the modeling of adsorption isotherm systems. Chem. Eng. J. 2010, 156, 2–10.
59. Chen, P.; Li, H.; Song, S.; Weng, X.; He, D.; Zhao, Y. Adsorption of dodecylamine hydrochloride on graphene oxide in water. Results Phys. 2017, 7, 2281–2288.
60. Wu, F.; Tseng, R.; Juang, R. Initial behavior of intraparticle diffusion model used in the description of adsorption kinetics. Chem. Eng. J. 2009, 153, 1–8.
61. Vijayakumar, G.; Tamilarasan, R.; Dharmendirakumar, M. Adsorption, Kinetic, Equilibrium and Thermodynamic studies on the removal of basic dye Rhodamine-B from aqueous solution by the use of natural adsorbent perlite. J. Mater. Environ. Sci. 2012, 3, 157–170. [Google Scholar]
62. Dreyer, D.R.; Park, S.; Bielawski, C.W.; Ruoff, R.S. The chemistry of graphene oxide. Chem. Soc. Rev. 2009, 39, 228–240.
63. Mohan Kumar, T.M.; Praveen, D. Impedance analysis of sodium alginate. Graphene oxide composite. In IOP Conference Series. Materials Science and Engineering; IOP Science. Bengaluru, India, 2018; Volume 310, p. 12150.
64. Kostarelos, K.; Vincent, M.; Hebert, C.; Garrido, J.A. Graphene in the design and engineering of next-generation neural interfaces. Adv. Mater. Weinheim. 2017, 29.
65. Reina, G.; González-Domínguez, J.M.; Criado, A.; Vázquez, E.; Bianco, A.; Prato, M. Promises, facts and challenges for graphene in biomedical applications. Chem. Soc. Rev. 2017, 46, 4400–4416.
66. Shin, S.R.; Li, Y.; Jang, H.L.; Khoshakhlagh, P.; Akbari, M.; Nasajpour, A.; Zhang, Y.S.; Tamayol, A.; Khademhosseini, A. Graphene-based materials for tissue engineering. Adv. Drug Deliv. Rev. 2016, 105, 255–274.
67. Qhatani, M.; Fadl-allah, S.; El-Shenawy, N. Electrochemical impedance spectroscopy study of the adsorption behavior of bovine serum albumin at biomimetic calcium–phosphate coating. Int. J. Electrochem. Sci. 2012, 7, 4510–4527.
68. Ero-Tolliver, I.A.; Hudson, B.G.; Bhave, G. The ancient immunoglobulin domains of peroxidasin are required to form sulfilimine cross-links in collagen
69. Zhou, H.; Xu, H.H.K. The fast release of stem cells from alginate-fibrin microbeads in injectable scaffolds for bone tissue engineering. Biomaterials 2011, 32, 7503–7513.
70. Hernández, R.M.A.; Orive, G.; Murua, A.; Pedraz, J.L. Microcapsules and microcarriers for in situ cell delivery. Adv. Drug Deliv. Rev. 2010, 62, 711–730.
71. Toyoda, T.; Arakawa, T.; Yamaguchi, H. N-Glycans stabilize human erythropoietin through hydrophobic interactions with the hydrophobic protein surface. Studies by surface plasmon resonance analysis. J. Biochem. 2002, 131, 511–515.
72. IV. J. Biol. Chem. 2015, 290, 21741–21748.
1. 73. Bhave, G.; Cummings, C.F.; Vanacore, R.M.; Kumagai-Cresse, C.; Ero-Tolliver, I.A.; Rafi, M.; Kang, J.; Pedchenko, V.; Fessler, L.I.; Fessler, J.H.; et al. Peroxidasin forms sulfilimine chemical bonds using hypohalous acids in tissue genesis. Nat. Chem. Biol. 2012, 8, 784–790.

Appendix 3

Modulation of Conductivity of Alginate Hydrogels Containing Reduced Graphene Oxide through the Addition of Proteins

Pharmaceutics 2021, *13*(9), 1473;

IF 6.321(2020).

CATEGORY: PHARMACOLOGY & PHARMACY

Rank 29/276 (Q1)

https://doi.org/10.3390/pharmaceutics13091473

Modulation of Conductivity of Alginate Hydrogels Containing Reduced Graphene Oxide through the Addition of Proteins.

Ahmed Raslan[1,†],Jesús Ciriza [2,3,4,†],Ana María Ochoa de Retana [5],María Luisa Sanjuán [6],Muhammet S. Toprak [7],Patricia Galvez-Martin [8],Laura Saenz-del-Burgo [1,2,9,*]andJose Luis Pedraz [1,2,9]

1 NanoBioCel Group, Laboratory of Pharmacy and Pharmaceutical Technology, Faculty of Pharmacy, University of the Basque Country UPV/EHU, 01006 Vitoria-Gasteiz, Spain; drrayad@gmail.com

2 Biomedical Research Networking Center in Bioengineering, Biomaterials, and Nanomedicine, CIBER-BBN, Paseo de la Universidad 7, 01006 Vitoria-Gasteiz, Spain; jeciriza@gmail.com

3 Tissue Microenvironment (TME) Lab, Aragón Institute of Engineering Research (I3A), University of Zaragoza, C/Mariano Esquillor s/n, 50018 Zaragoza, Spain

4 Institute for Health Research Aragón (IIS Aragón), 50009 Zaragoza, Spain

5 Department of Organic Chemistry I, Faculty of Pharmacy and Lascaray Research Center,

University of the Basque Country (UPV/EHU), Paseo de la Universidad 7, 01006 Vitoria-Gasteiz, Spain; anamaria.ochoaderetana@ehu.eus

6 Instituto de Ciencia de Materiales de Aragón (Universidad de Zaragoza-CSIC), Facultad de Ciencias, 50009 Zaragoza, Spain; sanjuan@unizar.es

7 Biomedical and X-ray Physics, Department of Applied Physics, KTH-Royal Institute of Technology, 10691 Stockholm, Sweden; toprak@kth.se

8 R&D Animal and Human Health, Bioibérica S.A.U., 08029 Barcelona, Spain; pgalvez@bioiberica.com

9 Bioaraba Health Research Institute, Jose Atxotegi, s/n, 01009 Vitoria-Gasteiz, Spain

* Correspondence. laura.saenzdelburgo@ehu.eus (L.S.-d.-B.); joseluis.pedraz@ehu.eus (J.L.P.); Tel.. +34-945014542 (L.S.-d.-B.); +34-945013091 (J.L.P.

Abstract.

Modifying hydrogels in order to enhance their conductivity is an exciting field with ap- plications in cardio and neuro-regenerative medicine. Therefore, we have designed hybrid alginate hydrogels containing uncoated and protein-coated reduced graphene oxide (rGO). We specifically studied the adsorption of three different proteins, BSA, elastin, and collagen, and the outcomes when these protein-coated rGO nanocomposites are embedded within the hydrogels. Our results demon- strate that BSA, elastin, and collagen are adsorbed onto the rGO surface, through a non-spontaneous phenomenon that fits Langmuir and pseudo-second-order adsorption models. Protein-coated rGOs are able to preclude further adsorption of erythropoietin, but not insulin. Collagen showed better adsorption capacity than BSA and elastin due to its hydrophobic nature, although requiring more energy. Moreover, collagen-coated rGO hybrid alginate hydrogels showed an enhancement in conductivity, showing that it could be a promising conductive scaffold for regenerative medicine.

Keywords. hydrogel; alginate; reduced graphene oxide; conductivity; collagen

1. Introduction.

Hydrogels are three-dimensional scaffolds made up of highly hydrophilic polymers. Because they absorb so much water, these hydrogels swell, representing a high degree of flexibility, closer to that of natural tissue [1]. Hydrogels also represent high porosity, excellent biocompatibility, and controllable degradability [2], triggering their application in biomedicine including, applications of soft contact lenses in the correction of vision [3], developing a tissue engineering process [2,4,5], diagnostics [6], and embolizing cells [7]. Depending on the type of bonding, these hydrogels can be classified as either physical or chemical. Physical bonding, such as hydrogen bonding, and hydrophobicity result in physical gels, which are often reversible and affected by environmental factors [1]. Chemical gels, in contrast, are formed by covalent bonding between polymers. These hydrogels are permanent and stable [8,9].

However, there are many limitations to the applications of nature hydrogels in clinical applications. These include high water content, large pores, weak mechanical strength, and fast drug release [3,10].

In the course of time, natural hydrogels have been gradually replaced by synthetic hydrogels that have a longer half lifetime and high mechanical strength [11].

Incorporating a special chemical group into the hydrogel will improve its functionality and allow the hydrogel to be switched by heat, light, magnetic fields, chemical agents, or pH alterations [2,12,13]. Functionalized hydrogels with therapeutic peptides and proteins are also possible. These can be used to treat diseases, such as cancer, immune disorders, mental disorders, hypertension, and certain cardiovascular and metabolic problems.

Extracellular matrix (ECM) is a non-cellular component of tissue that provides physical support to cells. Emerging research has shown that ECM provides tissue-specific biochemical and biophysical cues required for tissue morphogenesis [14].

For decades, alginate was considered one of the best biomaterials for assembling and fabricating functional hydrogels, owing to its excellent biocompatibility and high porosity [15,16]. However, several drawbacks, such as its mechanical strength, weakness, the leak of cell adhesion, and its rapid drug release, have limited its clinical application [17,18]. To solve these drawbacks, different materials have been integrated into the alginate matrix, also creating biomimetic support. In this regard, graphene has been

applied in various fields based on this excellent characteristic, including electronics [19], being considered a strong candidate in the field of biomedicine, both for fabricating drug delivery vehicles and gene therapy [19,20,21,22]. However, studies with graphene are contradictory [22]. On one hand, some reports describe graphene as a material that does not cause any alteration in cell function [23,24], with acceptable hemocompatibility, and without induction of immune response, even at high concentrations [24]. On the other hand, reports show a cytotoxic effect even at a low dosage [23,25]. Graphene oxide (GO), a derivative from graphene, can be produced through Hummer's method [26,27,28,29,30] and shows unique physical and mechanical properties, including high thermal conductivity [26,31,32], colossal surface area [33,34], and a robust mechanical strength [35,36]. The oxidation process of graphene alters the surface of graphene, increasing its affinity to water [37,38] and, therefore, mediating a vast number of biochemical reactions and bio-conjugations along its surface [39]. GO biocompatibility is affected in two-dimensional cultures by factors such as GO surface processing and the particle size of surface functionality, with impact on adhesion or cell proliferation [40]. In this regard, our group combined GO with alginate to modify alginate surface properties and its mechanical strength, showing good biocompatibility with myoblasts in alginate microcapsules, within a range of GO concentrations. Concisely, GO concentrations between 25 and 50 µg/mL enhanced the viability of C_2C_{12} myoblasts [16,40,41,42]. However, the integration of GO within alginate matrices reduced the release of therapeutic factors, since GO could sorb the secreted therapeutic factors on its surface due to its high surface activity. GO sorption was solved by applying a pre-coating layer on the GO surface with fetal bovine serum [16,40,41,42].

An alternative graphene derivate is reduced GO, with low surface absorbability compared to GO [43]. Several techniques have been utilized to reduce GO, including mechanical reduction or chemical reduction [43], adding alterations in rGO surface, such as the chemical structure and hydrophilicity [37,44]. However, there is again conflicting information comparing the biocompatibility of GO and rGO [43,45,46]. It has been described that the irradiated light reduction in GO yields an immense reactive oxygen species generation and oxidative stress [43], while the small particle size of thermally reduced oxide can stimulate cytotoxicity, facilitating its cell membrane penetration [43]. However, chemically reduced rGO shows lower toxicity than other rGO forms [47]. Modified scaffolds with rGO have shown strong mechanical strength and ultra-high electrical conductivity [48], with favorable impacts on cell viability, proliferation, and

differentiation [48]. Hydrothermal processing of alginate and graphene oxide in an aqueous solution yields hybrid alginate-rGO hydrogels with high porosity. In the hydrothermal process, graphene nanosheets and alginate form a porous structure as a result of auto-assembly; afterwards, the hybrid hydrogel is produced by ionically linking polymer networks of alginate [49]. Thus, rGO has become more applicable in tissue engineering, particularly for neuronal regeneration [48,50] or cardiomyocytes regeneration [51]. Here, we are using reduced graphene-based materials, as it is one of the best redox species that could be studied on an electrode. The redox peaks will give a clear indication of changes to the double layer on the electrode's surface. When rGO-protein-alginate is incorporated over an electrode the double layer changes, this can affect the double-layer capacitance and the electron transfer resistance. Therefore, by monitoring the charge transfer resistance, we could understand the charge transfer properties of the double layer. Cyclic voltammetry (CV) and electrochemical impedance spectroscopy (EIS) are interrelated electroanalytical methods to examine the electrochemical double layer on the electrodes. In this work, we aimed to create conductive protein-rGO-alginate hydrogels using different proteins in order to study their adsorption capacity and electrochemical characteristics to identify the best composition.

2. Materials and Methods

2.1. Materials

The chemically reduced graphene oxide (rGO) powder was provided by Graphenea (San Sebastian, Spain). Bovine Serum Albumin (BSA) and type 1 Collagen were purchased from Sigma Aldrich (Saint Louis, MO, USA). Elastin was provided by Bioiberica (Barcelona, Spain). High pure, low-viscosity, and ultra guluronic (LVG) acid alginate was purchased from FMC Biopolymer (Drammen, Norway).

2.2. Protein Adsorption

rGO powder in a 3/1 mixture of water and DMSO (v/v) to get a suspension of 4 mg/mL rGO, homogenizing by sonication for 60 min in a bath. The resulting rGO dispersion was diluted to 2.5 mg/mL with 18 MΩ cm resistivity deionize water (DI). Then, 90 µL of 200 µg/mL BSA, 200 µg/mL elastin, or 500 µg/mL collagen were mixed with 10 µL of 250 µg/mL rGO suspension for 120 min at 37 °C under agitation at 400 rpm. The samples were spun down at 15,000 rpm for 15 min to collect supernatants. The lack of adsorbed protein was determined with the BCA kit (Thermo Fisher, Massachusetts, MA,

USA) in a M 200 TECAN microplate reader (TECAN Trading AG, Männedorf, Switzerland) at 562 nm. At least three samples were quantified to ensure accuracy and repeatability. The % of protein sorption was estimated by Equation (1), and the adsorption capacity qe (µg/µg) was estimated by Equation (2), where C0 (µg/mL) and Ce (µg/mL) are the original protein concentration and the protein concentration at steadiness, respectively, S is the sample volume (mL), and m is the mass of rGO (µg).

$$\text{Adsorbability (\%)} = (C_0 - Ce) \times 100/C_0 \quad (1)$$

$$\text{Adsorption capacity qe} = (C_0 - C_e) \times S/m \quad (2)$$

Freundlich and Langmuir's adsorption isotherm models were implemented to estimate the adsorption isotherm. The Langmuir model is displayed in Equations (3) and (4), where the concentration of the adsorbed protein at steady-state is Ce (µg/mL), qe is the adsorption capacity (µg/ug), qmax (µg/µg) is the maximum quantity of protein sorbed per unit mass of rGO, K_L (mL/µg) is the Langmuir factor associated with the surface affinity for the protein, C_0 is the initial protein concentration, and R_L is the separation factor that specifies the Langmuir isotherm's fundamental aspects [52].

$$Ce/qe = Ce/qmax + 1/(qmax \cdot K_L) \quad (3)$$

$$R_L = 1/ (1 + K_L \cdot C_0) \quad (4)$$

Freundlich model is described as follows (Equation (5)), where K_F and m are the Freundlich constant and intensity adsorption, respectively.

$$\text{Log qe} = \log K_F + 1/m \cdot \log Ce \quad (5)$$

2.3. Kinetics of Protein Adsorption

250 µg/mL rGO was suspended either in 50 µg/mL BSA, 200 µg/mL collagen, or 50 µg/mL elastin by agitation at 37 °C. After spinning down at 15,000 rpm for 10 min, supernatants were collected after the following incubation times. 5, 10, 20, 30, and 80 min. Adsorbed protein was quantified with a BCA kit (Thermo Fisher) in a M 200 TECAN microplate reader (TECAN Trading AG, Männedorf, Switzerland) at 562 nm. At least three samples were quantified to ensure accuracy and repeatability. Intra-particle diffusion model, pseudo-first-order, and pseudo-second-order rate adsorption were applied to the results to determine the most appropriate adsorption kinetic model. At least three samples were quantified for each condition. Several models were evaluated to elucidate the

adsorption mechanism and the adsorption rate (Equations (6)–(9)) [16], where qt (µg/µg) is the quantity of the adsorbed protein vs. time (*t*) (min.), Kp is the intra-particle diffusion rate constant (µg/µg. $min^{1/2}$), and C (µg/µg) is a constant for the intra-particle diffusion model, which provides a piece of information about the thickness of the barrier layer [52,53], qe (µg/µg) is the adsorption capacity at equilibrium, K_1 (min^{-1}) is the constant rate of the pseudo-first-order model, and K_2 ($\mu g \cdot \mu g^{-1} min^{-1}$) is the pseudo-second-order model's constant rate.

2.4. Thermodynamics of Protein Adsorption

250 µg/mL rGO was suspended either in 50 µg/mL BSA, 200 µg/mL collagen, or 50 µg/mL elastin solution. Mixtures with each protein were incubated and agitated at the following temperatures. 5, 10, 15, 25, 37, and 39 °C. After spinning down at 15,000 rpm for ten minutes, supernatants were collected to quantify the amount of non-adsorbed protein with BCA kit (Thermo Fisher) in a M 200 TECAN microplate reader (TECAN Trading AG, Männedorf, Switzerland) at 562 nm. At least three samples were quantified for each condition. The fundamental thermodynamic factors, such as entropy change (∆S°), enthalpy change (∆H°), and Gibbs free energy change (∆G°), were calculated using Equations (10)–(13) [53,54,55], where R is the gas constant (8.314 J/mol K), T the absolute temperature (K), K_d the equilibrium constant, qe (µg/µg) the quantity of protein adsorbed per mass unit of rGO at equilibrium, and Ce (µg/mL) the equilibrium concentration of each protein.

$$qt = Kp.t^{1/2} + C \quad (6)$$

$$\log (qe - qt) = \log (qe) - (K_1 \cdot t)/2.303 \quad (7)$$

$$t/qt = t/qe + 1/K_2 \cdot 1/(qe)^2 \quad (8)$$

$$1/qt = 1/(K_2 + qe^2) \cdot 1/t + 1/qe \quad (9)$$

2.5. Characterization of the rGO-Protein Binding.

The binding of each protein to rGO surface was studied by Raman and Fourier transform infrared spectroscopy. First, 250 µg/mL rGO was suspended either in 50 µg/mL BSA, 200 µg/mL collagen, or 50 µg/mL elastin solution, and agitated at 37 °C for 2 h. The supernatants were collected after spinning down at rpm for 15 min and lyophilized in a Telstar Lyobeta 15 lyophilizer. rGO without protein incubation and proteins without rGO were also studied. At least three samples were studied for each condition. Raman spectrum was obtained by confocal Raman imaging (Alpha 300 M, Company WITec, Ulm,

Germany) with a 532 nm laser (5% laser power, a contact time of the 50 s, and four accumulations). FT-IR, using an attenuated total reflectance (ATR) technique, was performed in a FT-IR Bruker IFS 66/S Spectrometer, with 32 scans at a resolution of 4 cm^{-1} between the wavelength ranges of 4000–400 cm^{-1}. Air background was applied as a blank. At least three samples were analyzed for each condition.

2.6. EPO and Insulin Adsorption Blocking Study

100 µg/mL rGO was suspended either in DI water, 50 µg/mL BSA, 200 µg/mL collagen, or elastin and incubated for two hours at 37 °C. After being spun down at 15,000 rpm for 15 min, supernatants were removed, and protein-coated rGO was incubated with 200 µL of 200 mIU/mL recombinant EPO or 150 mIU/mL recombinant insulin for 24 h at 37 °C. Uncoated rGO was used as a reference. Next, samples were spun down by centrifuging for 15 min at 15,000 rpm and supernatants were collected. Non adsorbed EPO and insulin were quantified with Quantikine IVD EPO (R&D Systems) and Insulin Elisa (Mercodia), respectively, following manufacturer recommendation. At least three samples were analyzed for each condition.

2.7. Preparation of Alginate Hydrogels Containing rGO and Protein-Coated rGO

At room temperature, 1.87 g of high pure sodium alginate was dissolved in 1% mannitol by magnetic string at 200 rpm for 2 h; then, it was mixed and homogenized with either rGO or protein-coated rGO suspension, obtaining a final concentration of 1.5% alginate and 50 µg/mL rGO. To prepare hybrid alginate hydrogels, alginate solutions were mixed with 60 µL of 1.22 M calcium sulfate through a connector (Braun) between two Luer Lock syringes (BS Syringe). The mixed solutions were dispensed between two glass slides with 2 mm spacing, leaving them for 30 min to form hydrogel disks, 14 mm in diameter.

2.8. Conductivity of Alginate Hydrogels Containing Protein-Coated rGO

Electrochemical impedance spectra (EIS) were measured using a potentiostat (Princeton Applied research, Oak Ridge, TN, USA), with a screen-printed electrode (Dropsens, Oviedo, Spain) based on carbon, and a silver electrode as reference. Samples were immersed in 0.1 M PBS buffer at room temperature, applying frequency series from 10^{-1} to 105 Hz. Cyclic Voltammetry (CV) measurements were performed in 0.1 M PBS buffer between the potential range from −0.2 to 0.5 V and at different scan

speeds (100 mVs^{-1}). Specific capacitance was estimated from CV curves by Equation (14) [16,56], where C ($F \cdot g^{-1}$) is the specific capacitance, Q the mean charge throughout the charging and discharging procedure, the potential range V (Volt), and the mass m (g) of the hydrogel disk.

$$C = Q/(2Vm) \quad (14)$$

2.9. Statistical Analysis

Statistical analysis was performed with GraphPad Prism 9.0 (GraphPad Inc., San Diego, CA, USA) and SPSS (version 27.00, IBM, New York, NY, USA) software. Results were presented as mean ± standard deviation. A normality test was performed, considering $p < 0.05$ as statistically significant values after ANOVA and Tukey's post hoc test bivariate correlation testing.

3. Results and Discussion

3.1. Adsorption of Proteins on rGO Surface.

We began studying the adsorption capacity of rGO to several proteins usually located in FBS. Thus, we observed that rGO adsorption capacity (qe) was enhanced at low protein dose values, indicating the presence of available active groups on the rGO surface. However, no significant modifications in qe values at high initial protein doses (Co) were quantified, suggesting that no further protein loading on the rGO surface was allowed. Among the studied proteins, collagen showed the highest adsorption capacity (qe = 0.022 µg/µg), while other hydrophilic proteins, such as BSA and elastin showed a low affinity for rGO surface (qe between 0.0049–0.0067 µg/µg) (**Figure 1**a).

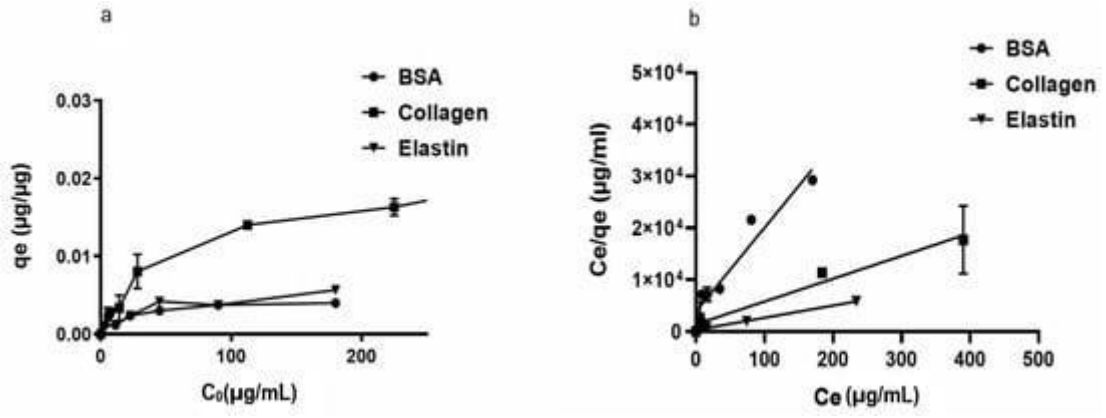

Figure 1. (**a**). Adsorption capacity (qe) of rGO (250 µg/mL) with initial concentrations of 200 µg/mL BSA, 200 µg/mL elastin and 500 µg/mL collagen after two hours of incubation at 37 °C. (**b**) Langmuir models for BSA, collagen, and BSA adsorption on the rGO surface.

In order to understand the adsorption phenomena involved on rGO surface, Langmuir and Freundlich's models were applied to the qe values recorded at a constant temperature, calculating the required parameters for the aforementioned models (Table 1 and Figure 1b). Protein adsorption phenomena on the rGO surface was better specified by the Langmuir than the Freundlich model, with R2 values between 0.968 and 0.996 for the Langmuir model and convergence between calculated qmax values and experimental qe results. Therefore, we suggest that adsorption phenomena occur on a homogeneous surface of rGO, with a specific number of adsorption sites on rGO surface binding to protein active sites and forming a monolayer [56]. In fact, Langmuir variable values (RL) < 1 would suggest advantageous adsorption onto the rGO surface for the studied proteins, with irreversibile adsorption for collagen and elastin (RL ≈ 0) [57].

Table 1. Parameters required for Langmuir and Freundlich adsorption isotherms. qe (µg/µg) is the Adsorption capacity at equilibrium, KL (mL/µg) is the Langmuir factor, R2 is the coefficient of determination for the Langmuir model, and qmax (µg/µg) is the maximum adsorption capacity of the proteins by rGO. For the Freundlich model, where KF is the Freundlich constant and m is the intensity adsorption, R2 is the coefficient of determination for the Freundlich isotherm.

	Langmuir Model				**Freundlich Model**				
	q_e µg/µg	**K_L ml/µg**	**R_L**	**R^2**	**qmax µg/µg**	**1/m**	**M**	**K_f**	**R^2**
BSA	0.0070	0.0297	0.1570	0.968	0.0091	0.345	2.896	0.00197	0.95
Collagen	0.0220	0.0313	0.0660	0.987	0.0230	0.386	2.590	0.00228	0.92
Elastin	0.0049	0.1980	0.0271	0.996	0.0049	0.161	6.184	0.00230	0.83

Studying the adsorption capacity (qt) of rGO over time, we observed a quick adsorption process, completed after 20 min (Figure 2a). The intraparticle-diffusion model was implemented to attain a suitable mechanism that fits the protein adsorption on rGO surface (Figure 2b). However, since q*t* vs. $t_{1/2}$ plotting showed linearity without going across zero, we think that intraparticle-diffusion is not the only process controlling protein adsorption on the rGO surface; film diffusion also contributes to the protein adsorption [40]. Calculated intraparticle-diffusion parameters, such as the diffusion rate constant (KP) and the impediment layer wideness (C) (Table 2), showed collagen with the highest intra-particle diffusion rate Kp (0.0001 $\mu g \cdot \mu g^{-1} min^{-1/2}$) and boundary layer thickness (0.0132), correlating to a strong hydrophobic attraction between collagen and the hydrophobic rGO surface. This result suggests that π–π bonding between collagen and rGO might also be responsible for this bonding [57]. However, the hydrophilicity of BSA and elastin would result in the decrease in interference forces and therefore the affinity with rGO.

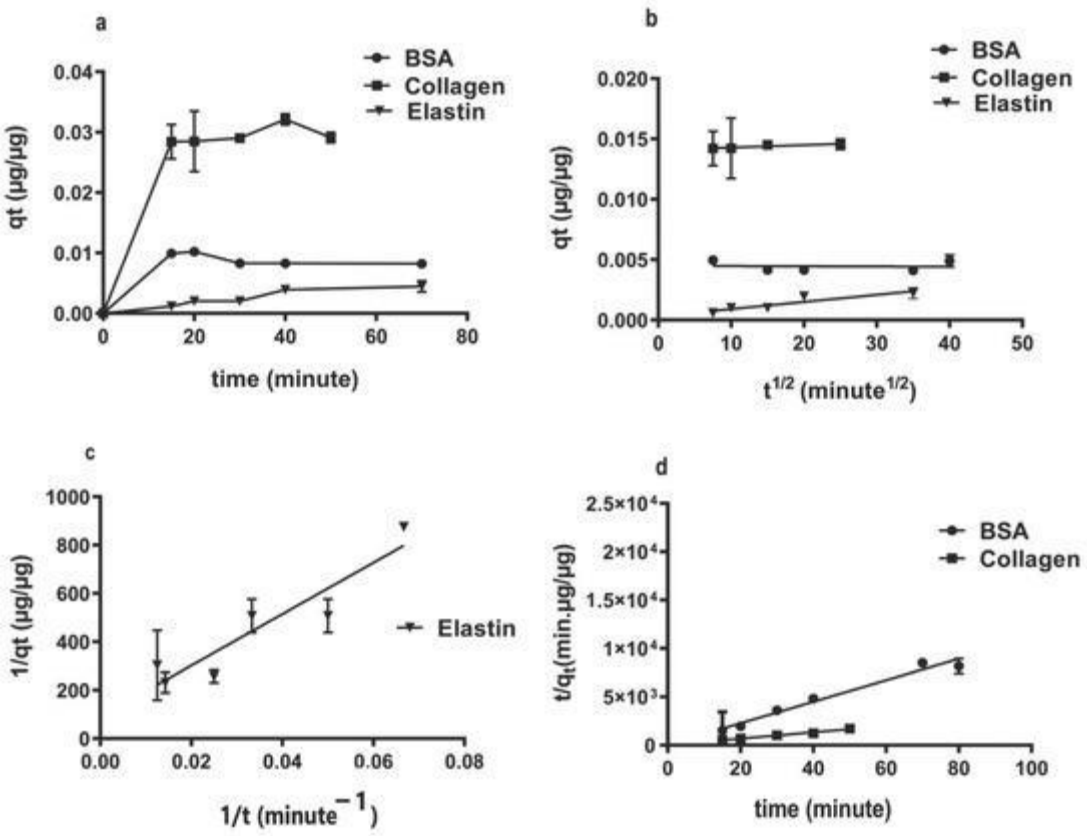

Figure 2. Kinetic protein adsorption models on rGO surface. (**a**) Adsorption capacity over time; (**b**) intra-particle diffusion model plot; (**c**) pseudo-second-order model plot for BSA and collagen; (**d**) nonlinear plot of pseudo-second-order for elastin.

Table 2. Calculated parameters from intra-particle diffusion pseudo-first-order and pseudo-second-order model. Calculated parameters from intra-particle diffusion are the intra-particle diffusion rate constant (K_p), constant for the intra-particle diffusion model (C) and coefficient of determination (R^2). The presented parameters for the pseudo-first-order are the adsorption capacity at equilibrium (qe), rate constant (K_1), and the coefficient of determination (R^2). For the pseudo-second-order model, the parameters are the rate constant (K_2) and the adsorption cap

	Intra-Particle-Diffusion Model			**Pseudo First Order Model**			**Pseudo Second Order Model**			
	K_p			**K_1**	**qe**		**Qe**	**K_2**		**q*t***
	$\mu g \cdot \mu g^{-1} min^{-1/2}$	**C**	**R^2**	**min^{-1}**	**µg/µg**	**R^2**	**µg/µg**	**$\mu g \cdot \mu g^{-1} min^{-1}$**	**R^2**	**µg/µg**
BSA	0.00002	0.0037	0.67	22.1	0.0074	0.35	0.009	2.34	0.98	0.0091
Collagen	0.0001	0.0132	0.96	16.3	0.0019	0.65	0.0307	27.27	0.99	0.0294
Elastin	0.00005	0.0004	0.91	67.7	0.0379	0.82	0.0067	2.16	0.93	0.0044

at different times (q*t*).Among adsorption kinetic mathematical models, the low R^2 values calculated in the pseudo-first-order model (0.35–0.82), with vast difference between estimated qe and experimental qt [139]discarded this model for describing adsorption phenomena on the rGO surface. However, the pseudo-second-order model showed high R^2 values (0.93–0.99) and convergence between the estimated qe and the experimental qt values (Table 2); therefore, this model can be considered the best kinetic model to define the studied protein adsorption phenomena on the rGO surface [58,59]. Interestingly, pseudo-second-order constant K_2 reduced while hydrophilicity increased with the lowest K_2 for elastin ($2.16 \cdot \mu g^{-1} \cdot in^{-1}$) and with the highest for collagen (27.27 $\mu g \cdot \mu g^{-1} \cdot min^{-1}$). Representing qt values versus time, while a linear pseudo-second-order plot was more suitable for collagen and BSA (Figure 2c), a nonlinear pseudo-second-order plot was fit for elastin adsorption (Figure 2d) [60]. Collagen showed a ten-fold higher adsorption rate constant (K_2) than BSA and elastin, indicating the highest affinity for rGO than elastin or BSA and due to the strong hydrophobic–hydrophobic interactions between rGO surface and collagen [61].

3.2. Thermodynamics of Protein Adsorption onto rGO Surface.

The study of adsorption capacity (qT) with BSA and elastin on rGO surface increasing temperature revealed the exothermic character ($\Delta H° < 0$) of the adsorption (Figure 3a, Table 3). However, collagen showed endothermic adsorption when the temperature was increased ($\Delta H° = 2.44$ kJ/mol). We consider that the protein adsorption could start with an endothermic hydration step, followed by exothermic adsorption, but in collagen, there would be a hydration step caused by its hydrophobic nature that requires more

energy than the other studied proteins [62]. This hypothesis would explain why an increase in the temperature would enhance the adsorption capacity of collagen, while it would increase the kinetic energy of BSA and elastin causing their elution from rGO surface. Moreover, the low ΔG° values (Table 3) indicated the physio-sorption nature of the adsorption [58], a non-spontaneous phenomenon that is a feature of positive ΔG° values. It could be attributed to the presence of an energy barrier in the migration of the studied proteins towards the rGO surface, with water forming a hydration shell around the proteins that would hinder their adsorption on rGO. Finally, the remarkable reduction in entropy during the adsorption of the studied proteins [58] suggests that molecular motion at the solid–liquid interface is more organized [63].

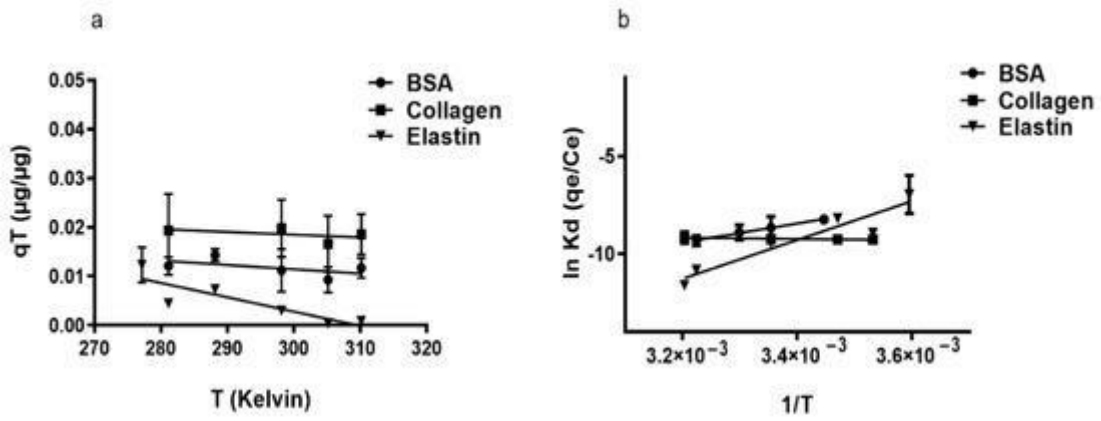

Figure 3. (**a**) Influence of temperature on the adsorption of proteins. Where mixtures of 250 µg/mL rGO were suspended either in 50 µg/mL BSA, 200 µg/mL collagen, or 50 µg/mL elastin solution and incubated for 2 h at the following temperatures. 5, 10, 15, 25, 37, and 39 °C. (**b**) Van't Hoff linear plot of ln Kd against 1/T for proteins adsorption on rGO. ΔH° was estimated from the slope (= −ΔH°/R) and ΔS° from the y-intercept (= +ΔS°/R).

Table 3. Thermodynamic parameters for protein adsorption by rGO. enthalpy of adsorption, ΔH° (kJ/mol); entropy of adsorption, ΔS° (kJ/mol·K); Gibbs free energy of adsorption, ΔG° (kJ/mol); coefficient of determination, R^2.

	ΔH° kJ/mol	**ΔS° kJ/mol.K**	**ΔG° kJ/mol**	**R^2**
BSA	−40.34	−0.207	23.95	0.99
Collagen	2.44	−0.069	23.68	0.95
Elastin	−89.96	−0.358	28.40	0.94

3.3. Surface Chemistry of Protein Adsorbed rGO

In order to confirm the adsorption of the studied proteins onto the rGO surface, we studied rGO and protein-adsorbed rGO by Raman spectroscopy and FT-IR. In Raman spectra, G and D bands at ~1595 cm^{-1} and ~342 cm^{-1} in rGO Raman spectrum indicated the occurrence of defects due to the reduction process of GO [52] (Figure 4a), also detected in protein adsorbed-rGO samples (Figure 4b–d). After proteins were adsorbed on the rGO surface, the G and D bands shifted to ~1588–1601 cm^{-1} and ~1342–1351 cm^{-1}, respectively. The intensity ratio between those bands (ID/IG) suggested an sp^2 electron distribution in all the samples [63], being higher than those ID/IG ratios previously described in graphene [64], and slightly increased when proteins were adsorbed on rGO (Table 4). Finally, the 2D band position and their intensity ratio with G band (2D/G) increase would indicate more structural defects, most likely attributed to protein adsorption on rGO [65], confirming the adsorption of the studied proteins on the rGO surface [66].

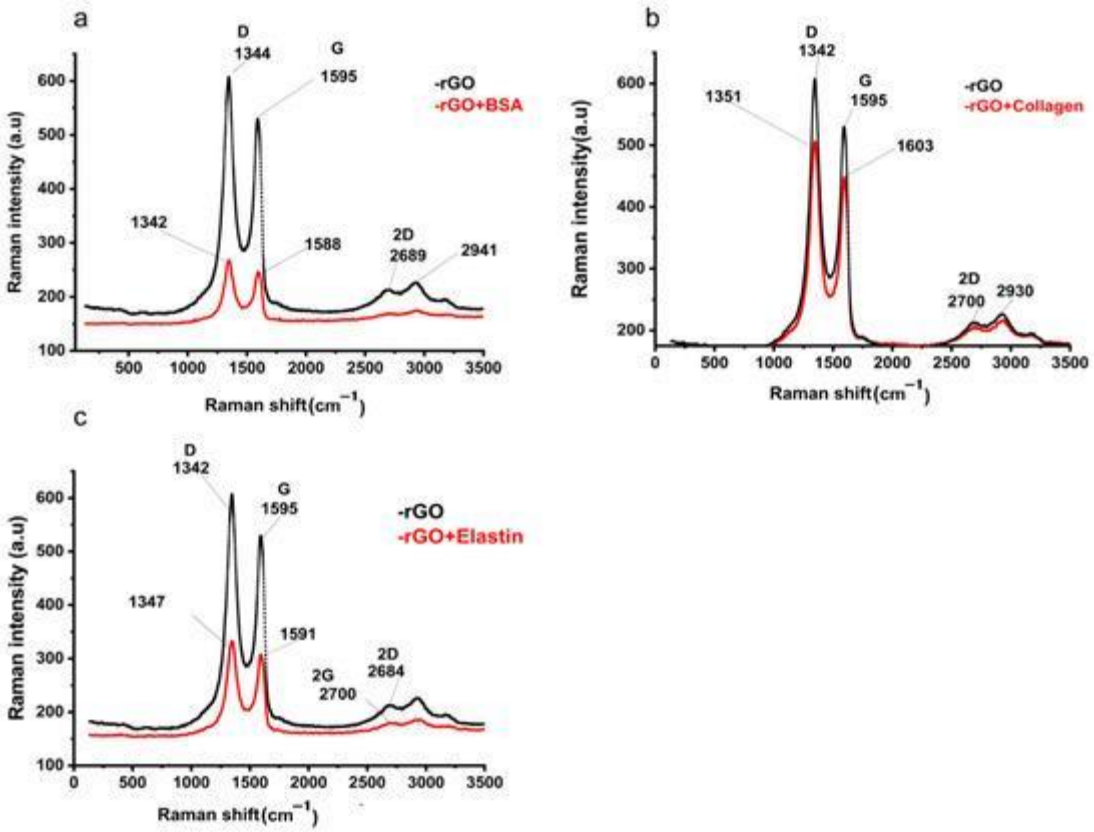

Figure 4. Raman spectra of rGO before and after the adsorption of (**a**) BSA (rGO + BSA), (**b**) collagen (rGO + collagen), and (**c**) elastin (rGO + elastin).

Table 4. Parameters from Raman spectra. the D band is related to scattering from local defects or disorders present in carbon, and the G bands arise from the in-plane diverging stretching of the C–C bonds in the graphitic structure, and (2D) is related to the number of graphene layers. ID/IG is the intensity ratio of the D and G bands, which refers to the amount of defects existing in the graphene matter. The intensity ratio of 2D/G is related to the number of graphene layers in the matrix.

Sample	D cm^{-1}	G cm^{-1}	2D	ID/IG	2D/G
rGO	1342	1595	2664	1.17	0.142
rGO-BSA	1342	1588	2669	1.19	0.226
rGO-Collagen	1342	1610	1692	1.20	0.144
rGO-Elastin	1347	1591	2700	1.16	0.173

Then, we confirmed the adsorption of the studied proteins on the rGO surface by FT-IR using an attenuated total reflectance (ATR) technique. Thus, we detected an absorption peak in rGO sample at 1603 cm^{-1} related to C=C stretching vibration, and at 1736 cm^{-1} and 1266 cm^{-1}, corresponding to carboxyl C=O and carbonyl C-O stretching vibrations, respectively [56] (Figure 5). When rGO incubated with the studied proteins was analyzed by FT-IR, an obvious shift of the C=C stretching band from 1603 cm^{-1} to 1590–1600 cm^{-1} and a shift of the C-O stretching band from 1266 cm^{-1} to 1227–1250 cm^{-1} were detected, which were ascribed to the π–π bonding between the benzene ring from proteins and the rGO surface (Table 5) [67]. Although due to the incomplete reduction in rGO, a hydroxyl signal was detected in FT-IR spectra, forming H-bonding when incubated with proteins (3692–3701 cm^{-1}), these slight changes are not strong enough for stable H-bond formation. Therefore, we consider that the studied protein adsorption on the rGO surface is attributed mainly to π–π interactions between the rGO surface and the proteins [52,68].

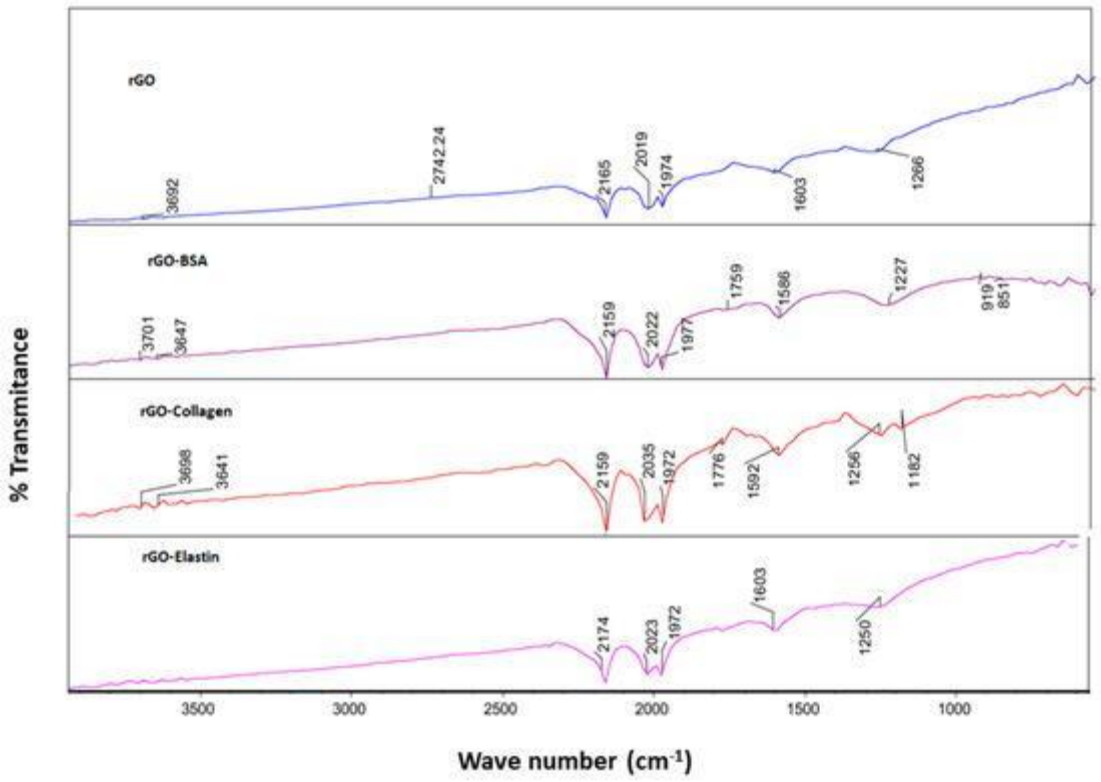

Figure 5. FT-IR spectra of rGO before and after the adsorption of BSA (rGO-BSA), collagen (rGO-collagen), and elastin (rGO-elastin).

Table 5. Parameters from FT-IR using an attenuated total reflectance (ATR) for rGO and rGO-proteins.

	C=C (cm^{-1})	Carboxyl C=O (cm^{-1})	Carbonyl C-O (cm^{-1})	H-Bonding (cm^{-1})
rGO	1603	1736	1266	3650
rGO+BSA	1590	1760	1227	3701
rGO+Collagen	1592	1774	1247	3618
rGO+Elastin	1600	1770	1250	3655

3.4. Therapeutic Protein Adsorption on Protein Coated rGO.

In order to determine if blocking the rGO surface with the studied proteins precluded further adsorption of other proteins, we studied the adsorption of two different therapeutic proteins as erythropoietin and insulin (Figure 6) for 24 h at 37 °C. No differences were detected among the studied coating proteins when adsorption studies were performed with either erythropoietin (EPO) or insulin. However, this behavior with the therapeutic proteins was slightly different, since EPO trapping was lower than insulin, indicating a higher blocking for EPO protein by the protein coating.

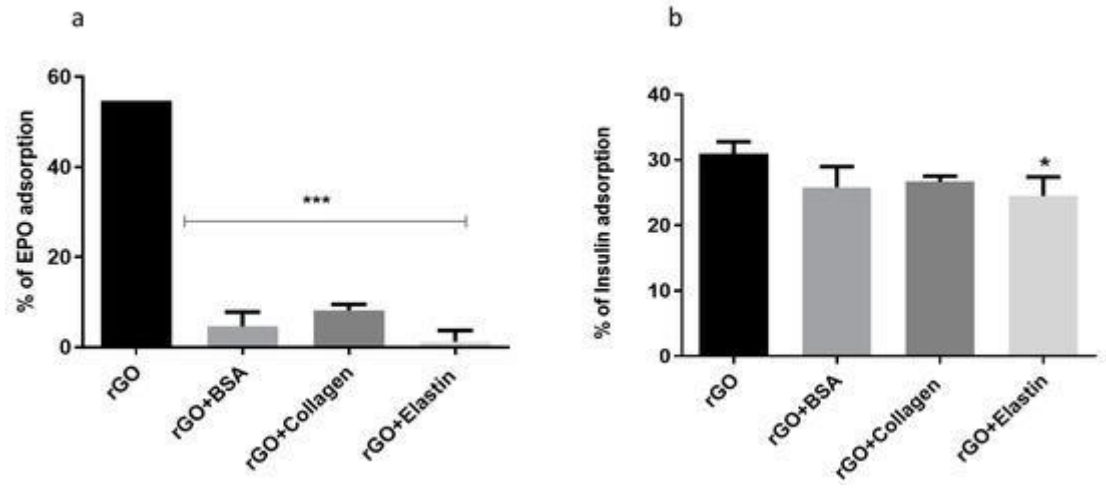

Figure 6. (**a**) Erythropoietin (EPO) and (**b**) insulin adsorption on rGO and rGO-protein matrix. Note. *. $p < 0.05$, ***. $p < 0.001$, compared to rGO without protein coating.

The mechanism of insulin adsorption by graphene and GO was shown to be different. The high adsorption of insulin hormone by graphene can be explained by a strong π–π interaction between the phenyl rings of insulin and the graphene surfaces [69]. On the other hand, insulin adsorption on the GO surface was attributed to electrostatic interactions and hydrogen bonds with the oxygenated functional groups. This interaction would be enough to overcome the blocking exerted by the coated studied proteins onto rGO, being unable to block the adsorption of further proteins with low molecular weight (6 kDa) and high hydrophilicity, such as insulin [16].

3.5. Conductivity Studies of Alginate Hydrogels Containing Protein Coated rGO

rGO has properties close to graphene and shows excellent electrical properties, including high electrical conductivity and high mobility [43]. During the reduction process, structural defects are formed, such as physical holes after removing the oxygen functional groups or alkyl groups. These holes can act as charge carriers and are responsible for the high conductivity of rGO [56]. In fact, the incorporation of rGO within scaffold matrices has improved their conductivity, such as rGO–gelatin methacryloyl (GelMA) hybrid hydrogels displaying improved electrical conductivity and mechanical properties [63]. Hybrid scaffolds with carbon nanofibers (CNFs) incorporated in alginate and gelatin hydrogels have demonstrated high electroconduction. Furthermore, this preparation method permits the elaboration of homogeneously dispersed hydrogels with integrated CNFs. The hybrid composite hydrogels including rGO were reported to display excellent electrical conductivity in the range of $4.1 \times 10^{-4} \pm 2 \times 10^{-5}$ S/cm [70]. Therefore, we decided to study the electrochemical activity of protein-coated-rGO embedded within alginate

hydrogels through the impedance spectroscopy (EIS) and cyclic voltammetry (CV) measurements. We quantified the phase angle (deg) and impedance modulus |Z| (ohms) within a range of frequencies between 10^{-1} and 10^{6} Hz in EIS, followed by analyzing the experimental data by Bode model (Figure 7) to determine the insulating or conducting behavior for the studied hydrogels. We determined that the addition of rGO or protein-coated-rGO to alginate matrix induced a slight decrease in hydrogel impedance at low frequencies. Moreover, we observed that the phase angle stayed close to 90° at low frequencies, decreasing towards zero at ultra-high frequencies in all the hydrogels studied (Figure 7a), quantifying the highest phase angle in collagen-coated rGO-alginate hydrogels. The magnitude of the impedance is inversely proportional to capacitance. ideal capacitors have lower impedance [71]. With rising frequency, the impedance of any given capacitance decreases. The frequency response of impedance is depicted in two portions on the Bode plot (Figure 7a). The first is associated with the hydrogel and is below 10^{1} Hz, whereas the second is related to the charge transfer resistance between the hybrid hydrogel and the electrolyte [72].

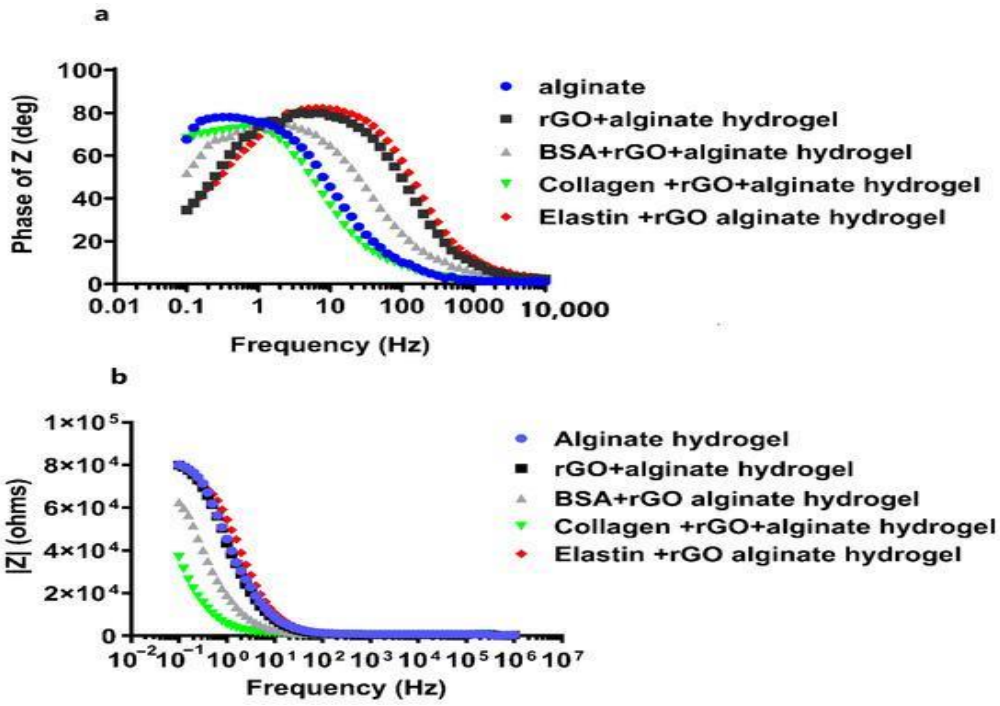

Figure 7. Electrochemical impedance spectroscopy (EIS) measurements for pristine alginate hydrogel, and hybrid alginate hydrogels containing protein-coated rGOs (rGO-BSA, rGO-Collagen, and rGO-Elastin). Bode plots representing (a) phase angle Z vs. frequency, and (b) the impedance modulus |Z| (ohms) vs. frequency. Measurements were performed in 0.1 M PBS buffer at room temperature.

The charge transfer resistance, as seen in Figure 7b, has the largest variance, where alginate hydrogels showed the highest impedance value, decreasing when rGO or protein-rGO was introduced into the hydrogels, especially with collagen that showed the lowest impedance value. At low frequencies, the charge transfer resistance can be obtained by interpolating the semi-circle to the real x-axis [73]. The current density of the rGO-proteins alginate hydrogels rises as the hydrogel resistance and charge transfer resistance fall [73]. Figure 8 depicts the charge transfer resistance (Rct) derived by analyzing the EIS spectra. Because the charge transfer resistance characterizes the electron flow at the counter electrode to a great extent, the lower the resistance, the faster the electron flow rate in the hydrogel [73].

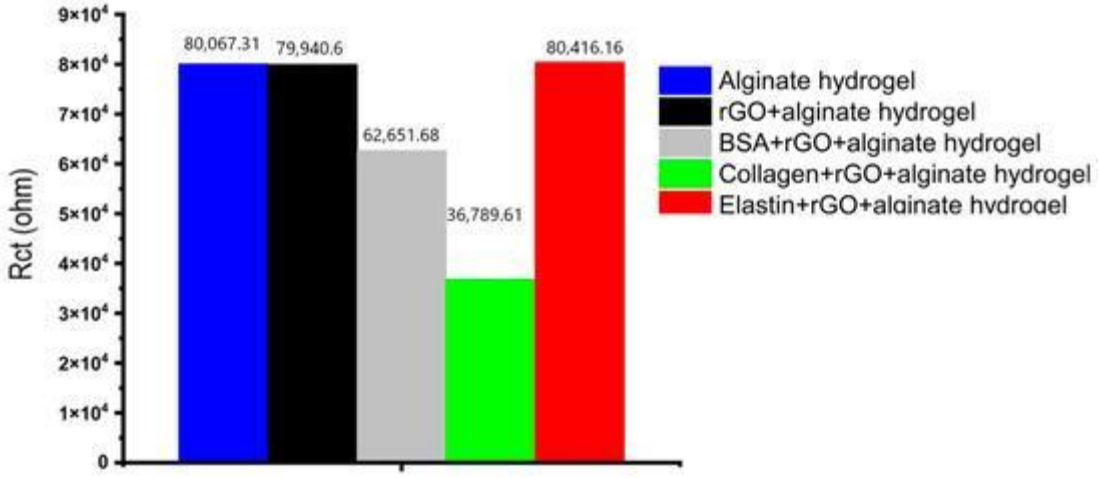

Figure 8. The charge transfer resistance (Rct) derived by analyzing the EIS spectra.

The impedance of rGO-proteins alginate hydrogels reduced greater and that was attributed to the π–π bonding between rGO and the adsorbed proteins [74], the electrons of the π–π bonding have higher mobility than that of the holes in rGO, which is the main charge carrier in rGO [75,76]. Cyclic voltammetry (CV) is a technique used to assess redox properties, stability, and surface area of electrodes for biosensing, using materials such as graphene [77]. In this work, we applied the CV to study the electrochemical activity of the alginate hydrogel and hybrid alginate hydrogel with rGO and rGO-proteins. Through the CV the specific capacitance of each hydrogel can be estimated. Voltammetry (CV) measurements showed excellent capacitance for all the tested hydrogels, maintaining the box-like shape even at different scan rates (Figure 9)

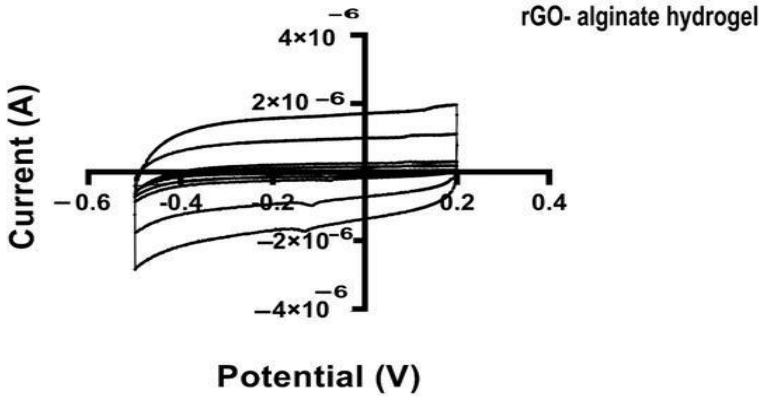

Figure 9. Cyclic voltammograms (CV) for hybrid rGO-alginate hydrogel at various scan rates. The potential (V) was plotted against the current (A). All specimens were dipped in 0.1M PBS and CV measurements were done at the potential range from −0.2 to 0.5 V at different scan rates (100 mVs^{-1}).

When rGO-proteins were added to the alginate matrix, the specific capacitance of the hybrid alginate hydrogel was modified (Figure 10). Collagen-coated rGO maximized the capacitance reaching the highest value (3.17×10^{-5} F/g), while BSA-rGO-alginate hydrogel and elastin-rGO-alginate hydrogel minimized it (to 1.88×10^{-5} F/g and 1.20×10^{-5} F/g, respectively) (Table 6). Therefore, CV results confirmed the measurement quantified in EIS, indicating that collagen-coated rGO hydrogel enhances the conducting behavior of rGO hydrogels [74], modifying the electrical properties of alginate hydrogel.

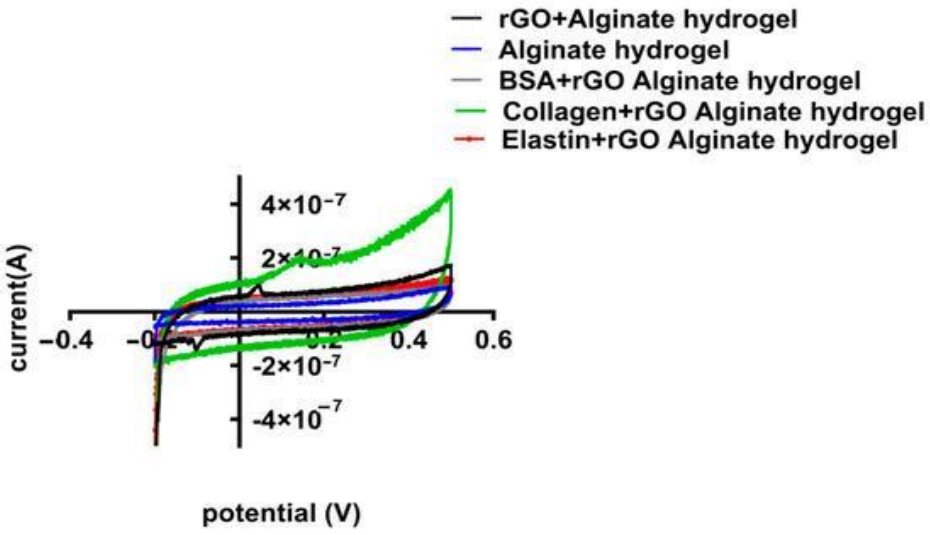

Figure 10. Cyclic voltammetry (CV) potential (V) vs. current curves for different hybrid alginate hydrogels containing uncoated and protein-coated rGOs (rGO-BSA, rGO-Collagen, and rGO-Elastin). All specimens were dipped in 0.1M PBS and CV measurements have been done at the potential range of −0.2 to 0.5 V, though the rate is specified as 100 mV/s.

Table 6. Specific capacitance for the tested hydrogels.

Hydrogels	Specific Capacitance (F/g)
Alginate	6.60×10^{-6}
rGO + alginate	1.84×10^{-5}
BSA + rGO + alginate	1.88×10^{-5}
Collagen + rGO + alginate	3.17×10^{-5}
elastin + rGO + alginate	1.20×10^{-5}

4. Conclusions

Aiming to improve alginate hydrogels, we incorporated reduced graphene oxide (rGO) coated with proteins—BSA, collagen, or elastin—into the alginate hydrogel matrix. Our finding demonstrated that the adsorption of these three proteins onto the rGO surface occurs through the π–π interactions. Moreover, the hydrophobic nature of the rGO surface has increased its affinity for hydrophobic protein and decreased its affinity for hydrophilic proteins. Among the studied proteins, the rGO surface showed the highest adsorption capacity to collagen (qe = 0.0220 µg/µg), while BSA and elastin represented three to five times lower qe values (0.0070 µg/µg and 0.0049 µg/µg, respectively). The thermodynamic study showed that the adsorption of these proteins onto rGO is a non-spontaneous phenomenon. Moreover, the adsorption of collagen by rGO is an endothermic process, while the adsorption of BSA and elastin is exothermic. When rGO-protein matrices were incorporated into the alginate hydrogels, the protein coat on the rGO surface was able to preclude further adsorption of erythropoietin. This collagen-coated rGO addition to alginate hydrogel enhanced alginate's conductivity, leading to the lowest impedance modulus and the highest specific capacitance, 3.17×10^{-5} (F/g). This enhancement would be extremely helpful for its application in tissue engineering for neuronal or cardiomyocyte regeneration, cell-based therapy, and tissue engineering.

Author Contributions

Conceptualization, J.L.P. and L.S.-d.-B.; methodology, J.C., A.M.O.d.R., M.L.S.; validation, A.R., J.C., A.M.O.d.R., M.S.T.; formal analysis, A.R., J.C., A.M.O.d.R., L.S.-d.-B., J.L.P.; investigation, A.R., J.C., A.M.O.d.R., M.L.S.; resources, P.G.-M., J.L.P.; data curation, A.R., A.M.O.d.R., M.L.S.; writing—original draft preparation, A.R., J.C., L.S.-d.-B., J.L.P.; writing—review and editing, A.R., J.C., M.S.T., L.S.-d.-B., J.L.P.; supervision, L.S.-d.-B., J.L.P.; project administration, J.L.P.; funding acquisition, J.L.P. All authors have read and agreed to the published version of the manuscript.

Funding

This study was financially supported by the Basque Country Government [grant number T907-16].

Institutional Review Board Statement

Not applicable.

Informed Consent Statement

Not applicable.

Acknowledgments

We wish to thank the intellectual and technical assistance from the ICTS “NANBIOSIS”, more specifically by the Drug Formulation Unit (U10) of the CIBER in Bioengineering, Biomaterials, and Nanomedicine (CIBER-BBN) at the University of Basque Country UPV/EHU.

Conflicts of Interest. The authors declare no conflict of interest.

4. References

1. Caló, E.; Khutoryanskiy, V. Biomedical applications of hydrogels. A review of patents and commercial products. Eur. Polym. J. 2015, 65, 252–267.
2. Chai, Q.; Jiao, Y.; Yu, X. Hydrogels for biomedical applications. Their characteristics and the mechanisms behind them. Gels 2017, 3, 6.
3. Hoare, T.R.; Kohane, D.S. Hydrogels in drug delivery. Progress and challenges. Polymer 2008, 49, 1993–2007.
4. Mei, L.; Zeng, X.; Ma, C.; Yi, H.; Ali, Z.; Mou, X.; Li, S.; Deng, Y.; He, N. Injectable hydrogels for cartilage and bone tissue engineering. Bone Res. 2017, 5, 75–94.
5. Tsou, Y.-H.; Khoneisser, J.; Huang, P.-C.; Xu, X. Hydrogel as a bioactive material to regulate stem cell fate. Bioact. Mater. 2016, 1, 39–55.
6. Van Der Linden, H.J.; Herber, S.; Olthuis, W.; Bergveld, P. Stimulus-sensitive hydrogels and their applications in chemical (micro)analysis. Analyst 2003, 128, 325–331.
7. Hudson, B.N.; Dawes, C.S.; Liu, H.-Y.; Dimmitt, N.; Chen, F.; Konig, H.; Lin, C.-C. Stabilization of enzyme-immobilized hydrogels for extended hypoxic cell culture. Emergent Mater. 2019, 2, 263–272.
8. Kaczmarek, B.; Nadolna, K.; Owczarek, A. Chapter 6—The physical and chemical properties of hydrogels based on natural polymers. In Hydrogels Based on Natural Polymers; Chen, Y., Ed.; Elsevier. Amsterdam, The Netherlands, 2020; pp. 151–172.
9. Hoffman, A.S. Hydrogels for biomedical applications. Adv. Drug Deliv. Rev. 2012, 64, 18–23.
10. Raza, F.; Zafar, H.; Zhu, Y.; Ren, Y.; Ullah, A.; Khan, A.U.; He, X.; Han, H.; Aquib, M.; Boakye-Yiadom, K.O.; et al. A Review on Recent Advances in Stabilizing Peptides/Proteins upon Fabrication in Hydrogels from Biodegradable Polymers. Pharmaceutics 2018, 10, 16.
11. Billiet, T.; Vandenhaute, M.; Schelfhout, J.; Van Vlierberghe, S.; Dubruel, P. A review of trends and limitations in hydrogel-rapid prototyping for tissue engineering. Biomaterials 2012, 33, 6020–6041.
12. Pan, G.; Guo, Q.; Ma, Y.; Yang, H.; Li, B. Thermo-responsive hydrogel layers imprinted with RGDS peptide. A system for harvesting cell sheets. Angew. Chem. Int. Ed. Engl. 2013, 52, 6907–6911.
13. Li, L.; Wang, Y.; Pan, L.; Shi, Y.; Cheng, W.; Shi, Y.; Yu, G. A Nanostructured Conductive Hydrogels-Based Biosensor Platform for Human Metabolite Detection. Nano Lett. 2015, 15, 1146–1151.
14. González-Díaz, E.C.; Varghese, S. Hydrogels as extracellular matrix analogs. Gels 2016, 2, 20.
15. Noguera, A.E.; Ciriza, J.; Cañibano-Hernández, A.; Fernandez, L.; Ochoa, I.; del Burgo, L.S.; Pedraz, J.L. Tunable injectable alginate-based hydrogel for cell therapy in Type 1 Diabetes Mellitus. Int. J. Biol. Macromol. 2018, 107, 1261–1269.
16. Raslan, A.; Burgo, L.; Espona-Noguera, A.; Retana, A.; Sanjuán, M.; Cañibano-Hernández, A.; Gálvez-Martín, P.; Ciriza, J.; Pedraz, J. BSA- and elastin-coated GO, but not collagen-coated GO, enhance the biological performance of alginate hydrogels. Pharmaceutics 2020, 12, 543.
17. Zhou, H.; Xu, H.H. The fast release of stem cells from alginate-fibrin microbeads in injectable scaffolds for bone tissue engineering. Biomaterials 2011, 32, 7503–7513.
18. Hernández, R.M.A.; Orive, G.; Murua, A.; Pedraz, J.L. Microcapsules and microcarriers for in situ cell delivery. Adv. Drug Deliv. Rev. 2010, 62, 711–730.
19. Liu, J.; Cui, L.; Losic, D. Graphene and graphene oxide as new nanocarriers for drug delivery applications. Acta Biomater. 2013, 9, 9243–9257.
20. Feng, L.; Liu, Z. Graphene in biomedicine. Opportunities and challenges. Nanomedicine 2011, 6, 317–324.
21. Yan, L.; Zhao, F.; Li, S.; Hu, Z.; Zhao, Y. Low-toxic and safe nanomaterials by surface-chemical design, carbon nanotubes, fullerenes, metallofullerenes, and graphenes. Nanoscale 2010, 3, 362–382.
22. Sasidharan, A.; Panchakarla, L.S.; Sadanandan, A.R.; Ashokan, A.; Chandran, P.; Girish, C.M.; Menon, D.; Nair, S.V.; Rao, C.N.R.; Koyakutty, M. Hemocompatibility and macrophage response of pristine and functionalized graphene. Small 2012, 8, 1251–1263.
23. Hu, W.; Peng, C.; Luo, W.; Lv, M.; Li, X.; Li, D.; Huang, Q.; Fan, C. Graphene-based antibacterial paper. ACS Nano 2010, 4, 4317–4323.
24. Yue, H.; Wei, W.; Yue, Z.; Wang, B.; Luo, N.; Gao, Y.; Ma, D.; Ma, G.; Su, Z. The role of the lateral dimension of graphene oxide in the regulation of cellular responses. Biomaterials 2012, 33, 4013–4021.
25. Kang, Y.; Liu, J.; Wu, J.; Yin, Q.; Liang, H.; Chen, A.; Shao, L. Graphene oxide and reduced graphene oxide induced neural pheochromocytoma-derived PC12 cell lines apoptosis and cell cycle alterations via the ERK signaling pathways. Int. J. Nanomed. 2017, 12, 5501–5510.
26. Casero, E.; Parra-Alfambra, A.; Domínguez, M.D.P.; Pariente, F.; Lorenzo, E.; Alonso, F.P. Differentiation between graphene oxide and reduced graphene by electrochemical impedance spectroscopy (EIS). Electrochem. Commun. 2012, 20, 63–66.
27. Eigler, S.; Dotzer, C.; Hirsch, A. Visualization of defect densities in reduced graphene oxide. Carbon 2012, 50, 3666–3673.
28. Kannappan, S.; Kaliyappan, K.; Manian, R.K.; Pandian, A.S.; Yang, H.; Lee, Y.S.; Jang, J.-H.; Lu, H. Graphene based supercapacitors with improved specific capacitance and fast charging time at high current density. arXiv 2013, arXiv.1311.1548.
29. Pokharel, P.; Lee, D.S. Thermal and mechanical properties of reduced graphene oxide/polyurethane nanocomposite. J. Nanosci. Nanotechnol. 2014, 14, 5718–5721.
30. Yan, H.; Tao, X.; Yang, Z.; Li, K.; Yang, H.; Li, A.; Cheng, R. Effects of the oxidation degree of graphene oxide on the adsorption of methylene blue. J. Hazard. Mater. 2014, 268, 191–198.
31. Molina, J.; Fernández, J.; Inés, J.; del Río, A.; Bonastre, J.; Cases, F. Electrochemical characterization of reduced graphene oxide-coated polyester fabrics. Electrochimica Acta 2013, 93, 44–52.
32. Rose, A.; Raghavan, N.; Thangavel, S.; Maheswari, B.U.; Nair, D.P.; Venugopal, G. Investigation of cyclic voltammetry of graphene oxide/polyaniline/polyvinylidene fluoride nanofibers prepared via electrospinning. Mater. Sci. Semicond. Process. 2015, 31, 281–286.
33. Bai, H.; Li, C.; Shi, G. Functional composite materials based on chemically converted graphene. Adv. Mater. 2011, 23, 1089–1115.
34. Raslan, A.; del Burgo, L.S.; Ciriza, J.; Pedraz, J.L. Graphene oxide and reduced graphene oxide-based scaffolds in regenerative medicine. Int. J. Pharm. 2020, 580, 119226.
35. Chen, D.; Feng, H.; Li, J. Graphene oxide. Preparation, functionalization, and electrochemical applications. Chem. Rev. 2012, 112, 6027–6053.
36. Mohan, V.B.; Lau, K.-t.; Hui, D.; Bhattacharyya, D. Graphene-based materials and their composites. A review on pro-duction, applications and product limitations. Compos. Part B Eng. 2018, 142, 200–220.

37. Park, S.; An, J.; Jung, I.; Piner, R.D.; An, S.J.; Li, X.; Velamakanni, A.; Ruoff, R.S. Colloidal suspensions of highly reduced graphene oxide in a wide variety of organic solvents. Nano Lett. 2009, 9, 1593–1597.
38. Konkena, B.; Vasudevan, S. Understanding aqueous dispersibility of graphene oxide and reduced graphene oxide through pKa measurements. J. Phys. Chem. Lett. 2012, 3, 867–872.
39. Park, S.; Ruoff, R.S. Chemical methods for the production of graphenes. Nat. Nanotechnol. 2009, 4, 217–224.
40. Ciriza, J.; del Burgo, L.S.; Muñoz, J.L.P.; Ochoa, I.; Fernandez, L.; Orive, G.; Hernandez, R.; Pedraz, J. Graphene oxide increases the viability of C2C12 myoblasts microencapsulated in alginate. Int. J. Pharm. 2015, 493, 260–270.
41. Ciriza, J.; Del Burgo, L.S.; Gurruchaga, H.; Borras, F.E.; Franquesa, M.; Orive, G.; Hernández, R.M.; Pedraz, J.L. Graphene oxide enhances alginate encapsulated cells viability and functionality while not affecting the foreign body response. Drug Deliv. 2018, 25, 1147–1160.
42. Del Burgo, L.S.; Ciriza, J.; Acarregui, A.; Gurruchaga, H.; Blanco, F.J.; Orive, G.; Hernández, R.M.; Pedraz, J.L. Hybrid alginate–protein-coated graphene oxide microcapsules enhance the functionality of erythropoietin secreting C2C12 myoblasts. Mol. Pharm. 2017, 14, 885–898.
43. Zhang, Q.; Liu, X.; Meng, H.; Liu, S.; Zhang, C. Reduction pathway-dependent cytotoxicity of reduced graphene oxide. Environ. Sci. Nano 2018, 5, 1361–1371.
44. Konios, D.; Stylianakis, M.M.; Stratakis, E.; Kymakis, E. Dispersion behaviour of graphene oxide and reduced graphene oxide. J. Colloid Interface Sci. 2014, 430, 108–112.
45. Liao, K.-H.; Lin, Y.-S.; Macosko, C.W.; Haynes, C. Cytotoxicity of graphene oxide and graphene in human erythrocytes and skin fibroblasts. ACS Appl. Mater. Interfaces 2011, 3, 2607–2615.
46. Tabish, T.; Pranjol, M.Z.I.; Hayat, H.; Rahat, A.A.M.; Abdullah, T.M.; Whatmore, J.L.; Zhang, Z. In vitro toxic effects of reduced graphene oxide nanosheets on lung cancer cells. Nanotechnology 2017, 28, 504001.
47. Mittal, S.; Kumar, V.; Dhiman, N.; Chauhan, L.K.S.; Pasricha, R.; Pandey, A.K. Physico-chemical properties based differential toxicity of graphene oxide/reduced graphene oxide in human lung cells mediated through oxidative stress. Sci. Rep. 2016, 6, 39548.
48. Guo, W.; Wang, S.; Yu, X.; Qiu, J.; Li, J.; Tang, W.; Li, Z.; Mou, X.; Liu, H.; Wang, Z.L. Construction of a 3D rGO–collagen hybrid scaffold for enhancement of the neural differentiation of mesenchymal stem cells. Nanoscale 2016, 8, 1897–1904.
49. Xiao, D.; He, M.; Liu, Y.; Xiong, L.; Zhang, Q.; Wei, L.; Li, L.; Yu, X. Strong alginate/reduced graphene oxide composite hydrogels with enhanced dye adsorption performance. Polym. Bull. 2020, 77, 6609–6623.
50. Jea, A.; Palejwala, A.; Fridley, J.; Mata, J.; Samuel, E.G.; Luerssen, T.; Perlaky, L.; Kent, T.; Tour, J. Biocompatibility of reduced graphene oxide nanoscaffolds following acute spinal cord injury in rats. Surg. Neurol. Int. 2016, 7, 75.
51. Mihic, A.; Cui, Z.; Wu, J.; Vlacic, G.; Miyagi, Y.; Li, S.-H.; Lu, S.; Sung, H.-W.; Weisel, R.D.; Li, R.-K. A conductive polymer hydrogel supports cell electrical signaling and improves cardiac function after implantation into myocardial infarct. Circulation 2015, 132, 772–784.
52. Nuengmatcha, P.; Mahachai, R.; Chanthai, S. Adsorption capacity of the as-synthetic graphene oxide for the removal of alizarin red S dye from aqueous solution. Orient. J. Chem. 2016, 32, 1399–1410.
53. Fierro, V.; Torné-Fernández, V.; Montane, D.; Celzard, A. Adsorption of phenol onto activated carbons having different textural and surface properties. Microporous Mesoporous Mater. 2008, 111, 276–284.
54. Xu, X.; Mao, X.; Wang, Y.; Li, D.; Du, Z.; Wu, W.; Jiang, L.; Yang, J.; Li, J. Study on the interaction of graphene oxide-silver nanocomposites with bovine serum albumin and the formation of nanoparticle-protein corona. Int. J. Biol. Macromol. 2018, 116, 492–501.
55. Ahmad, M.A.; Puad, N.A.A.; Bello, O.S. Kinetic, equilibrium and thermodynamic studies of synthetic dye removal using pomegranate peel activated carbon prepared by microwave-induced KOH activation. Water Resour. Ind. 2014, 6, 18–35.
56. Peng, B.; Chen, L.; Que, C.; Yang, K.; Deng, F.; Deng, X.; Shi, G.; Xu, G.; Wu, M. Adsorption of antibiotics on graphene and biochar in aqueous solutions induced by π-π interactions. Sci. Rep. 2016, 6, 31920.
57. Chen, P.; Li, H.; Song, S.; Weng, X.; He, D.; Zhao, Y. Adsorption of dodecylamine hydrochloride on graphene oxide in water. Results Phys. 2017, 7, 2281–2288.
58. Nethaji, S.; Sivasamy, A.; Mandal, A.B. Adsorption isotherms, kinetics and mechanism for the adsorption of cationic and anionic dyes onto carbonaceous particles prepared from Juglans regia shell biomass. Int. J. Environ. Sci. Technol. 2012, 10, 231–242.
59. Yang, A.; Zhu, Y.; Huang, C.P. Facile preparation and adsorption performance of graphene oxide-manganese oxide composite for uranium. Sci. Rep. 2018, 8, 9058.
60. Moussout, H.; Ahlafi, H.; Aazza, M.; Maghat, H. Critical of linear and nonlinear equations of pseudo-first order and pseudo-second order kinetic models. Karbala Int. J. Mod. Sci. 2018, 4, 244–254.
61. Wang, W.; Liu, P.; Wu, K.; Tan, S.; Li, W.; Yang, Y. Preparation of hydrophobic reduced graphene oxide supported Ni-B-P-O and Co-B-P-O catalysts and their high hydrodeoxygenation activities. Green Chem. 2015, 18, 984–988.
62. Hong, F.; Yue, B.; Hirao, N.; Liu, Z.; Chen, B. Significant improvement in Mn2O3 transition metal oxide electrical conductivity via high pressure. Sci. Rep. 2017, 7, srep44078.
63. Wang, J.; Chen, B. Adsorption and coadsorption of organic pollutants and a heavy metal by graphene oxide and reduced graphene materials. Chem. Eng. J. 2015, 281, 379–388.
64. Ossonon, B.D.; Bélanger, D. Synthesis and characterization of sulfophenyl-functionalized reduced graphene oxide sheets. RSC Adv. 2017, 7, 27224–27234.
65. Kim, K.H.; Yang, M.; Cho, K.M.; Jun, Y.-S.; Lee, S.B.; Jung, H.-T. High quality reduced graphene oxide through repairing with multi-layered graphene ball nanostructures. Sci. Rep. 2013, 3, 3251.
66. Li, L.; Xu, D.; Pei, Z. Kinetics and thermodynamics studies for bisphenol S adsorption on reduced graphene oxide. RSC Adv. 2016, 6, 60145–60151.
67. Peng, S.; Feng, P.; Wu, P.; Huang, W.; Yang, Y.; Guo, W.; Gao, C.; Shuai, C. Graphene oxide as an interface phase between polyetheretherketone and hydroxyapatite for tissue engineering scaffolds. Sci. Rep. 2017, 7, srep46604.
68. Shin, S.R.; Zihlmann, C.; Akbari, M.; Assawes, P.; Cheung, L.; Zhang, K.; Manoharan, V.; Zhang, Y.S.; Yüksekkaya, M.; Wan, K.; et al. Reduced graphene oxide-GelMA hybrid hydrogels as scaffolds for cardiac tissue engineering. Small 2016, 12, 3677–3689.
69. Kumar, S.; Parekh, S.H. Linking graphene-based material physicochemical properties with molecular adsorption, structure and cell fate. Commun. Chem. 2020, 3, 1–11.
70. Serafin, A.; Murphy, C.; Rubio, M.C.; Collins, M.N. Printable alginate/gelatin hydrogel reinforced with carbon nanofibers as electrically conductive scaffolds for tissue engineering. Mater. Sci. Eng. C 2021, 122, 111927

71. Krishnamoorthy, K.; Ananth, A.; Mok, Y.S.; Kim, S.-J. Plasma assisted synthesis of graphene nanosheets and their supercapacitor applications. Sci. Adv. Mater. 2014, 6, 349–353.
72. Ruano, G.; Iribarren, J.I.; Pérez-Madrigal, M.M.; Torras, J.; Alemán, C. Electrical and capacitive response of hydrogel solid-like electrolytes for supercapacitors. Polymers 2021, 13, 1337.
73. Ghann, W.E.; Kang, H.; Uddin, J.; Chowdhury, F.A.; Khondaker, S.I.; Moniruzzaman, M.; Kabir, H.; Rahman, M.M. Synthesis and characterization of reduced graphene oxide and their application in dye-sensitized solar cells. ChemEngineering 2019, 3, 7.
74. Mavrič, T.; Benčina, M.; Imani, R.; Junkar, I.; Valant, M.; Kralj-Iglič, V.; Iglič, A. Chapter three—Electrochemical biosensor based on tio2 nanomaterials for cancer diagnostics. In Advances in Biomembranes and Lipid Self-Assembly; Iglič, A., Rappolt, M., García-Sáez, A.J., Eds.; Academic Press. Cambridge, MA, USA, 2018; Volume 27, pp. 63–1

Resumen

Los hidrogeles son estructuras 3D diseñadas para ayudar a la supervivencia de las células embebidas y crear un microambiente óptimo dentro del cual puedan prosperar y persistir. La porosidad de estos hidrogeles permite que los nutrientes entren en el gel para mantener las células y que los productos de desecho secretados por las células se liberen en el gel para mantener la viabilidad celular. El hidrogel también protege las células embebidas del entorno externo, que incluye inmunoglobulinas de alto peso molecular y células del sistema inmunitario, cuando se implanta in vivo.

El alginato es uno de los mejores biomateriales para la preparación de estos hidrogeles debido a sus excelentes propiedades, entre ellas su alta biocompatibilidad y facilidad de gelificación. Los hidrogeles de alginato han sido particularmente efectivos en la curación de heridas, administración de fármacos, terapias basadas en células y aplicaciones de ingeniería de tejidos. Estos hidrogeles a base de alginato conservan una estructura similar a las matrices extracelulares. Sin embargo, los hidrogeles de alginato tienen una adhesión celular deficiente, una resistencia mecánica débil y una liberación rápida del fármaco. Para compensar este inconveniente, muchos investigadores han incorporado diferentes materiales en la matriz de alginato para proporcionar soporte biomimético. El grafeno y sus derivados (óxido de grafeno y óxido de grafeno reducido) han demostrado ser candidatos adecuados para mejorar las propiedades superficiales y la resistencia mecánica del alginato. Debido a sus propiedades químicas y físicas únicas, la utilización de grafeno abarca una amplia gama de aplicaciones en muchos campos, como la electrónica, la óptica y el almacenamiento de energía, debido a sus excelentes propiedades químicas y físicas, que incluyen un área de superficie alta y excelentes propiedades electroquímicas, como alta capacitancia y alta conductividad, el grafeno se utiliza cada vez más en el campo biomédico para el desarrollo de nuevos sistemas de administración de fármacos, en terapia génica o en la mejora de medios de contraste para diagnóstico por imágenes.

En los últimos años, los avances en nanotecnología, por ejemplo, GO y rGO, parecen ser materiales muy prometedores para su aplicación en hidrogeles de alginato, que contienen células vivas y crean un microambiente adecuado.

En cuanto a los mecanismos de adsorción de proteínas en GO, varían según factores como la morfología, la hidrofobicidad de GO y la naturaleza de la proteína adsorbida. En este sentido, la proteína se puede adsorber en la superficie del GO mediante adsorción física o covalente. La adsorción física incluye interacción hidrofóbica, fuerzas de Van der Waals, interacciones electrostáticas y enlaces de hidrógeno. El GO tiene la hibridación sp2 por lo que la interacción GO-proteína ocurre principalmente a través de la interacción hidrofóbica-hidrofóbica, donde los sitios hidrofóbicos de la proteína tienen una alta afinidad por la red de carbono hidrofóbico en el GO. Al mismo tiempo, las fuerzas de van der Waals tienen un papel fundamental en la adsorción de fármacos hidrofóbicos o nanocompuestos en la superficie del GO.

Además, las interacciones electrostáticas son más obvias en el GO y ocurren principalmente en condiciones de pH fuertes (a pH < 6,0, la superficie del GO tiene una carga más negativa). Además, la formación de enlaces de hidrógeno se utiliza para explicar la formación de segmentos de ssDNA adsorbidos en GO. Finalmente, las interacciones de apilamiento π–π se han atribuido a la abundancia de electrones π en el plano basal de la superficie del GO. Las interacciones de apilamiento π-π son uno de los mecanismos más importantes para la adsorción de proteínas al GO.

Varios estudios han investigado los efectos de GO y rGO en la diferenciación de células madre en medicina regenerativa. Una observación general ha sido que el GO y el rGO mejoran la diferenciación de células madre. Los cardiomiocitos, las neuronas y las células madre mesenquimales (MSC) se ven muy afectados por la superficie del GO en su capacidad de adhesión, proliferación celular y diferenciación en linajes osteogénicos.

Con respecto a las propiedades de la superficie del GO en términos de unión y proliferación celular, se ha observado que el GO tiene un fuerte impacto, mediando la

unión y adhesión celular tanto en cultivos bidimensionales (2D) como en cultivos tridimensionales (3D).

El GO podría inducir la proliferación celular en cultivos bidimensionales (2D). De hecho, en los cultivos 2D, las partículas de GO se comportan de forma diferente con la membrana de los mioblastos C2C12 dependiendo de su tamaño, donde las partículas grandes son fagocitadas, mientras que las partículas más pequeñas entran en la célula por endocitosis mediada por clatrina. Sin embargo, algunos otros parámetros, como las dimensiones de las nanopartículas y la química de su superficie, podrían tener un impacto significativo en sus efectos biológicos. Asimismo, la inducción de estrés oxidativo en las células A549 en función de la dosis utilizada y el tamaño de las partículas GO también podría tener un impacto significativo en sus efectos biológicos. Aun así, se cree que este material podría tener una buena biocompatibilidad.

Con respecto a los efectos del GO sobre la proliferación celular en cultivos tridimensionales (3D), encontramos que concentraciones de GO de 50 µg/ml mejoraron la viabilidad, la actividad metabólica y la integridad de la membrana de los mioblastos C2C12-EPO.

Sin embargo, debido a la actividad superficial del GO, se ha observado que el GO tiene una gran afinidad para adsorber la EPO producida, lo que reduce la cantidad de EPO liberada cuando se integra con microcápsulas de células de mioblastos C2C12-EPO. Por lo tanto, es interesante desarrollar una capa de proteína de recubrimiento previo para reducir la alta capacidad de adsorción de GO. Esta aproximación se basa en los resultados de un estudio en el que la incorporación de una capa de albumina bovina o suero fetal, mejoró la liberación de EPO y redujo la toxicidad de las células al GO cuando se integró con células microencapsuladas.

Esta tesis demuestra métodos novedosos para fabricar nuevos hidrogeles de alginato modificados mediante la incorporacion de GO y rGO para imitar la matriz acelular de las células encapsulada con el fin de reducir la alta captura de las proteínas secretadas.

La incorporación de proteínas de matriz extracelular con GO y rGO dio como resultado una corona protectora en sus superficies. Cuando analizamos las diferentes bandas de espectros Raman en los espectros y la relación entre algunas de las bandas, observamos que la relación de intensidad aumenta cuando las proteínas se mezclan con las nanopartículas de GO o rGO, lo que sugiere una mejora del grado de funcionalización de la superficie. Además, la espectroscopia FTIR confirmó la formación de una biocorona proteica donde el pico característico de GO a 1645 cm-1 (grupo aromático C=C) ya no era detectable. Para rGO , este pico fe desplazado lo que sugiere que la formación de la biocorona en las superficies de GO ocurre a través de la interacción π-π entre el anillo de benceno de las proteínas y el C=C del GO.

Según nuestros hallazgos, a medida que aumentamos la concentración de proteínas, también aumenta la capacidad de GO y rGO para adsorber proteínas. Este efecto varió entre las proteínas estudiadas, la albumina bovina y la elastina tienen mayor afinidad mientras que el colágeno manifiesta una menor afinidad por la superficie del GO. Por el contrario, rGO tiene una mayor afinidad por el colágeno y una baja afinidad por albumina bovina y elastina.

Además, se haobservado un aumento en la capacidad de adsorción del GO para BSA, colágeno y elastina con un aumento de la temperatura. Los valores positivos de $\Delta H°$ indican que el proceso de adsorción de las proteínas en la superficie GO es endotérmico. Por otro lado, se ha observado una disminución en la capacidad de adsorción de rGO para albumina bovina y elastina, y solo el incremento de temperatura mejoró la adsorción de colágeno en la superficie de rGO .

El análisis de los datos electroquímicos reveló que las partículas GO recubiertas de proteína y rGO recubiertas de proteína actúan como mediadores electroquímicos en los hidrogeles de alginato.

Por lo tanto, recubrimos las nanopartículas de GO con las proteínas de estudio (BSA, elastina y colágeno) y analizamos el efecto sobre los mioblastos C2C12 productores de EPO mediante microscopía de fluorescencia. Las partículas de GO cubiertas de proteína mejoraron la viabilidad de las células C2C12 embebidas en hidrogeles de

alginato, siendo el impacto más significativo en los hidrogeles que contienen partículas de colágeno-GO y elastina-GO. Este efecto ya era visible después de una semana, y fue aún más relevante durante la segunda semana después de la encapsulación.

Paralelamente, la medición de la actividad metabólica de las células reveló que incluso después de un día después de la encapsulación, los hidrogeles de alginato que contenían GO recubiertos con elastina mostraron una actividad significativamente mayor. A partir de este tieempo, el efecto de todas las proteínas adsorbidas pareció tener el mismo impacto, y estadísticamente solo se detectaron diferencias significativas en la segunda semana de análisis.

Según los resultados, los hidrogeles de alginato GO recubiertos con BSA fueron los más efectivos en la liberación de EPO. Por el contrario, los hidrogeles de alginato GO recubiertos de colágeno mostraron una liberación más baja que el control. Se podría esperear que a medida que aumenta la viabilidad celular, también debería aumentar la cantidad de EPO liberada en los medios, sin embargo, la biocorona que se forma alrededor de las nanopartículas de GO es diferente dependiendo de la proteína utilizada (BSA, elastina o Colágeno), por lo que el bloqueo que se logra es diferente, lo que repercute en la cantidad de proteína terapéutica que se libera. Parece que la elastina y el Colágeno no pueden formar una biocorona estable y homogenea alrededor de GO. En consecuencia, no evitan por completo la adsorción de EPO en la superficie GO y aunque las células tienen una alta actividad metabólica y, probablemente, están produciendo una gran cantidad de EPO, esta proteína no se libera al medio ya que se une a las partículas GO.

En cuanto al estudio de bloqueo, observamos que cuando se mezclan GO y EPO, el derivado de grafeno adsorbe alrededor del 70% de la proteína. Curiosamente, cuando BSA se usa para hacer una biocorona previamente, y luego las nanoparticulas BSA-GO se mezclan con EPO, se observa que esta proteína podría bloquear casi por completo la adsorción de EPO en la superficie GO. En consecuencia, toda la EPO producida por las células encapsuladas en estos hidrogeles de BSA-GO-alginato puede liberarse al medio. Por el contrario, las otras dos proteínas no bloquean completamente

la adsorción de EPO y, por lo tanto, la proteína terapéutica producida por las células se retiene dentro de los hidrogeles. Esto explicaría por qué en estas dos proteínas, aunque las células mostraron altos niveles de viabilidad, la cantidad de EPO detectada en el medio fue menor.

Para investigar si este fenómeno se produce con otras proteínas terapéuticas además de la EPO, realizamos el mismo experimento con insulina ya que las células productoras de insulina en microcápsulas de alginato o hidrogeles podrían ser un área de investigación para el tratamiento de la diabetes mellitus tipo 1. La adsorción de insulina en la superficie GO fue similar a la de la EPO y fue de aproximadamente el 70 %. Sin embargo, a diferencia de la EPO, las tres proteínas estudiadas redujeron la adsorción de insulina en la superficie GO en alrededor de un 60 %. A la luz de estos hallazgos, especulamos que debido a que la BSA y la elastina son hidrofílicas, interfieren con la naturaleza hidrofóbica de la EPO, lo que reduce su afinidad para adsorberse en las superficies GO. Por el contrario, el colágeno, que es hidrofóbico, interactuaría con la proteína terapéutica, disminuyendo así su capacidad para prevenir la adsorción de EPO en la superficie GO. Por otro lado, debido a su bajo peso molecular y alta naturaleza hidrofílica, la insulina podría competir con BSA, elastina y colágeno por los sitios de unión de GO, reemplazando así una porción de las proteínas de recubrimiento.

Para comparar la adsorción de proteínas terapéuticas en la superficie de rGO y el efecto de bloquear estos sitios activos de rGO con diferentes recubrimientos previos (BSA, elastina y colágeno), realizamos los mismos estudios con rGO. Los resultados ponen de manifiesto que el rGO tiene mayor afinidad por la EPO (54,67%) que por la insulina (30,94%). En particular, se observó una reducción significativa en la adsorción de EPO con las tres biocoronas estudiadas. Entre los tres recubrimientos previos, la elastina exhibió la mayor capacidad para evitar la adsorción de EPO en la superficie rGO .

Cuando se analizó el bloqueo de la adsorción de insulina, las proteínas de recubrimiento BSA y Colágeno no pudieron bloquear la interacción entre las partículas

de rGO y la insulina. La elastina, sin embargo, mostró una capacidad ligeramente superior para evitar que la insulina quedara atrapada en la superficie de rGO y pudiera ser liberada al medio.